Substituting,

$$B = -(m_{\dot{\theta}} + m_{\dot{\alpha}} - f_\alpha) \tag{9-24}$$

and

$$C = -(m_\alpha + f_\alpha m_{\dot{\theta}}) \tag{9-25}$$

we get

$$\lambda(\lambda^2 + B\lambda + C) = 0 \tag{9-26}$$

or

$$\lambda_{1,2} = \frac{-B \pm \sqrt{B^2 - 4C}}{2} \tag{9-27}$$

and

$$\lambda_3 = 0 \tag{9-28}$$

The roots λ_1 and λ_2, which are the only roots of interest in this analysis, may be expressed in the complex form

$$\lambda_{1,2} = -\xi_1 \pm i\eta_{1,2} \tag{9-29}$$

The period P and time to damp to half amplitude $T_{1/2}$ (see Fig. 9-3) may be calculated by the following equations:

$$P = \frac{2\pi}{\eta} \quad \text{sec} \tag{9-30}$$

$$T_{1/2} = \frac{\ln 2}{\xi} \quad \text{sec} \tag{9-31}$$

It is apparent from Eq. (9-31) that the time to damp to half amplitude is dependent upon the value of ξ or B in Eq. (9-24). Since the value of B is primarily a function of the damping characteristics of the airframe (i.e., $M_{\dot{\theta}}$ and M_α), it is appropriate to discuss here the source and magnitude of these damping terms before going into the three-degree-of-freedom analysis.

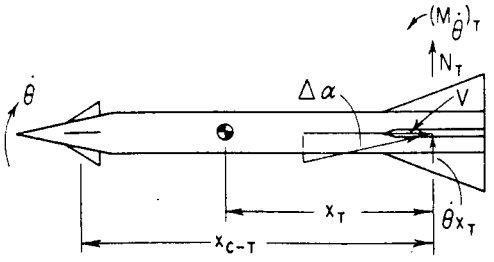

FIG. 9-4. Tail contribution to damping in pitch.

$M_{\dot{\theta}}$. This is a damping moment which arises from the pitching velocity $\dot{\theta}$ of the missile and is commonly known as the damping in pitch. From Fig. 9-4, it is seen that, as a result of missile rotation about the center of gravity, an angle of attack is induced at the tail (or any other aerodynamic component, i.e., nose, canard, or wing). The resultant force and hence moment is in a direction which opposes the rotation of the missile; hence the term damping arises and has a negative sign. In most missile configurations, the tail surfaces contribute

the largest portion to the complete model damping. The magnitude of this damping in pitch may be determined as follows:

$$\Delta M_T = -N_T x_T = -(C_{N_\alpha})_T[K_{T(B)} + K_{B(T)}]\,\Delta\alpha_T q S_T x_T \qquad (9\text{-}32)$$

where $K_{T(B)}$ and $K_{B(T)}$ are the body-tail interference factors discussed in Chap. 5.

It has been assumed in Eq. (9-32) that the damping due to the tail surfaces includes the body-carry-over normal force, i.e., $(C_{N_\alpha})_T K_{B(T)}$ and that the center of pressure of this part of the normal force is the same as that on the tail surfaces. For preliminary-design purposes, this assumption appears to be adequate, particularly for configurations with tail surfaces located near or at the end of the body (i.e., little or no afterbody). This assumption is used throughout the entire derivation of the complete model damping in pitch. In this derivation a canard-control design is used. The error introduced by the above assumption is negligible since the canard contribution to damping is of secondary importance.

Dividing Eq. (9-32) by $qS_\pi d$, we get

$$\Delta C_{m_T} = -(C_{N_\alpha})_T[K_{T(B)} + K_{B(T)}]\,\Delta\alpha_T \frac{S_T}{S_\pi}\left(\frac{x}{d}\right)_T \qquad (9\text{-}33)$$

The induced angle of attack due to pitching velocity $\dot\theta$ is

$$\Delta\alpha_T = \tan^{-1}\frac{\dot\theta x_T}{V} \qquad (9\text{-}34)$$

or, for small values of $\Delta\alpha_T$,

$$\Delta\alpha_T \cong \frac{\dot\theta x_T}{V} \qquad (9\text{-}35)$$

Substituting Eq. (9-35) into (9-33), we get

$$\Delta C_{m_T} = -(C_{N_\alpha})_T[K_{T(B)} + K_{B(T)}]\,\frac{\dot\theta}{V}\frac{S_T}{S_\pi}\frac{x_T^2}{d} \qquad (9\text{-}36)$$

Defining

$$C_{m_{\dot\theta}} = \frac{\partial C_m}{\partial(\dot\theta d/2V)} \qquad (9\text{-}37)$$

we get

$$C_{m_{\dot\theta}} = -2(C_{N_\alpha})_T[K_{T(B)} + K_{B(T)}]\,\frac{S_T}{S_\pi}\left(\frac{x}{d}\right)_T^2 \qquad (9\text{-}38)$$

It is apparent from Eq. (9-38) that the tail contribution to damping in pitch varies directly with the tail area and as the square of the tail length. Hence it is much more effective to increase the length of the

tail than to increase the tail area to obtain increased damping. Moreover, tail area has the disadvantage of increased weight and drag. The complete model damping in pitch is the sum of the contributions from the nose, canard, and tail surfaces and may be expressed as

$$(C_{m_{\dot\theta}})_{CM} = -\left\{2(C_{N_\alpha})_B\left(\frac{x}{d}\right)_B^2 + 2(C_{N_\alpha})_C[K_{C(B)} + K_{B(C)}]\frac{S_C}{S_\pi}\left(\frac{x}{d}\right)_C^2 + 2(C_{N_\alpha})_T[K_{T(B)} + K_{B(T)}]\frac{S_T}{S_\pi}\left(\frac{x}{d}\right)_T^2\right\} \quad (9\text{-}39)$$

M_α. This damping term arises because of the time lag in the canard downwash getting to the tail surfaces (in the case of a wing- or tail-control design, the lag in the wing downwash getting to the tail surfaces is used). Since $\alpha_T = \alpha - \epsilon$ and $\epsilon = (d\epsilon/d\alpha)\alpha$,

$$\epsilon = \frac{d\epsilon}{d\alpha}\left(\alpha - \frac{d\alpha}{dt}\,\Delta t\right) \quad (9\text{-}40)$$

where Δt is the time it takes the air to go from the canard to the tail, i.e., $\Delta t = x_{C-T}/V$. Hence the damping moment due to this downwash lag is

$$M_T = -(C_{N_\alpha})_T[K_{T(B)} + K_{B(T)}]\alpha_T q S_T x_T \quad (9\text{-}41)$$

Substituting Eq. (9-40) into Eq. (9-41), we get

$$M_T = -(C_{N_\alpha})_T[K_{T(B)} + K_{B(T)}]\left[\alpha - \frac{d\epsilon}{d\alpha}\left(\alpha - \frac{d\alpha}{dt}\frac{x_{C-T}}{V}\right)\right]qS_T x_T \quad (9\text{-}42)$$

Dividing Eq. (9-42) by $qS_\pi d$, we get

$$C_{m_T} = -(C_{N_\alpha})_T[K_{T(B)} + K_{B(T)}]\left[\alpha - \epsilon_\alpha\left(\alpha - \dot\alpha\,\frac{x_{C-T}}{V}\right)\right]\frac{S_T}{S_\pi}\frac{x_T}{d} \quad (9\text{-}43)$$

Defining

$$C_{m_{\dot\alpha}} = \frac{\partial C_m}{\partial(\dot\alpha d/2V)} \quad (9\text{-}43a)$$

we get

$$C_{m_{\dot\alpha}} = -2(C_{N_\alpha})_T[K_{T(B)} + K_{B(T)}]\frac{S_T}{S_\pi}\frac{x_T}{d}\epsilon_\alpha\frac{x_{C-T}}{d} \quad (9\text{-}44)$$

Equation (9-44) is applicable for a canard-control design. For a wing-control design (see Fig. 2-2) where the wing is located at or near the center of gravity of the missile, the following simplification may be made since the length x_{W-T} is approximately equal to x_T.

$$C_{m_{\dot\alpha}} = -2(C_{N_\alpha})_T[K_{T(B)} + K_{B(T)}]\frac{S_T}{S_\pi}\left(\frac{x}{d}\right)_T^2\epsilon_\alpha \quad (9\text{-}45)$$

It is apparent that $C_{m_{\dot{\alpha}}}$ is of secondary importance since the value of ϵ_α is generally low. This is particularly true for the case of the canard-control design.

Another damping which is similar in nature to $C_{m_{\dot{\alpha}}}$ is $C_{m_{\dot{\delta}}}$. The latter is generally negligible because of the very low value of ϵ_δ as shown in Eq. (9-46) below for the canard-control design.

$$C_{m_{\dot{\delta}}} = -2(C_{N_\alpha})_T[K_{T(B)} + K_{B(T)}]\frac{S_T}{S_\pi}\frac{x_T}{d}\epsilon_\delta\frac{x_{C-T}}{d} \tag{9-46}$$

A note of caution is injected here that, in most airplane applications, these dynamic rotary derivatives are expressed as $\partial(\ )/\partial(\dot{\theta}\bar{c}/2V)$ where $\bar{c}$ is the aerodynamic chord of the wing. However, in most missile analysis, these derivations are expressed as $\partial(\ )/\partial(\dot{\theta}d/2V)$ and hence the added factor of $(d/2V)$ must appear in all the damping coefficients such as those shown in Eq. (5-1) and subsequent equations where these damping coefficients occur.

The values of these aerodynamic damping or rotary derivatives $C_{m_{\dot{\theta}}}$, $C_{m_{\dot{\alpha}}}$, and $C_{m_{\dot{\delta}}}$ may be readily determined from the static derivatives, i.e., C_{N_α}, C_{m_α}, etc., obtained from wind-tunnel-test results. The method of calculation is presented in Appendix G. A summary of the pitch-damping derivatives of complete airplane and missile configurations as measured in flight at transonic and supersonic speeds is presented in ref. 7.

2. Three Degrees of Freedom. In the analysis of longitudinal dynamics with three degrees of freedom, the equation relating the change in missile forward speed, i.e., $\Sigma F_x = m(\dot{U})$ from Eq. (9-10), is used in addition to Eqs. (9-17) and (9-18). The characteristic equation for this case may be solved by the same procedure used previously for the two-degree-of-freedom analysis. The resultant characteristic equation is the familiar quartic as shown below.

$$A\lambda^4 + B\lambda^3 + C\lambda^2 + D\lambda + E = 0 \tag{9-47}$$

The coefficients A, B, . . . are a function of the aerodynamic derivatives, mass, and moment of inertia of the missile. If all the coefficients of λ are positive, no positive real roots exist and hence no pure divergence will be exhibited in the dynamic motion of the missile. When the combination of coefficients $(BCD - AD^2 - B^2E)$, known as Routh's discriminant,[8] is positive, the motion is stable. A zero value for Routh's discriminant indicates neutral stability whereas a negative value indicates a divergent (undamped) oscillation for one of the modes. If any of the coefficients is negative, a pure divergent or increasing oscillatory motion in one of the modes is present.

In general it is of interest to determine the roots of the characteristic equation in order that the periods of the motion and the damping characteristics may be determined. Of the many available methods of solution for the roots, the method by Lin[9] appears to be the easiest. In this method the form of one of the quadratics is assumed and the second quadratic is determined by division as indicated below.

$$\lambda^4 + B'\lambda^3 + C'\lambda^2 + D'\lambda + E' = 0 \tag{9-48}$$

where $B' = B/A, C' = C/A$, etc. The first trial quadratic is assumed to be

$$\lambda^2 + \frac{D'}{C'}\lambda + \frac{E'}{C'}$$

and is used as a divisor as shown below:

$$\begin{array}{r} \lambda^2 + a_1\lambda + b_1 \\ \lambda^2 + \frac{D'}{C'}\lambda + \frac{E'}{C'} \;\overline{)\; \lambda^4 + B'\lambda^3 + C'\lambda^2 + D'\lambda + E'} \\ \underline{\text{x} \quad \text{x} \quad \text{x}} \\ \text{x} \quad \text{x} \quad D'\lambda \\ \underline{\text{x} \quad \text{x} \quad \text{x}} \\ R_1 \quad R_2 \quad E' \\ \underline{\text{x} \quad \text{x} \quad \text{x}} \\ \text{x} \quad \text{x} \text{ (remainder)} \end{array}$$

In the division process shown above, if there is a remainder, the first trial quadratic assumed, $\lambda^2 + (D'/C')\lambda + (E'/C')$, is not a factor of the quartic. In this case, a second trial quadratic must be assumed. It is of the following form:

$$\lambda^2 + \frac{R_2}{R_1}\lambda + \frac{E'}{R_1}$$

and is derived from the result of the first division previously shown. If the frequencies of the two oscillatory modes are considerably different (such is the case in the longitudinal dynamic motions) this method will converge on the second or third try. This is illustrated by a sample calculation shown in Table 9-1 for the following quartic:

$$\lambda^4 + 3.05\lambda^3 + 5.12\lambda^2 + 0.0412\lambda + 0.0205 = 0$$

Before proceeding with Lin's method of determining the roots of the quartic, a quick check should be performed to determine qualitatively the nature of the dynamic motion. Since all the coefficients are positive, no divergent motion is present. The value of Routh's discriminant is calculated to be

$$(3.05)(5.12)(0.0412) - (1)(0.0412)^2 - (3.05)^2(0.0205) > 0$$

TABLE 9-1. SAMPLE QUARTIC SOLUTION BY LIN'S METHOD[9]

Sample quartic: $\lambda^4 + 3.05\lambda^3 + 5.12\lambda^2 + 0.0412\lambda + 0.0205 = 0$

First trial quadratic: $\lambda^2 + \frac{0.0412}{5.12}\lambda + \frac{0.0205}{5.12} = \lambda^2 + 0.00805\lambda + 0.00401$

$$
\begin{array}{r}
\lambda^2 + 3.04\lambda + 5.10 \\
\lambda^2 + 0.00805\lambda + 0.00401 \;\overline{)\;\lambda^4 + 3.05\lambda^3 + 5.12\lambda^2 + 0.0412\lambda + 0.0205} \\
\underline{\lambda^4 + 0.01\lambda^3 + 0.00\lambda^2} \\
3.04\lambda^3 + 5.12\lambda^2 + 0.0412\lambda \\
\underline{3.04\lambda^3 + 0.02\lambda^2 + 0.0122\lambda} \\
5.10\lambda^2 + 0.0290\lambda + 0.0205 \\
\underline{5.10\lambda^2 + 0.0410\lambda + 0.0205} \\
-\,0.0120\lambda + 0
\end{array}
$$

Second trial quadratic: $\lambda^2 + \frac{0.0290\lambda}{5.10} + \frac{0.0205}{5.10} = \lambda^2 + 0.00569\lambda + 0.00402$

$$
\begin{array}{r}
\lambda^2 + 3.04\lambda + 5.10 \\
\lambda^2 + 0.00569\lambda + 0.00402 \;\overline{)\;\lambda^4 + 3.05\lambda^3 + 5.12\lambda^2 + 0.0412\lambda + 0.0205} \\
\underline{\lambda^4 + 0.01\lambda^3 + 0.00\lambda^2} \\
3.04\lambda^3 + 5.12\lambda^2 + 0.0412\lambda \\
\underline{3.04\lambda^3 + 0.02\lambda^2 + 0.0122\lambda} \\
5.10\lambda^2 + 0.0290\lambda + 0.0205 \\
\underline{5.10\lambda^2 + 0.0290\lambda + 0.0205} \\
0 \qquad\qquad 0
\end{array}
$$

$$\therefore (\lambda^2 + 0.00569\lambda + 0.00402)(\lambda^2 + 3.04\lambda + 5.10) = 0$$

$$\lambda_{1,2} = \frac{-0.00569 \pm \sqrt{(0.00569)^2 - 4(0.00402)}}{2} = -0.00285 \pm 0.063j$$

$$P_{1,2} = \frac{2\pi}{0.063} = 99.6 \text{ sec}, \quad (T_{1/2})_{1,2} = \frac{0.693}{0.00285} = 243 \text{ sec}$$

$$\lambda_{3,4} = \frac{-3.04 \pm \sqrt{(3.04)^2 - 4(5.10)}}{2} = \pm 1.52 \pm 1.67j$$

$$P_{3,4} = \frac{2\pi}{1.67} = 3.76 \text{ sec}, \quad (T_{1/2})_{3,4} = \frac{0.693}{1.52} = 0.456 \text{ sec}$$

Since the value of Routh's discriminant is positive and greater than zero, a stable motion is anticipated.

The results derived from Table 9-1 indicate the roots for the two modes

$$\lambda_{1,2} = -0.00285 \pm 0.063j$$
$$\lambda_{3,4} = -1.52 \pm 1.67j$$

where $j = \sqrt{-1}$, an imaginary number. The period and time to

damp to half amplitude for the two modes [using Eqs. (9-30) and (9-31)] are

$$P_{1,2} = \frac{2\pi}{0.063} = 99.6 \text{ sec}$$

$$(T_{1/2})_{1,2} = \frac{0.693}{0.00285} = 243 \text{ sec}$$

$$P_{3,4} = \frac{2\pi}{1.67} = 3.76 \text{ sec}$$

$$(T_{1/2})_{3,4} = \frac{0.693}{1.52} = 0.456 \text{ sec}$$

From the above results, it is seen that the longitudinal dynamic motion in three degrees of freedom consists of two distinct and separate modes: a long-period oscillation which is lightly damped and a very-short-period heavily damped oscillation. The former mode, called the phugoid, is of interest on cruise-type missiles whereas the short-period motion is usually more important on short-range missiles such as an AAM.

9-4. CLASSICAL SOLUTION—LATERAL DYNAMICS

The dynamic motions of a monowing missile about its lateral and directional (x and z) axes may be conveniently analyzed by assuming a three-degree-of-freedom study. The equations involved are [from Eq. (9-10)]

$$\begin{aligned} \Sigma F_y &= m(\dot{V} + UR) && \Sigma \text{ side force} \\ \Sigma M_z &= I_z\dot{R} - I_{xz}\dot{P} && \Sigma \text{ yawing moment} \\ \Sigma M_x &= I_x\dot{P} - I_{xz}\dot{R} && \Sigma \text{ rolling moment} \end{aligned} \tag{9-49}$$

In the above analysis, constant forward speed and no pitching motions are assumed. It is emphasized, however, that in most dynamic analysis of this kind, careful considerations must be given to the inertia cross-coupling effects whenever pitching motions are present. These cross-coupling effects arise from the fact that the roll moment of inertia of a missile is generally small relative to the pitch or yaw moments of inertia, i.e., $(I_y - I_x)$ and $(I_x - I_z)$ in Eq. (9-10) are large. In such cases, a more complete analysis involving five or six degrees of freedom must be conducted on automatic computing equipment.

Substituting $\beta \cong V/U$, $\dot{V} = U\dot{\beta}$, $R = \dot{\psi}$, and $P = \dot{\phi}$ (see Fig. 9-5), Eq. (9-49) becomes

$$\begin{aligned} \Sigma F_y &= mU(\dot{\psi} + \dot{\beta}) \\ \Sigma M_y &= I_z\ddot{\psi} - I_{xz}\ddot{\phi} \\ \Sigma M &= I_x\ddot{\phi} - I_{xz}\ddot{\psi} \end{aligned} \tag{9-50}$$

Equation (9-50) may be solved by the method previously described for the longitudinal case.

In the analysis of the flight dynamics of the missile, the dynamics of the missile airframe alone are only part of the over-all system. The response of the control and autopilot systems must be included in order to determine the response of the over-all missile system. The study of the complete missile dynamics is most conveniently made with the Laplace-transform and transfer-function technique discussed in the next section.

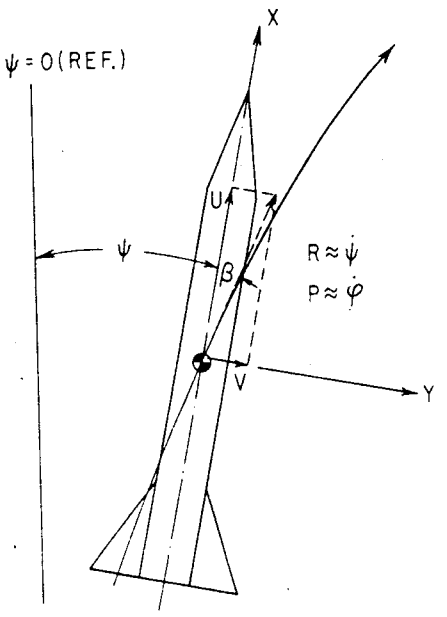

FIG. 9-5. Nomenclature for lateral-directional dynamic analysis.

9-5. TRANSFER FUNCTION

1. Derivation. A transfer function is the ratio of output to input of a linear system and is expressed in the Laplace transform variable s. The Laplace transform is a mathematical technique involving the use of the transform variable s, which is a complex variable of the form $\sigma + j\omega$, where σ is the real part and $j\omega$ is the imaginary part ($j = \sqrt{-1}$). For example, suppose the angle θ varies as a function of time and is expressed as $\theta(t)$. The Laplace transform of this function is $\theta(s)$ or $\theta(s) = \mathscr{L}\,\theta(t)$, where $\mathscr{L}$ denotes application of the transform integral. The Laplace transform of a function of the time $\mathscr{L}f(t)$ is of the following form:

$$\mathscr{L}f(t) \equiv F(s) = \int_0^\infty e^{-st} f(t)\, dt,$$

where $F(s)$ is a function of the transform variable s.

The transfer functions of the missile airframe without control and autopilot are usually expressed as the ratio of the rate of change of angle of attack, flight-path angle, etc., as an output to control-surface deflection δ. For example,

$$\frac{\dot{\gamma}}{\delta} = \frac{K}{s^2 + 2\zeta\omega s + \omega^2} \tag{9-51}$$

is the aerodynamic transfer function of the second order which relates the rate of change of flight-path angle to control-surface deflection.

In most preliminary-design studies, a two-degree-of-freedom analysis is adequate in the evaluation of the response characteristics of the airframe in conjunction with those of the autopilot and control system for pitch and/or yaw motions for the cruciform design. For the lateral-directional motions of a monowing design, a three-degree-of-freedom analysis involving Eq. (9-50) may be used. In each case, a constant forward speed is assumed regardless of the actual velocity profile of the missile. Linear aerodynamics are also assumed in these analyses.

In the development of the transfer functions for the longitudinal motions, the gravity term $W \cos \theta$ may be conveniently omitted since it represents an initial input or condition which can be biased (i.e., by fixed control-surface deflection). Since only the disturbed or perturbation motions are of interest, the initial conditions may be assumed to be zero. However, where flight kinematics (i.e., missile displacement relative to the inertial axes) are involved, the gravity terms must be accounted for. The equations of motion involved in the derivation of the transfer functions for the longitudinal case are

$$I_y\ddot{\theta} = \Sigma M_y = M_\alpha\alpha + M_\delta\delta + M_{\dot\theta}\dot\theta + M_{\dot\alpha}\dot\alpha + M_{\dot\delta}\dot\delta \tag{9-52}$$

$$mV\dot\gamma = \Sigma F = N_\alpha\alpha + N_\delta\delta \tag{9-53}$$

$$\theta = \alpha + \gamma \tag{9-54}$$

where V is used in lieu of U to denote missile forward velocity, and m is the mass of the missile and is assumed to be a constant or

$$I_y\ddot{\theta} = C_{m_\alpha}\alpha qSd + C_{m_\delta}\delta qSd + C_{m_{\dot\theta}}\dot\theta\frac{qSd^2}{2V} + C_{m_{\dot\alpha}}\dot\alpha\frac{qSd^2}{2V} + C_{m_{\dot\delta}}\dot\delta\frac{qSd^2}{2V} \tag{9-55}$$

$$mV\dot\gamma = C_{N_\alpha}\alpha qS + C_{N_\delta}\delta qS \tag{9-56}$$

Dividing Eq. (9-52) by I_y and Eq. (9-53) by mV,

$$\ddot{\theta} = m_\alpha\alpha + m_\delta\delta + m_{\dot\theta}\dot\theta + m_{\dot\alpha}\dot\alpha + m_{\dot\delta}\dot\delta \tag{9-57}$$

$$\dot\gamma = f_\alpha\alpha + f_\delta\delta \tag{9-58}$$

where $m_\alpha = M_\alpha/I_y$, . . . etc.

$f_\alpha = N_\alpha/mV$, . . . etc.

Rearranging and letting $s = d/dt$ and $s^2 = d^2/dt^2$, Eqs. (9-57), (9-58), and (9-54) become

$$(1)\alpha + (-1)\theta + (1)\gamma = 0 \tag{9-59}$$

$$(m_\alpha + sm_{\dot\alpha})\alpha + (sm_{\dot\theta} - s^2)\theta + (0)\gamma = -(m_\delta + m_{\dot\delta}s)\delta \tag{9-60}$$

$$(f_\alpha)\alpha + (0)\theta + (-s)\gamma = (-f_\delta)\delta \tag{9-61}$$

Solving Eqs. (9-59) through (9-61) by determinants, we get

$$\gamma = \frac{\begin{vmatrix} 1 & -1 & 0 \\ m_\alpha + sm_{\dot\alpha} & s(m_{\dot\theta} - s) & -(m_\delta + m_{\dot\delta}s)\delta \\ f_\alpha & 0 & -f_\delta\delta \end{vmatrix}}{\begin{vmatrix} 1 & -1 & 1 \\ m_\alpha + sm_{\dot\alpha} & s(m_{\dot\theta} - s) & 0 \\ f_\alpha & 0 & -s \end{vmatrix}}$$

$$= \frac{[-sf_\delta(m_{\dot\theta} - s) + f_\alpha(m_\delta + m_{\dot\delta}s) - f_\delta(m_\alpha + sm_{\dot\alpha})]\delta}{-s^2(m_{\dot\theta} - s) - sf_\alpha(m_{\dot\theta} - s) - s(m_\alpha + sm_{\dot\alpha})} \tag{9-62}$$

The transfer function γ/δ is thus

$$\frac{\gamma}{\delta} = \frac{f_\delta s^2 + (f_\alpha m_{\dot\delta} - f_\delta m_{\dot\theta} - f_\delta m_{\dot\alpha})s + (f_\alpha m_\delta - f_\delta m_\alpha)}{s[s^2 - (m_{\dot\theta} - f_\alpha + m_{\dot\alpha})s - (m_\alpha + f_\alpha m_{\dot\theta})]} \tag{9-63}$$

Defining $$\Delta = [s^2 - (m_{\dot\theta} - f_\alpha + m_{\dot\alpha})s - (m_\alpha + f_\alpha m_{\dot\theta})] \tag{9-64}$$

$$\frac{\gamma}{\delta} = \frac{f_\delta s^2 + (f_\alpha m_{\dot\delta} - f_\delta m_{\dot\theta} - f_\delta m_{\dot\alpha})s + (f_\alpha m_\delta - f_\delta m_\alpha)}{s\Delta} \tag{9-65}$$

Since $\dot\gamma = s\gamma$, the transfer function $\dot\gamma/\delta$ becomes

$$\frac{\dot\gamma}{\delta} = \frac{f_\delta s^2 + (f_\alpha m_{\dot\delta} - f_\delta m_{\dot\theta} - f_\delta m_{\dot\alpha})s + (f_\alpha m_\delta - f_\delta m_\alpha)}{\Delta} \tag{9-66}$$

Similarly,

$$\theta = \frac{\begin{vmatrix} 1 & 0 & 1 \\ (m_\alpha + sm_{\dot\alpha}) & -(m_\delta + m_{\dot\delta}s) & 0 \\ f_\alpha & -f_\delta\delta & -s \end{vmatrix}}{\Delta}$$

$$= \frac{s(m_\delta + m_{\dot\delta}s) - f_\delta(m_\alpha + sm_{\dot\alpha}) + f_\alpha(m_\delta + m_{\dot\delta}s)}{s\Delta} \tag{9-67}$$

or $$\frac{\theta}{\delta} = \frac{m_{\dot\delta}s^2 + (m_\delta - f_\delta m_{\dot\alpha} + f_\alpha m_{\dot\delta})s + (f_\alpha m_\delta - f_\delta m_\alpha)}{s\Delta} \tag{9-68}$$

and

$$\frac{\dot{\theta}}{\delta} = \frac{m_{\dot{\delta}}s^2 + (m_\delta - f_\delta m_{\dot{\alpha}} + f_\alpha m_{\dot{\delta}})s + (f_\alpha m_\delta - f_\delta m_\alpha)}{\Delta} \tag{9-69}$$

$$\alpha = \frac{\begin{vmatrix} 0 & -1 & 1 \\ -(m_\delta + m_{\dot{\delta}}s) & s(m_{\dot{\theta}} - s) & 0 \\ -f_\delta\delta & 0 & -s \end{vmatrix}}{s\Delta} = \frac{[s(m_\delta + m_{\dot{\delta}}s) + f_\delta s(m_{\dot{\theta}} - s)]\delta}{s\Delta} \tag{9-70}$$

or

$$\frac{\alpha}{\delta} = \frac{(m_{\dot{\delta}} - f_\delta)s + (m_\delta + f_\delta m_{\dot{\theta}})}{\Delta} \tag{9-71}$$

and

$$\frac{\dot{\alpha}}{\delta} = \frac{(m_{\dot{\delta}} - f_\delta)s^2 + (m_\delta + f_\delta m_{\dot{\theta}})s}{\Delta} \tag{9-72}$$

Other transfer functions may be derived as follows:

$$\frac{\alpha}{\gamma} = \frac{\alpha}{\delta} \times \frac{\delta}{\gamma} = \frac{[(m_{\dot{\delta}} - f_\delta)s + (m_\delta + f_\delta m_{\dot{\theta}})]s}{f_\delta s^2 + (f_\alpha m_{\dot{\delta}} - f_\delta m_{\dot{\theta}} - f_\delta m_{\dot{\alpha}})s + (f_\alpha m_\delta - f_\delta m_\alpha)} \tag{9-73}$$

$$\frac{\alpha}{\theta} = \frac{\alpha}{\delta} \times \frac{\delta}{\theta} = \frac{[(m_{\dot{\delta}} - f_\delta)s + (m_\delta + f_\delta m_{\dot{\theta}})]s}{m_{\dot{\delta}}s + (m_\delta - f_\delta m_{\dot{\alpha}} + f_\alpha m_{\dot{\delta}})s + (f_\alpha m_\delta - f_\delta m_\alpha)} \tag{9-74}$$

$$\frac{\gamma}{\theta} = \frac{\gamma}{\delta} \times \frac{\delta}{\theta} = \frac{f_\delta s^2 + (f_\alpha m_{\dot{\delta}} - f_\delta m_{\dot{\theta}} - f_\delta m_{\dot{\alpha}})s + (f_\alpha m_\delta - f_\delta m_\alpha)}{m_{\dot{\delta}}s^2 + (m_\delta - f_\delta m_{\dot{\alpha}} + f_\alpha m_{\dot{\delta}})s + (f_\alpha m_\delta - f_\delta m_\alpha)} \tag{9-75}$$

For a highly maneuverable missile where $n \gg 1$, the following approximate transfer function of n/δ may be expressed as

$$\frac{n}{\delta} = \frac{V\dot{\gamma}}{g\delta} = \frac{V}{g}\left[\frac{f_\delta s^2 + (f_\alpha m_{\dot{\delta}} - f_\delta m_{\dot{\theta}} - f_\delta m_{\dot{\alpha}})s + (f_\alpha m_\delta - f_\delta m_\alpha)}{\Delta}\right] \tag{9-76}$$

Let

$$\begin{aligned} a &= f_\delta \\ b &= f_\delta m_{\dot{\theta}} + f_\delta m_{\dot{\alpha}} - f_\alpha m_{\dot{\delta}} \\ c &= f_\alpha m_\delta - f_\delta m_\alpha \\ d &= f_\delta m_{\dot{\theta}} + m_\delta \\ e &= m_{\dot{\alpha}} - f_\alpha + m_{\dot{\theta}} \\ h &= m_\alpha + m_{\dot{\theta}} f_\alpha \\ i &= f_\delta m_{\dot{\alpha}} - m_{\dot{\delta}} - f_\alpha m_{\dot{\delta}} \\ l &= m_{\dot{\delta}} \\ (b - i) &= m_\delta + f_\delta m_{\dot{\theta}} \\ (l - a) &= m_{\dot{\delta}} - f_\delta \end{aligned} \tag{9-77}$$

The above transfer functions become

$$\frac{\gamma}{\delta} = \frac{as^2 - bs + c}{s(s^2 - es - h)} \tag{9-78}$$

$$\frac{\dot{\gamma}}{\delta} = \frac{as^2 - bs + c}{(s^2 - es - h)} \tag{9-79}$$

$$\frac{\theta}{\delta} = \frac{ls^2 - is + c}{s(s^2 - es - h)} \tag{9-80}$$

$$\frac{\dot{\theta}}{\delta} = \frac{ls^2 - is + c}{(s^2 - es - h)} \tag{9-81}$$

$$\frac{\alpha}{\delta} = \frac{(l - a)s + (b - i)}{(s^2 - es - h)} \tag{9-82}$$

$$\frac{\dot{\alpha}}{\delta} = \frac{(l - a)s^2 + (b - i)s}{(s^2 - es - h)} \tag{9-83}$$

$$\frac{\alpha}{\gamma} = \frac{\alpha}{\delta} \times \frac{\delta}{\gamma} = \frac{s[(l - a)s + (b - i)]}{as^2 - bs + c} \tag{9-84}$$

$$\frac{\alpha}{\theta} = \frac{\alpha}{\delta} \times \frac{\delta}{\theta} = \frac{s[(l - a)s + (b - i)]}{ls^2 - is + c} \tag{9-85}$$

$$\frac{\gamma}{\theta} = \frac{\gamma}{\delta} \times \frac{\delta}{\theta} = \frac{as^2 - bs + c}{ls^2 - is + c} \tag{9-86}$$

$$\frac{n}{\delta} = \frac{V\dot{\gamma}}{g\delta} = \frac{V}{g}\left[\frac{as^2 - bs + c}{(s^2 - es - h)}\right] \tag{9-87}$$

The aerodynamic transfer function is usually expressed in the following general form, i.e.,

$$\frac{\dot{\gamma}}{\delta} = \frac{K}{s^2 + 2\zeta\omega s + \omega^2} \tag{9-88}$$

where K/ω^2 is the aerodynamic static "gain" of the system and $(s^2 + 2\zeta\omega s + \omega^2)$ is the characteristic equation. In this case, $\omega = \sqrt{-h}$ and is defined as the undamped natural frequency of the missile. The term ζ equal to $(-e/2\omega)$ is the damping constant of the (airframe) system and is defined as the ratio of the actual damping of the airframe to critical damping. The value of the critical damping for a second-order linear system, such as that expressed by Eq. (9-88), is one. By

solving for the roots in the characteristic equation, the period and time to damp to half amplitude of the dynamic motion are determined as shown below.

$$s_{1,2} = \frac{-2\zeta\omega \pm \sqrt{4\zeta^2\omega^2 - 4\omega^2}}{2} \tag{9-89}$$

or

$$s_{1,2} = -\zeta\omega \pm \sqrt{-\omega^2(1-\zeta^2)} \equiv (\xi + i\eta) \tag{9-90}$$

[see Eq. (9–29)]

$$P_{1,2} = \frac{2\pi}{\eta} = \frac{2\pi}{\sqrt{-\omega^2(1-\zeta^2)}} \cong \frac{2\pi}{\omega} \quad \text{sec} \tag{9-91}$$

$$(T_{1/2})_{1,2} = \ln\frac{2}{\xi} = \frac{0.693}{\zeta\omega} \tag{9-92}$$

The transfer function for rolling motion in a single degree of freedom is readily derived as follows:

$$I_x\dot{p} = \mathscr{L}_p p + \mathscr{L}_\delta \delta$$

$$= C_{l_p} p \frac{qSd^2}{2V} + C_{l_\delta}\,\delta qSd \tag{9-93}$$

$$\dot{p} = l_p p + l_\delta \delta \tag{9-94}$$

where $l_p = \dfrac{\mathscr{L}_p}{I_x}$ and $l_\delta = \dfrac{\mathscr{L}_\delta}{I_x}$

Let $$s = \frac{d}{dt}$$

then $$sp - l_p p = l_\delta \delta \tag{9-95}$$

or $$\frac{p}{\delta} = \frac{l_\delta}{s - l_p} \tag{9-96}$$

2. Application. The transfer functions derived above may be used to determine the dynamic-response characteristics of the airframe (i.e., open loop) together with those associated with the autopilot and control system. Several methods which are available and used by the servomechanical engineers include the Nyquist technique and the root-locus method. These methods are extensively discussed in many published works (i.e., refs. 10 to 14). For the purpose of this

volume, a simple example is worked up to illustrate the usefulness of the transfer function in a frequency-response study.

The illustrative problem involves the determination of the proper time lag of the control system in order to prevent the missile from attaining an excessively high dynamic overshoot whenever the frequency of the sinusoidal input approaches the undamped natural frequency (denoted as ω_n in lieu of ω used previously) of the missile. In this example, a typical canard configuration is used in order to simplify the calculation. Since the values of $C_{N\delta}$, $C_{m\dot{\alpha}}$, and $C_{m\dot{\delta}}$ for this type of design are relatively low, they are assumed to be zero. The resultant transfer function of α/δ is simply

$$\frac{\alpha}{\delta} = \frac{m_\delta}{s^2 - (m_{\dot{\theta}} - f_\alpha)s - (m_\alpha - m_{\dot{\theta}} f_\alpha)} \tag{9-97}$$

For the condition investigated,

$$\frac{\alpha}{\delta} = \frac{300}{s^2 + 8.00s + 1{,}600} \tag{9-98}$$

Substituting $j\omega = s$ where $j = \sqrt{-1}$, an imaginary number, this transfer function can be rewritten as

$$\frac{\alpha}{\delta} = \frac{300}{(-\omega^2 + 1{,}600 + 8.00j\omega)} \tag{9-99}$$

or

$$\frac{\alpha}{\delta} = \frac{300}{(-\omega^2 + 1{,}600 + 8.00j\omega)} \frac{(-\omega^2 + 1{,}600) - 8.00j\omega}{(-\omega^2 + 1{,}600) - 8.00j\omega}$$

$$= \frac{\overset{\text{(real part)}}{(-300\omega^2 + 480{,}000)} - \overset{\text{(imaginary part)}}{2{,}400j\omega}}{(-\omega^2 + 1{,}600)^2 + (8.00\omega)^2} \tag{9-99a}$$

Since the amplitude is equal to the square root of the sum of the squares of the real and imaginary parts, i.e., $A = \sqrt{r^2 + i^2}$, we get

$$A = \frac{\sqrt{(-300\omega^2 + 480{,}000)^2 + (2{,}400\omega)^2}}{(-\omega^2 + 1{,}600)^2 + (8.00\omega)^2} \tag{9-100}$$

Substituting various values of the input frequency ω_i we get the following amplitude or dynamic overshoot ratio A/A_0, where A_0 is the amplitude at $\omega_i = 0$ radians/sec.

ω_i	ω_i/ω_n	A	A/A_0 = overshoot ratio
0	0	$0.183 = A_0$	1.00
10	0.250	0.200	1.09
20	0.500	0.248	1.32
30	0.750	0.405	2.15
37	0.925	0.802	4.27
38	0.950	0.878	4.67
39	0.975	0.932	4.96
40	1.000	0.938	4.99
41	1.005	0.888	4.72
42	1.050	0.802	4.27
45	1.125	0.539	2.87
50	1.25	0.305	1.6

In the above example, the value of α/δ (i.e., trim angle of attack per degree of control deflection) for the static condition is 0.183 and is obtained from $\omega_i = 0$ condition. This value is often referred to as the static gain of the system. The above results, plotted in Fig. 9-6, indicate that, as the frequency of the input approaches the undamped natural frequency of the missile, the dynamic gain or overshoot ratio A/A_0 increases considerably since the damping constant ζ for the sample configuration is low [i.e., $\zeta = 0.09$ from Eqs. (9-88) and (9-98)]. Since the above results do not include the time lag in the servo-control system, the above values of the amplitude ratio are valid for the air-frame loop only.

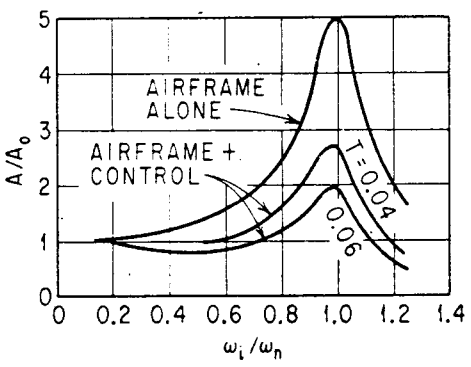

FIG. 9-6. Frequency-response characteristics of airframe and control system.

The effect of the servo loop on the combined airframe-control-system (see Fig. 9-6) response characteristics must be taken into account. This may be done conveniently by assuming that the servo has the response characteristics of a first-order linear system whose transfer function of δ_0/δ_i may be expressed as follows:

$$\frac{\delta_0}{\delta_i} = \frac{1}{1 + Ts} \tag{9-101}$$

where T is a time constant (i.e., time required for δ_0 to reach 63 per cent of its final value). Substituting $s = j\omega$, Eq. (9-101) becomes

$$\frac{\delta_0}{\delta_i} = \frac{1}{1+Ts} = \frac{1}{1+Ts} \times \frac{1-Ts}{1-Ts}$$
$$= \frac{1}{1+jTs} \times \frac{1-jT\omega}{1-jT\omega} = \frac{1-jT\omega}{1+T^2\omega^2} \tag{9-102}$$

The value of the amplitude ratio for the control system A_c may be calculated by the same method used previously.

$$A_c = \sqrt{r^2+i^2} = \frac{\sqrt{1+(T\omega)^2}}{1+T^2\omega^2} = \frac{\sqrt{1+T^2\omega^2}}{1+T^2\omega^2} = \frac{1}{\sqrt{1+T^2\omega^2}} \tag{9-103}$$

ω_i	ω_i/ω_n	A_c for ($T = 0.04$)	A_c for ($T = 0.06$)	$(A/A_0)(A_c)$ for ($T = 0.04$)	$(A/A_0)(A_c)$ for ($T = 0.06$)
0	0	1	1	1.000	1.000
10	0.250	0.929	0.857	1.014	0.936
20	0.500	0.780	0.640	1.029	0.845
30	0.750	0.640	0.486	1.375	1.045
37	0.925	0.565	0.413	2.410	1.762
38	0.950	0.555	0.404	2.590	1.885
39	0.975	0.545	0.397	2.705	1.970
40	1.000	0.530	0.384	2.640	1.915
41	1.005	0.526	0.378	2.480	1.783
42	1.050	0.517	0.369	2.208	1.575
45	1.125	0.488	0.348	1.400	0.999
50	1.250	0.448	0.316	0.725	0.512

The transfer function of α/δ for the combined servo-airframe open loop may expressed as

$$\frac{\alpha}{\delta_i} = \frac{\delta_0}{\delta_i} \times \frac{\alpha}{\delta_0} = \frac{1}{1+Ts} \frac{m_\delta}{s^2 - (m_{\dot\theta} - f_\alpha)s - (m_\alpha - m_{\dot\theta} f_\alpha)} \tag{9-104}$$

Hence it is apparent that the servo lag T attenuates the dynamic overshoot by the factor A_c. These effects are shown in Fig. 9-6. From Fig. 9-6, the time lag of the servo may be selected to prevent the missile from exceeding the designed dynamic overshoot under the most

severe input condition. Assume that the structural design overshoot ratio is 2.0; it is apparent from Fig. 9-6 that the desired time lag of the control system must be approximately 0.06 sec.

SYMBOLS

A	amplitude
A_c	amplitude ratio for the control system
A_0	amplitude at $\omega_i = 0$
A/A_0	overshoot ratio
A, B, C, D, E, K	general constants in Eqs. (9-1),(9-2), and (9-47)
B, C	constants in Eqs. (9-24) and (9-25)
B', C', D', E'	general constants in Eq. (9-48)
C_l	rolling-moment coefficient
C_m	pitching-moment coefficient
C_N	normal-force coefficient
F	force
$F(s)$	function of the transform variable s
I	moment of inertia
$K_{B(C)}, K_{B(T)}$	see Symbols in Chap. 5
$K_{C(B)}, K_{T(B)}$	see Symbols in Chap. 5
$\mathscr{L}$	rolling moment
$\mathscr{L}f(t)$	Laplace transform of a function of time $F(s)$
M	moment
N	normal force
P	period of oscillation
P, Q, R	angular velocities about the X, Y, Z axes (see Fig. 9-2)
S	reference area
T	time constant of first-order control system [see Eq. (9-101)]
$T_{1/2}$	time to damp to half amplitude
U, V, W	velocities along the X, Y, Z axes (see Fig. 9-2)
W	weight of missile
$a, b, c, \ldots$	constants defined in Eq. (9-77), also in Fig. 9-3
a_1, a_2	constants defined in Eq. (9-4)
d	body diameter
f	N/mV [see Eq. (9-58)]
h	moments of momentum
i	imaginary number in the complex form
j	an imaginary number, $\sqrt{-1}$

$j\omega$	imaginary part of a complex variable
l_p	$\mathscr{L}_p/I_x$ [see Eq. (9-94)]
m	mass, also M/I_y [see Eq. (9-57)]
n	load factor
p	rolling velocity, also operator to denote differentiation with respect to time
$p_{1,2}$	roots of the characteristic equation [see Eq. (9-3)]
q	dynamic pressure
s	Laplace operator
t	time
Δt	time it takes the air to go from the canard to the tail [see Eq. (9-40)]
x	moment arm
x_{C-T}	distance between canard and tail surfaces (see Fig. 9-4)
α	angle of attack
β	angle of sideslip
γ	flight-path angle
Δ	denominator as defined in Eq. (9-64)
δ	control-surface deflection
ϵ	downwash angle
ζ	damping constant defined as the ratio of the actual damping of the airframe to critical damping [see Eq. (9-88)]
η	term used in Eqs. (9-29), (9-30), and (9-91)
θ	missile attitude ($\alpha + \gamma$)
$\lambda_{1,2}$	roots of the characteristic equation [see Eq. (9-27)]
ξ	term used in Eqs. (9-29), (9-31), and (9-92)
σ	real part of a complex variable (see Sec. 9-5)
φ	roll (or bank) angle
ψ	yaw angle
ω, ω_n	undamped natural frequency of missile
ω_i	input frequency

Subscripts

B	body
C	canard
T	tail
x, y, z	about the X, Y, Z axes
π	body frontal area (i.e., S_π)
0	initial condition
1, 2	conditions other than zero

REFERENCES

1. Dynamics of the Airframe, BuAer *Rept.* AE-61-4II, Bureau of Aeronautics, Navy Department, September, 1952.

2. Perkins, C. D., and R. E. Hage: "Airplane Performance Stability and Control," John Wiley & Sons, Inc., New York, 1950.

3. Jones, B. M.: Dynamics of the Airplane, Durand's "Aerodynamic Theory," vol. V, Div. N, Springer-Verlag, Berlin, 1935.

4. Synge, J. L., and B. A. Griffith,: "Principles of Mechanics," 3d ed., McGraw-Hill Book Company, Inc., New York, 1959.

5. Goldstein, H.: "Classical Mechanics," Addison-Wesley Publishing Company, Reading, Mass., 1950.

6. Webster, A. G.: "The Dynamics of Particles and of Rigid, Elastic, and Fluid Bodies," Hafner Publishing Company, New York, 1950.

7. Gillis, C. L., and R. Chapman, Jr.: Summary of Pitch-damping Derivatives of Complete Airplane and Missile Configurations as Measured in Flight at Transonic and Supersonic Speeds, *NACA Research Mem.* L52K20, Jan. 22, 1953.

8. Routh, E. J.: "Dynamics of a System of Rigid Bodies," 3d ed., Macmillan & Co., Ltd., London, 1877.

9. Lin, S.: A Method of Successive Approximations for Evaluating the Real and Complex Roots of Cubic and Higher-order Equations, *J. Math. and Phys.*, vol. 20, no. 3, August, 1941.

10. Nixon, F. E.: "Principles of Automatic Controls," Prentice-Hall, Inc., Englewood Cliffs, N.J., 1953.

11. Brown, G. S., and D. P. Campbell: "Principles of Servomechanisms," John Wiley & Sons, Inc., New York, 1948.

12. Methods of Analysis and Synthesis of Piloted Aircraft Flight Control Systems, BuAer *Rept.* AE-61-4I, Bureau of Aeronautics, Navy Department, March, 1952.

13. Savant, C. J., Jr.: "Basic Feedback Control System Design," McGraw-Hill Book Company, Inc., New York, 1958.

14. Thaler, G. J., and R. G. Brown: "Servomechanism Analysis," McGraw-Hill Book Company, Inc., New York, 1953.

CHAPTER 10

AIR LOADS

10-1. INTRODUCTION

In most preliminary analyses, one is required to estimate the air loads on the missile and its components in order for the structural and stress engineers to "rough out" the detailed design of the various external components such as skin gauge on the nose and body or wing thickness. Since detailed design criteria are generally not specified at this stage of design, one must examine several conditions of flight which include both trim and dynamic flight conditions. These missile flight conditions may be examined by the methods discussed previously, particularly in Chap. 5 and 9. In addition to the air loads, the aerodynamic hinge moments are of interest for the determination of the type and capacity of the servo system for actuating the aerodynamic movable surfaces. Finally, thermal loading or aerodynamic heating must be estimated in order to determine the optimum type of material and construction for the airframe. This chapter is devoted to a discussion of some of the approaches and methods of analysis associated with the general aerodynamic air loads, load distribution, and heating problems.

10-2. DESIGN CRITERIA

A missile is often designed to operate over a wide range of speed, altitude, and dynamic pressure q conditions. Hence care must be exercised in selecting the correct or critical design loading condition or conditions for stress analyses. Since the aerodynamic loading on the missile is expressed as

$$N = C_{N_\alpha} \alpha q S = C_{N_\alpha} \alpha \tfrac{1}{2} \gamma p M^2 S \tag{10-1}$$

it is necessary to examine not only the individual terms C_{N_α}, α, M, etc.,

in Eq. (10-1) but also the product of these terms. Each of these terms is discussed below.

1. C_{N_α}. As discussed in Chap. 3, the normal-force-curve slope is a function of Mach number. In the supersonic case C_{N_α} varies approximately inversely as $\sqrt{M^2 - 1}$. Hence it is evident that the maximum value of C_{N_α} encountered in flight does not necessarily result in maximum aerodynamic loading.

2. α. In general, the maximum value of angle of attack including dynamic overshoot, gusts, etc., will result in the critical loading condition provided the product of $C_{N_\alpha} q$ is a maximum.

3. p. The effect of decreasing static pressure or increasing altitude is to decrease the aerodynamic loading on a missile. However, for medium- or long-range ballistic missiles, the effect of increasing altitude is generally overcompensated by the Mach-number increase such that the q is a maximum at the higher altitude (see Fig. 10-1) and hence results in maximum loading at altitude. For other types of missiles, the lowest operating altitude generally results in the maximum loading.

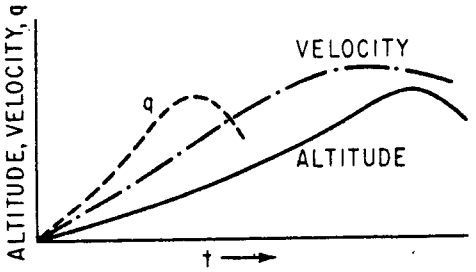

FIG. 10-1. Altitude, velocity, and dynamic pressure vs. time.

4. M. The effect of the Mach number is twofold: it decreases the value of C_{N_α} as previously mentioned and increases the dynamic pressure. Since the latter effect is more pronounced in that q varies as the Mach number squared, the general net effect of the Mach number is to increase the aerodynamic loading on the missile. An exception to this case may be one in which the control system is inadequate in overcoming the aerodynamic hinge moment of the control surfaces. In such a case, the restricted control deflection results in a lower trim or dynamic overshoot α and hence may result in a lower loading condition at the higher operating Mach numbers. The type of servo used in this case is commonly called the "proportional-torque" servo which "proportions" the loading of the missile as a function of the aerodynamic hinge moments on the control surfaces.

5. Dynamic pressure q. In the majority of the cases, maximum q results in the maximum air loads. In a very few cases, maximum loading may occur at somewhat lower values of q. One such may be the case in which the maximum speed of the missile is slightly supersonic, where C_{N_α} may be significantly reduced. In such a case the high

subsonic speed with its attendant rise in C_{N_α} may result in maximum loading even though maximum q is not yet attained.

From the above discussion, it is apparent that careful analysis must be made of the various factors involved before the maximum aerodynamic loading condition can be determined. Now that the effects of Mach number, altitude, q, etc., have been discussed the various missile flight attitudes (i.e., trim and out-of-trim conditions) must be examined next. These flight attitudes are described below for two common types of design: (1) forward canard or wing control and (2) rear or tail control.

1. Forward Control. The flight attitudes for this type of design are shown in Fig. 10-2 and are discussed below.

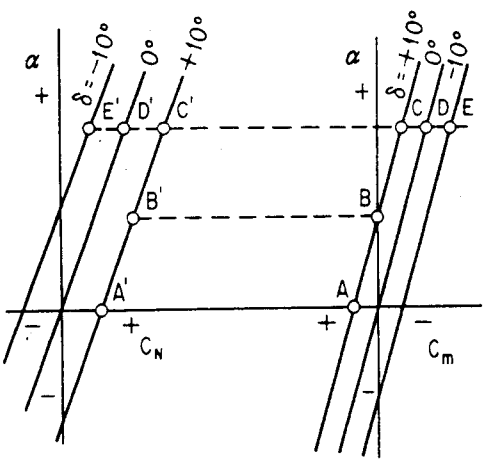

FIG. 10-2. Flight conditions for airloads analysis—forward control.

A. This is the condition which exists immediately after the forward movable control surfaces are deflected hard over onto their stops. Actually this condition rarely exists since it takes a finite time to reach maximum deflection, at which time some nominal angle of attack would have been developed. However, assuming $\alpha = 0$, maximum positive pitching acceleration occurs at point *A*.

B. This is the trimmed condition of the missile, since $C_m = 0$. Generally, this condition does not result in maximum design loads.

C. This is the maximum dynamic overshoot condition which results in maximum aerodynamic loads on the body and control (movable wings or canards) surfaces. The amount of overshoot depends primarily on the amount of aerodynamic damping and control-surface response characteristics as discussed in Chap. 9. For low aerodynamic damping and very fast control-surface (rates) responses, this overshoot can be many times that of the trimmed value *B*. In a given design, the response and overshoot loading must often be compromised.

D. This is a transient condition in which the forward movable control surfaces are returned to neutral at the peak of the dynamic overshoot condition. This condition may often result in maximum tail loads since the angle of the tail is at a maximum because of the absence of downwash.

E. Again this is a transient condition similar to *A*, *C*, and *D*. This condition obviously results in maximum negative pitching acceleration.

2. Rear Control. The flight attitudes for a rear-control design are shown in Fig. 10-3 and are similar to those shown in Fig. 10-2 for the forward-control design. However, because of the negative value of C_{m_δ} as pointed out in Sec. 5-8 the corresponding points A^1, B^1, C^1, etc., on the C_N vs. α curves are located differently from those of Fig. 10-2.

A. Same as for the forward-control design.

B. Same as for the forward-control design.

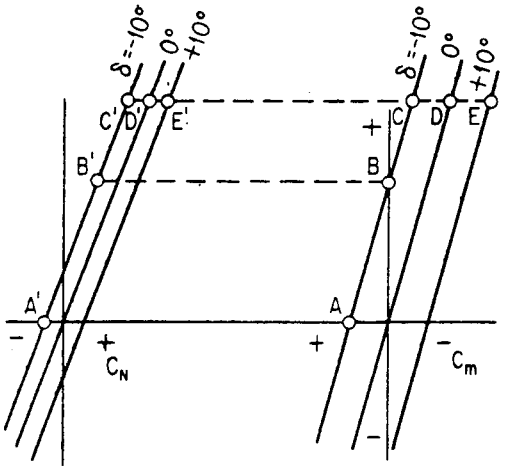

FIG. 10-3. Flight conditions for air-loads analysis—rear control.

C. This is the maximum dynamic overshoot condition which results in maximum loads on the body and forward fixed (wing) aerodynamic surfaces.

D. This is a transient condition in which the movable tail-control surfaces are returned to neutral at the peak of the overshoot condition. Large tail load is generally associated with this condition.

E. This transient condition is similar to that for the forward-control case. Maximum tail load (i.e., $\alpha_T = \alpha_W - \epsilon + \delta_T$) as well as maximum negative pitching acceleration are encountered in this condition.

The above conditions are generally more severe than the actual conditions the missile experiences since it requires a finite time for the control surfaces to deflect from one position to the next, during which time the angle of attack is changing in a direction so as to alleviate the loading problem. Hence, if a more refined definition of the dynamic conditions is desired, a simplified transient response study should be conducted.

Although maximum air loads on the various components seldom occur during any one flight attitude or condition, these components must be designed to withstand their respective maximum loads. It is very important, then, to investigate all these five (and possibly other) flight conditions and evaluate the loads and angular accelerations. The previously described conditions (i.e., *A*, *B*, *C*, etc.) should also be made for the range of center-of-gravity locations of the missile. The

effect of gust should be factored in the loads analysis. This may be done by increasing the angle of attack by an incremental value defined below:

$$\Delta\alpha_g \cong \frac{V_g}{V} \tag{10-2}$$

where $\Delta\alpha_g$ = angle of attack due to gust
V_g = gust velocity

The methods of evaluating the aerodynamic loads, loading distributions, and hinge moments are discussed next. Inertia loading will be discussed in Chap 14..

10-3. COMPONENT AIR LOADS

1. Body. As discussed in Chap. 3, the majority of the body load for the body-alone configuration is concentrated at the forebody or nose section. Therefore, the total load on the forebody may be approximated as

$$N_N = (C_{N_\alpha})_B \alpha_B q S_n \tag{10-3}$$

Owing to wing and/or tail-body interference effects, additional loads are incurred on the body because of the presence of these aerodynamic surfaces. For a forward-control design (i.e., a canard control) the "carry-over" load from the canards on the body [from Eqs. (5-8) and (5-9)] is

$$N_{B(C)} = (C_{N_\alpha})_C [K_{B(C)}\alpha_C + k_{B(C)}\delta_C] q S_C \tag{10-4}$$

The load on the body caused by the tail surfaces is

$$N_{B(T)} = (C_{N_\alpha})_T K_{B(T)}(\alpha - \epsilon) q S_T \tag{10-5}$$

For a rear-control (i.e., tail-control) design, the interference loads due to the forward fixed wing and movable tail surfaces may be written [see Eqs. (5-30) and (5-31)] as

$$N_{B(W)} = (C_{N_\alpha})_W K_{B(W)} \alpha_W q S_W \tag{10-6}$$

$$N_{B(T)} = (C_{N_\alpha})_T [K_{B(T)}(\alpha - \epsilon) + k_{B(T)}\delta_T] q S_T \tag{10-7}$$

2. Aerodynamic Surfaces. The normal force on the aerodynamic surfaces may also be calculated with the aid of Eqs. (5-8), (5-9), (5-30), (and 5-31) for the forward- and rear-control design. For the

former type of design, the forward (i.e., canard) control-surface load is

$$N_{C(B)} = (C_{N_\alpha})_C[K_{C(B)}\alpha_C + k_{C(B)}\delta_C]qS_C \tag{10-8}$$

For the aft (tail) surfaces, the load is

$$N_{T(B)} = (C_{N_\alpha})_T K_{T(B)}(\alpha - \epsilon)qS_T \tag{10-9}$$

For an aft (tail) control design, the load on the forward fixed wing surfaces is

$$N_{W(B)} = (C_{N_\alpha})_W K_{W(B)}\alpha_W qS_W \tag{10-10}$$

The load on the movable tail surfaces is

$$N_{T(B)} = (C_{N_\alpha})_T[K_{T(B)}(\alpha - \epsilon) + k_{T(B)}\delta_T]qS_T \tag{10-11}$$

The load on small movable control surfaces such as flaps and ailerons is generally obtained from test data. However, for preliminary design analysis, the load on these surfaces may be estimated by first analyzing the nature and magnitude of its pressure distribution, which is discussed in the following section.

10-4. COMPONENT LOAD DISTRIBUTION

1. Body. The theoretical pressure distribution and hence loading characteristics of a body of revolution at zero angle of attack may be predicted by many different methods.[1–5,13*] Comparison of the results obtained by the different theoretical methods indicates excellent agreement with those obtained experimentally.[6–8] Figure 10-4 shows the typically close agreement between the theoretical and experimental results for a common body of revolution of $l/d = 10$ with a three-caliber tangent ogive forebody.

For inclined bodies of revolution, many theoretical methods[9–13] are also available for the determination of the pressure distribution over their entire length. However, since these methods are based primarily on potential-flow theories, viscous and cross-flow compressibility effects were neglected. Hence these theoretical results could not be expected to agree exactly with those obtained from experiments which include these viscous effects. Figure 10-5 shows a typical comparison of the theoretical and experimental results. It can be seen that, as the angle of attack increases, flow separation due to viscous effects is a major cause of the discrepancy between the theoretical and experimental results.

* Superscript numbers indicate references listed at the end of the chapter.

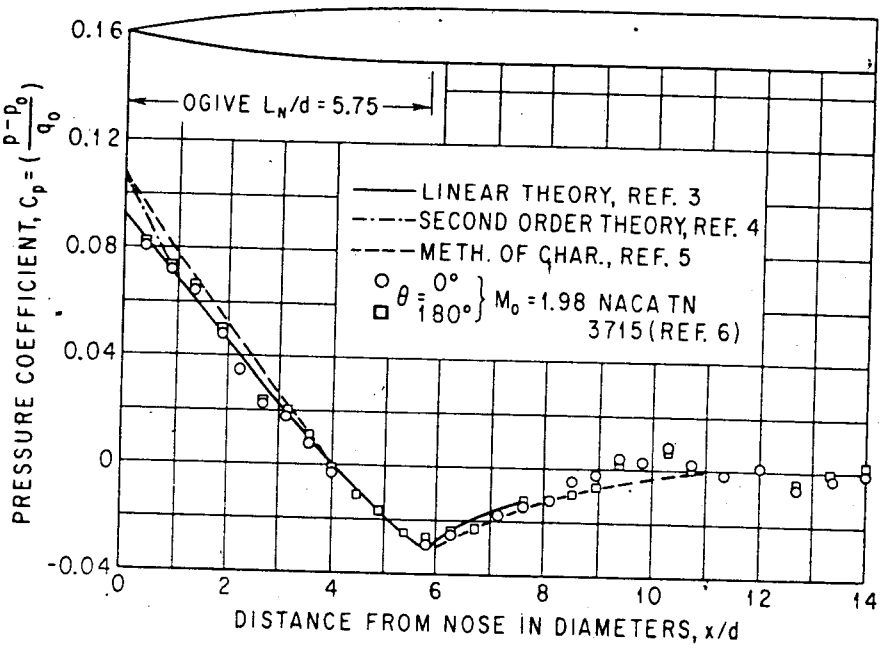

FIG. 10-4. Comparison of theoretical and experimental C_p at $\alpha = 0°$.

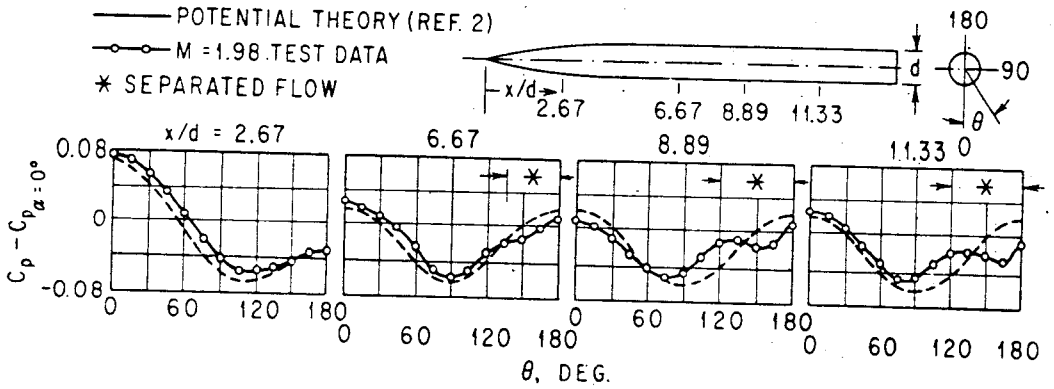

FIG. 10-5. Comparison of theoretical and experimental circumferential distribution of lifting pressure at $\alpha = 8°$. (*NACA Tech. Note* 3715.)

Once the peripheral pressure distribution is determined for the various stations along the body (such as those shown in Fig. 10-5), the local normal-force coefficient per inch may be determined as follows:

$$C_n = \frac{2r}{S_\pi} \int_0^\pi C_p \cos\theta \, d\theta \qquad (10\text{-}12)$$

where r = radius of the body
S_π = reference area
$C_p = (p - p_0)/q_0$

The value of C_n is next plotted vs. body station as shown in Fig. 10-6. Integration of the area under this curve yields the total normal-force

coefficient C_N on the complete-body configuration. The center of pressure is determined by taking the summation of the moments of area and dividing by the summation of the area of Fig. 10-6.

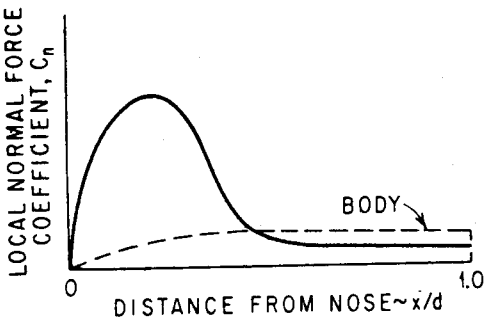

FIG. 10-6. Variation of local normal-force coefficient with body station.

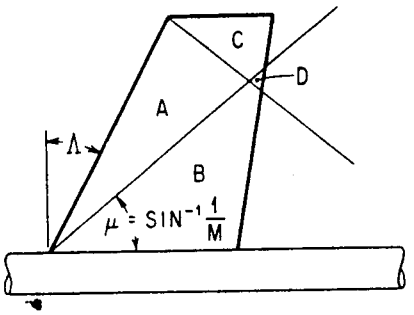

FIG. 10-7. Definition of regions for air-loads analysis.

2. Aerodynamic Surfaces. For preliminary analysis, the load on the aerodynamic surfaces may be assumed to be concentrated at the quarter chord at subsonic speeds and close to the mid-chord at supersonic speeds, as pointed out in Chap. 3. For detailed analysis, however, actual loading distribution is needed. This need may be fulfilled by either (1) using pressure-distribution data on a similar or identical configuration or (2) estimating the loading distribution by theoretical means. The latter approach for the determination of load distribution at supersonic speeds is presented below.

Figure 10-7 shows a typical wing planform with its Mach lines to represent a given flight Mach-number condition. In the application of the linear theory the following four important assumptions are made: (1) attached shock (i.e., sharp leading edge), (2) relatively low angles of attack ($\alpha < 10°$), (3) relatively thin airfoil, and (4) supersonic leading edge (i.e., $\mu > \Lambda$). The relationships for the local pressure coefficient C_p defined as $(p_{\text{upper}} - p_{\text{lower}})/q$, for the different areas A, B, etc., are

$$C_{p_{(A)}} = \frac{4\alpha}{\sqrt{\beta^2 - k^2}} \tag{10-13}$$

$$C_{p_{(B)}} = \frac{8\alpha}{\pi\sqrt{\beta^2 - k^2}} \left[\frac{\pi}{2} - \sin^{-1}\sqrt{\frac{n^2 - t_1^2}{1 - t_1^2}}\right] \tag{10-14}$$

$$C_{p_{(C)}} = \frac{4\alpha(a+1)}{\pi\beta\sqrt{a}} \tan^{-1}\sqrt{\frac{-2a\beta y_2}{(1+a)(x_2 + \beta y_2)}} \tag{10-15}$$

and

$$C_{p_{(D)}} = C_{p_{(B)}} + C_{p_{(C)}} - C_{p_{(A)}} \tag{10-16}$$

where α is the local angle of attack and must be corrected for body upwash effects. The local angle of attack at any spanwise wing location r may be related to the body radius R and the free-stream angle of attack α_0 as[14]

$$\alpha = \alpha_0\left[1 + \left(\frac{R}{r}\right)^2\right] \tag{10-17}$$

$$\beta = \sqrt{M^2 - 1} \tag{10-18a}$$

$$k = \tan \Lambda \tag{10-18b}$$

$$n = \frac{k}{\beta} \tag{10-18c}$$

$$t_1 = \frac{ky_1}{x_1} \tag{10-18d}$$

(See Fig. 10-8.)

$$a = \frac{\beta + k}{\beta - k} \tag{10-18e}$$

Using the above relationships, the chordwise pressure distribution may be readily calculated for several spanwise wing stations such as

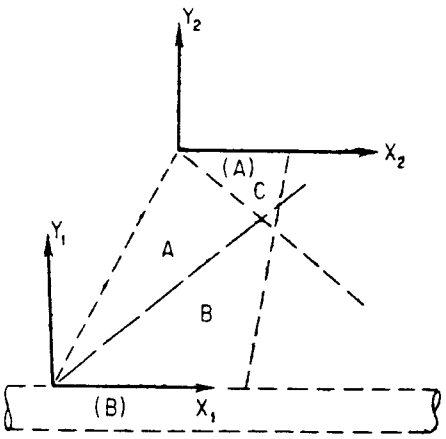

FIG. 10-8. Definition of coordinate systems for air-loads analysis.

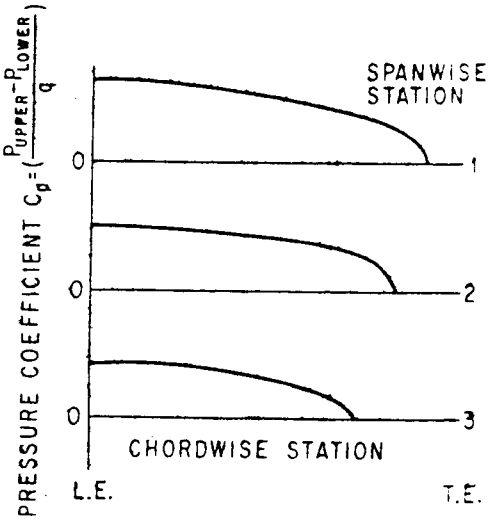

FIG. 10-9. Typical chordwise pressure distribution.

those shown in Fig. 10-9. The spanwise loading distribution and total load may be calculated as follows:

1. Integrate the area under the curves in Fig. 10-9:

$$N'(\text{lb/in.}) = FC_p cq \tag{10-19}$$

where F is a scale factor (i.e., if 1 in. = one unit of C_p and 1 in. = 2 in. span, then $F = 1 \times 2 = 2$).

2. Plot N' vs. spanwise stations (see Fig. 10-10) to get the spanwise distribution.

3. Integrate the area under Fig. 10-10 to obtain the total normal force N.

A comprehensive treatment of the spanwise load distributions for a variety of wing planforms at supersonic speeds may be found in refs. 15 to 17. For subsonic speeds, refs. 18 and 19 should be consulted.

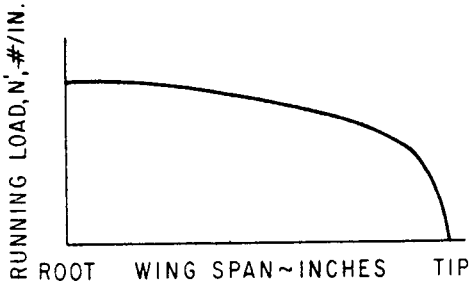

FIG. 10-10. Typical spanwise loads distribution.

Quite frequently, after the component loads and their locations have been determined, the summation of forces may not agree with the total load (or load factor), or the summation of moments about the center of gravity is not zero (for trimmed-flight condition), or the predetermined angular acceleration (out-of-trim condition) does not result. Hence it will be necessary to adjust either the individual component loads and/or locations to satisfy these predetermined values. Which component load or load location to be modified or adjusted to satisfy these predetermined values depends upon the magnitude or accuracy of these loadings. Hence, if the load of a particular component (say the wing, for instance) is much larger than that on other components, only slight modification of its magnitude and/or its location is required. Or, if the accuracy of the load or its location on a particular component is questionable, then modification should be made on that particular load or location.

10-5. AERODYNAMIC HINGE MOMENTS

Since the size and capacity of the servomechanism is dependent directly upon the magnitude of the hinge moments associated with the aerodynamic surfaces to which it is linked, it is important to be able to predict the approximate magnitude of the hinge moments for the critical flight conditions. Several flight conditions of Mach number, control-surface deflection, angle of attack, and dynamic pressure must be investigated since these parameters affect both the magnitude of the normal force and its center-of-pressure location. When only

supersonic speeds are concerned, maximum hinge moments generally occur at the highest supersonic Mach number, q, α, and δ condition.

Several methods may be used to estimate the magnitude of the hinge moment for preliminary analysis. These are (1) estimation of the load and center-of-pressure location, (2) integration of pressure-distribution data, and (3) use of hinge-moment data of similar configuration. The first method mentioned may be expressed mathematically (for a movable wing) as

$$(\mathrm{HM})_\alpha = (C_{N_\alpha})_W K_{W(B)}(x_{\mathrm{HL}} - \bar{x}_\alpha) q S_W \tag{10-20}$$

and

$$(\mathrm{HM})_\delta = (C_{N_\alpha})_W k_{W(B)}(x_{\mathrm{HL}} - \bar{x}_\delta) q S_W \tag{10-21}$$

where $(\mathrm{HM})_\alpha$ = hinge moment due to α, etc.
x_{HL} = hinge-line location
$\bar{x}_\alpha$ = center of pressure due to α
$\bar{x}_\delta$ = center of pressure due to δ

The values of $\bar{x}_\alpha$ and $\bar{x}_\delta$ for the wing-alone configuration (see Chap. 3) may be used since the body effect on the wing center of pressure appears to be negligible.

Another method of determining hinge moment is by integrating the theoretical pressure distribution as previously described to determine the load and chordwise center-of-pressure location. Since this method is rather tedious, it is generally not recommended for the sole purpose of hinge-moment determination. However, in the process of getting the loading distribution, the hinge moment may be also determined by this method. Perhaps the most direct method is to use experimental hinge-moment data of similar configurations. Theoretical values of hinge moments for trailing-edge-type controls for supersonic flights may be obtained from ref. 21. However, since theoretical values are subject to errors because of flow separation, viscous effects, etc., experimental wind-tunnel hinge-moment data when obtained under conditions reasonably close to those actually experienced in flight should be obtained for design purposes. Most of the experimental data on hinge-moment characteristics of various practical designs are classified for security reasons.

10-6. AERODYNAMIC HEATING

Thermal loading or aerodynamic heating may constitute a major problem in the design of a high-speed missile. Hence, during the preliminary-design phase of the missile project, it is important to estimate the heat-transfer rate and temperature on the critical portions

(i.e., nose, leading edge of aerodynamic surfaces, etc.) of the missile. Aerodynamic heating results from the airflow about the surface of the missile: friction of the air along the surface of the missile and compression at and near the stagnation regions of the missile external components. In these processes, a portion of the kinetic energy of the air is converted into thermal energy within the boundary layer of the missile.

The temperature rise for bringing the air to rest ΔT is expressed as

$$\Delta T = \frac{\gamma - 1}{2} M_\infty{}^2 T_\infty \tag{10-22}$$

where γ = ratio of specific heats at constant pressure C_p to specific heat at constant volume C_v.
M_∞ = free-stream Mach number
T_∞ = free-stream temperature, ° Rankine

The final or stagnation temperature T_0 is

$$T_0 = T_\infty \left(1 + \frac{\gamma - 1}{2} M_\infty{}^2\right) \tag{10-23}$$

Equation (10-23) is applicable for a compressible non-heat-conducting gas. Since there is a small amount of heat transfer within the boundary layer, the "recovery" temperature T_r differs from the stagnation temperature by the temperature-recovery factor r and is expressed as

$$T_r = T_\infty \left(1 + r \frac{\gamma - 1}{2} M_\infty{}^2\right) \tag{10-24}$$

The temperature-recovery factor r can thus be expressed as

$$r = \frac{T_r - T_\infty}{T_0 - T_\infty} \tag{10-25}$$

The value of r varies from approximately 0.85 for laminar flow to approximately 0.88 for turbulent flow. Hence it can be seen that the recovery temperature is relatively independent of the type of flow except at very high Mach numbers. For an insulated wall (i.e., no heat transfer through the skin of the missile) the recovery temperature T_r is identical to the adiabatic wall temperature T_{aw}:

$$T_{aw} = T_r = T_\infty \left(1 + r \frac{\gamma - 1}{2} M_\infty{}^2\right) \tag{10-26}$$

In most practical applications, heat transfer through the skin or wall of the missile occurs. The heat-transfer rate through the wall q_w is governed by the following classical relationship:

$$q_w = h(T_r - T_w) \tag{10-27}$$

where h = heat-transfer coefficient
T_w = wall temperature

It is more convenient to use a nondimensional coefficient called the Stanton number C_h, which is defined as

$$C_h = \frac{h}{\rho \mu C_p} \tag{10-28}$$

where ρ = fluid density
μ = coefficient of fluid viscosity

The Stanton number is related to the skin-friction coefficient C_f as

$$C_h = \frac{1}{s}\frac{C_f}{2} \tag{10-29}$$

where s is the Reynolds analogy factor and has a value of approximately 0.8.

Hence the heat-transfer rate may be expressed as

$$\begin{aligned} q_w &= \frac{1}{s}\frac{C_f}{2}\rho \mu C_p(T_r - T_w) \\ &= \frac{1}{s}\frac{C_f}{2}\rho \mu C_p\left[T_\infty\left(1 + r\frac{\gamma - 1}{2}M^2\right) - T_w\right] \end{aligned} \tag{10-30}$$

It is seen from Eq. (10-30) that the heat-transfer rate varies directly as the friction coefficient C_f. Since C_f for turbulent flow can be many times C_f for laminar flow, it is essential that laminar flow be maintained over as great a portion of the missile as possible.

In the calculation of aerodynamic heating of the missile, the following fundamental heat-balance equation is used:

$$\text{Heat input} = \text{heat stored} + \text{heat radiated} \tag{10-31}$$

where $\text{Heat stored} = (\text{weight})(\text{specific heat})(\text{temp. rise})$

$$= (W)(C)(T_1 - T_2) \tag{10-31a}$$

and $$\text{Heat radiated} = \sigma A \epsilon T_w^4 \tag{10-31b}$$

The term σ in Eq. (10-31b) is the Stefan-Boltzmann constant and has a value of 0.48×10^{-12} Btu/(ft^2)(sec)(°R)^4. The term A is the surface

area being checked for heating effects. The term ϵ is the emissivity factor of the surface material, which depends upon the surface temperature, degree of surface roughness, etc. Since the temperature of a body exposed to transient heating conditions at any instant depends upon the previous thermal history of the body, a time-step solution of the heat-balance equation is required.

Many methods and procedures exist for the determination of aerodynamic heating of the missile. Some of these methods are limited to the determination of heat transfer to a specified location on the missile (i.e., stagnation point only), flight condition (i.e., hypersonic speeds only), etc. Hence an extensive study on the subject of heat transfer is required before the proper method or methods are selected for a particular design condition. References 22 through 44 constitute a partial list of the many reports written on this subject.

SYMBOLS

A	surface area being checked for heating effects
C	specific heat [see Eq. (10-31a)]
C_f	skin-friction coefficient
C_h	Stanton number
C_N	normal-force coefficient
C_n	local normal-force coefficient
C_p	specific heat at constant pressure, or pressure coefficient
C_v	specific heat at constant volume
F	scale factor as used in Eq. (10-19)
HM	hinge moment
$K_{B(C)}$, $K_{B(W)}$, $K_{B(T)}$	see Symbols in Chap. 5
$K_{C(B)}$, $K_{W(B)}$, $K_{T(B)}$	see Symbols in Chap. 5
L_N	nose length (see Fig. 10-4)
M	Mach number
N	normal force
N'	spanwise loading distribution
S	reference area
T	temperature
T_{aw}	adiabatic wall temperature
T_r	recovery temperature
T_w	wall temperature
T_0	stagnation pressure
T_∞	free-stream temperature

V	forward velocity
V_g	gust velocity
W	weight
a	a term in Eq. (10-15) and defined by Eq. (10-18*e*)
c	local chord
d	body diameter
h	heat-transfer coefficient
k	a term in Eqs. (10-13) and (10-14) and defined by Eq. (10-18*b*)
$k_{B(C)}$, $k_{B(T)}$	see Symbols in Chap. 5
$k_{C(B)}$, $k_{T(B)}$	see Symbols in Chap. 5
n	a term in Eq. (10-14) and defined by Eq. (10-18*c*)
p	static pressure
q	dynamic pressure
q_w	heat-transfer rate through the wall
r	radius of body, spanwise wing location, temperature-recovery factor
s	Reynolds analogy factor [see Eq. (10-29)]
t_1	a term in Eq. (10-14) and defined by Eq. (10-18*d*)
x, y	coordinates as shown in Fig. 10-8
$\bar{x}_\alpha$, $\bar{x}_\delta$	center of pressure due to α and δ, respectively
α	angle of attack
$\Delta\alpha_g$	incremental angle of attack due to gust velocity
β	$\sqrt{M^2 - 1}$ [see Eq. (10-18*a*)]
γ	specific heat ratio of air
δ	control-surface deflection
ϵ	downwash angle, emissivity factor
θ	circumferential angle (see Fig. 10-5)
Λ	leading-edge sweep angle
μ	Mach angle [see Eq. (3-35)], coefficient of fluid viscosity
ρ	air or fluid density
σ	Stefan-Boltzmann constant [see Eq. (10-31*b*)]

REFERENCES

1. Allen, H. J.: Pressure Distribution and Some Effects of Viscosity on Slender Inclined Bodies of Revolution, *NACA Tech. Note* 2044, 1950.

2. Allen, H. J.: Estimation of the Forces and Moments Acting on Inclined Bodies of Revolution of High Fineness Ratio, *NACA Research Mem.* A9I26, 1949.

3. Von Kármán, T., and N. B. Moore: Resistance of Slender Bodies Moving with Supersonic Velocities with Special Reference to Projectiles, *Trans. ASME* vol. 54, no. 23, pp. 303–310, Dec. 15, 1932.

4. Van Dyke, M. D.: A Study of Second-order Supersonic-flow Theory, *NACA Rept.* 1081, 1952 (formerly *NACA Tech. Note* 2200).

5. Ehret, D. M., V. J. Rossow, and V. I. Stevens, Jr.: An Analysis of the Applicability of the Hypersonic Similarity Law to the Study of Flow about Bodies of Revolution at Zero Angle of Attack, *NACA Tech. Note* 2250, 1950.

6. Perkins, E. W., and D. M. Kuehn: Comparison of the Experimental and Theoretical Distribution of Lift on a Slender Inclined Body of Revolution at $M = 2$, *NACA Tech. Note* 3715, May, 1956.

7. Perkins, E. W., and L. H. Jorgensen: Comparison of Experimental and Theoretical Normal-force Distributions (Including Reynolds Number Effects) on an Ogive-cylinder Body at Mach Number 1.98, *NACA Tech. Note* 3716, May, 1956.

8. Perkins, E. W., F. E. Gowen, and L. H. Jorgensen: Aerodynamic Characteristics of the NACA RM-10 Research Missile in the Ames 1- by 3-foot Supersonic Wind Tunnel No. 2—Pressure and Force Measurements at Mach Numbers of 1.52 and 1.98, *NACA Research Mem.* A51G13, 1951.

9. Allen, H. J., and E. W. Perkins: Characteristics of Flow over Inclined Bodies of Revolution, *NACA Research Mem.* A50L07, 1951.

10. Rossow, V. J.: Applicability of the Hypersonic Similarity Rule to Pressure Distribution Which Include the Effects of Rotation for Bodies of Revolution at Zero Angle of Attack, *NACA Tech. Note* 2399, 1951 (extension of *NACA Tech. Note* 2250).

11. Bolton-Shaw, B. W., and H. K. Zienkiewicz: The Rapid, Accurate Prediction of Pressure on Non-lifting Ogival Heads of Arbitrary Shape at Supersonic Speeds, English Electric Company, Navigational Project Division, no. L.A.t. 034 (British), June 23, 1952.

12. Van Dyke, M. D.: Practical Calculation of Second-order Supersonic Flow Past Nonlifting Bodies of Revolution, *NACA Tech. Note* 2744, 1952.

13. Savin, R. C.: Application of the Generalized Shock-expansion Method to Inclined Bodies of Revolution Traveling at High Supersonic Airspeeds, *NACA Tech. Note* 3349, April, 1955.

14. Beskin, L.: Determination of Upwash around a Body of Revolution at Supersonic Velocities, CM-251, Applied Physics Laboratory, Johns Hopkins University, May 27, 1946.

15. Martin, J. C., and I. Jeffreys: Span Load Distributions Resulting from Angle of Attack, Rolling, and Pitching for Tapered Sweptback Wings with Streamwise Tips, Supersonic Leading and Trailing Edges, *NACA Tech. Note* 2643, July, 1952.

16. Hannah, M. E., and K. Margolis: Span Load Distributions Resulting from Constant Angle of Attack, Steady Rolling Velocity, Steady Pitching Velocity, and Constant Vertical Acceleration for Tapered Sweptback Wings with Streamwise Tips, Subsonic Leading Edges and Supersonic Trailing Edges, *NACA Tech. Note* 2831, December, 1952.

17. Margolis, Kenneth, Windors L. Sherman, and M. E. Hannah: Theoretical Calculation of the Pressure Distribution, Span Loading, and Rolling Moment Due to Sideslip at Supersonic Speeds for Thin Swept-back Tapered

Wings with Supersonic Trailing Edges and Wing Tips Parallel to the Axis of Wing Symmetry, *NACA Tech. Note* 2898, February, 1953.

18. Schrenk, O.: A Simple Approximation Method for Obtaining the Spanwise Lift Distribution, *NACA Tech. Mem.* 948, August, 1940.

19. DeYoung, J., and C. W. Harper: Theoretical Symmetric Span Loading at Subsonic Speeds for Wings Having Arbitrary Plan Form, *NACA Rept.* 921, 1948.

20. Czarnecki, K. R., and D. R. Lord: Load Distributions Associated with Controls at Supersonic Speeds, *NACA Research Mem.* L53D15a, May 29, 1953.

21. Goin, K. L.: Equations and Charts for the Rapid Estimation of Hinge-moment and Effectiveness Parameters for Trailing-edge Controls Having Leading and Trailing-edges Swept Ahead of the Mach Lines, *NACA Rept.* 1041, 1951.

22. Van Driest, E. R.: The Problem of Aerodynamic Heating, IAS Preprint 645, June, 1956 (also in *Aero. Eng. Rev.*, vol. 15, no. 10, pp. 26–41, October, 1956).

23. Kemp, N. H., and F. R. Riddell: Heat Transfer to Satellite Vehicles Re-entering the Atmosphere, *Jet Propulsion*, vol. 27, pp. 132–137, February, 1957 (addendum in *Jet Propulsion*, vol. 27, no. 12, pp. 1256–1257, December, 1957).

24. Romig, M. H.: Stagnation Point Heat Transfer for Hypersonic Flow, *Jet Propulsion*, vol. 26, no. 12, pp. 1098–1101, December, 1956 (addendum in *Jet Propulsion*, vol. 27, no. 12, p. 1255, December, 1957).

25. Van Driest, E. R.: Turbulent Boundary Layer in Compressible Fluids, *J. Aeronaut. Sci.*, vol. 18, no. 3, March, 1951.

26. Van Driest, E. R.: Turbulent Boundary Layer on a Cone in Supersonic Flow at Zero Angle of Attack, *J. Aeronaut. Sci.*, vol. 19, no. 1, January, 1952.

27. Slote, L., and W. D. Murray: A Method of Predicting Skin, Compartment, and Equipment Temperatures for Aircraft, *WADC AD* 19722, July, 1953.

28. Seiff, A.: Examination of the Existing Data on the Heat Transfer of Turbulent Boundary Layers at Supersonic Speeds from the Point of View of Reynolds Analogy, *NACA Tech. Note* 3284, August, 1954.

29. Reshotko, E., and I. E. Beckwith: Compressible Laminary Boundary Layer over a Yawed Infinite Cylinder with Heat Transfer and Arbitrary Prandtl Number, *NACA Tech. Note* 3986, June, 1957.

30. Englert, G. W.: Estimation of Compressible Boundary-layer Growth over Insulated Surfaces with Pressure Gradient, *NACA Tech. Note* 4022, June, 1957.

31. Czarnecki, K. R., and A. R. Sinclair: A Note on the Effect of Heat Transfer on Peak Pressure Rise Associated with Separation of Turbulent Boundary Layer on a Body of Revolution (NACA RM-10) at a Mach Number of 1.61, *NACA Tech. Note* 3997, April, 1957.

32. Reshotko, E., and C. B. Cohen: Heat Transfer at the Forward Stagnation Point of Blunt Bodies, *NACA Tech. Note* 3513, July, 1955.

33. Brinich, P. F., and N. Sands: Effect of Bluntness on Transition for a Cone and a Hollow Cylinder at Mach 3.1, *NACA Tech. Note* 3979, May, 1957.

34. Stine, H. A., and K. Wanlass: Theoretical and Experimental Investigation of Aerodynamic-heating and Isothermal Heat-transfer Parameters on a

Hemispherical Nose with Laminar Boundary Layer at Supersonic Mach Number, *NACA Tech. Note* 3344, December, 1954.

35. Rubesin, M. W.: A Theoretical Study of the Effect of Upstream Transpiration Cooling on the Heat Transfer and Skin-friction Characteristics of a Compressible, Laminar Boundary Layer, *NACA Tech. Note* 3969, May, 1957.

36. Eber, G. R.: Recent Investigation of Temperature Recovery and Heat Transmission on Cones and Cylinders in Axial Flow in the N. O. L. Aeroballistics Wind Tunnel, *J. Aeronaut. Sci.*, vol. 19, no. 1, pp. 1–6, 14, January, 1952.

37. Von Kármán, T.: The Analogy between Fluid Friction and Heat Transfer, *Trans. ASME*, vol. 61, no. 11, November, 1939.

38. des Clers, B., and J. Sternberg: On Boundary-layer Temperature Recovery Factors, *J. Aeronaut. Sci.*, vol. 19, no. 9, pp. 645, 646, September, 1952.

39. Eckert, E. R. G.: "Introduction to the Transfer of Heat and Mass," McGraw-Hill Book Company, Inc., New York, 1950.

40. Kemp, N. H., P. H. Rose, and R. W. Detra: Laminar Heat Transfer Around Blunt Bodies in Dissociated Air, *J. Aero/Space Sci.*, vol. 26, no. 7, pp. 421–430, July, 1959.

41. Biot, M. A.: Further Developments of New Methods in Heat-flow Analysis, *J. Aero/Space Sci.*, vol. 26, no. 6, pp. 367–381, June, 1959.

42. Lees, L.: Laminar Heat Transfer over Blunt-nosed Bodies at Hypersonic Flight Speeds, *Jet Propulsion*, vol. 26, no. 4, p. 259, 1956.

43. Allen, H. J., and A. J. Eggers, Jr.: A Study of the Motion and Aerodynamic Heating of Missiles Entering the Earth's Atmosphere at High Supersonic Speeds, *NACA Tech. Note* 4047, October, 1957.

44. Allen, H. J.: Motion of a Ballistic Missile Angularly Misaligned with the Flight Path upon Entering the Atmosphere and its Effects upon Aerodynamic Heating, Aerodynamic Loads, and Miss Distance, *NACA Tech. Note* 4048, October, 1957.

CHAPTER 11

AERODYNAMIC LAUNCHING PROBLEMS

11-1. INTRODUCTION

The aerodynamic problem of launching missiles from ground launchers, shipboard, and particularly from high-speed parent aircraft is indeed a difficult and challenging one. Careful design practice must be exercised in order to assure that the missile realizes clean and safe separation as well as minimum deviation from the intended flight path. "Beam-riding" missiles have occasionally lost "beam lock-on" during their boost or launching phase as the result of excessive flight-path excursion, resulting in aborted flights. Hence detailed analyses must be made of the sources and magnitudes of both internal and external forces acting on the missile during its launching phase. Should these forces cause undesirable launching dispersion proper design modifications must be incorporated to assure a satisfactory launch. In the case of an air-launched missile, aircraft-missile compatibility must be realized. Hence the requirement of over-all system performance and accuracy as well as safety of launch must be satisfied. Thus the designer must consider carefully all the numerous factors which may cause undesirable and detrimental launching characteristics. It is the purpose of this chapter to point out and discuss some of the more important aspects of missile launching.

11-2. SAFETY OF PARENT AIRCRAFT—AIR LAUNCH

In addition to satisfying the requirement that the dispersion of the missile during launch must not exceed the limit dictated by guidance considerations, safety of launch must be assured to the parent aircraft and its crew. Unfortunately, in the majority of the cases, the airplane and missile designers are foreign to each other and often make undue design compromises when the over-all missile-aircraft weapon system is ready to be integrated. One of the chief reasons leading to the difficulties of integrating the missile to the parent aircraft or vice

versa is the fact that the air-launched missile is usually designed to be carried by many different aircraft which are either operational or fairly well finalized in design. Hence the missile engineer is left with the problem of "retrofitting" his missile to the parent aircraft, the design of which is "frozen."

The problem of safety of launch is particularly severe in the case of "retrofitting" the missile to a particular parent aircraft because of the following limitations imposed by the design of the parent aircraft: (1) extreme inboard pylon or external store location, (2) restricted longitudinal center-of-gravity movement, (3) unduly long forebody for the missile to fly clear of, and (4) limited ground and wing clearance, etc. The above limitations can be alleviated to a great extent whenever the parent aircraft and missile are designed as an integrated system at their earliest design stages. In either case, however, detailed analysis must be conducted on the various factors which may contribute to the hazards of launching.

In many modern aircraft, pilots have reported and subsequently verified that bombs and external stores such as fuel tanks exhibited extremely erratic separation characteristics upon release or ejection. Bombs have been shown to pitch violently inside the bombbay prior to their eventual separation from the carrier aircraft while fuel tanks have been shown to travel from their wing-tip location inboard to hit the fuselage of the airplane during their release. Obviously such erratic release characteristics for a missile are totally unacceptable from the standpoint of safety to the parent aircraft, not to mention the strong possibility of a completely inaccurate and consequently ineffective round.

Although no detailed safety criteria are specified, they should consist of the following as a guide for the missile or airplane designer:

1. The missile should not strike the parent aircraft during boost or jettison.
2. The missile structure should not fail under any conditions of flight in the immediate vicinity of the parent aircraft.
3. The jet blast from the rocket of the missile should not adversely affect the parent-aircraft structures and its operating components such as air inlets and control surfaces.

1. Missile-aircraft Collision. Perhaps the two most important causes which may result in missile collision with the launch aircraft are (1) adverse aerodynamic forces on the missile induced by the flow field about the missile-pylon-wing combination and (2) control-system failure at launch, which causes the control surfaces to deflect

fully to their hard-over position in pitch, yaw, or roll. Other contributing factors are normal manufacturing malalignment of the control surfaces, thrust malalignment, missile center of gravity off center, and launch-aircraft manuevers. In general, the latter effects are small relative to those mentioned previously.

Over the past several years, the NACA (now NASA) and private companies in the aircraft-missile industry have conducted extensive experimental and theoretical studies on the nature and magnitude of

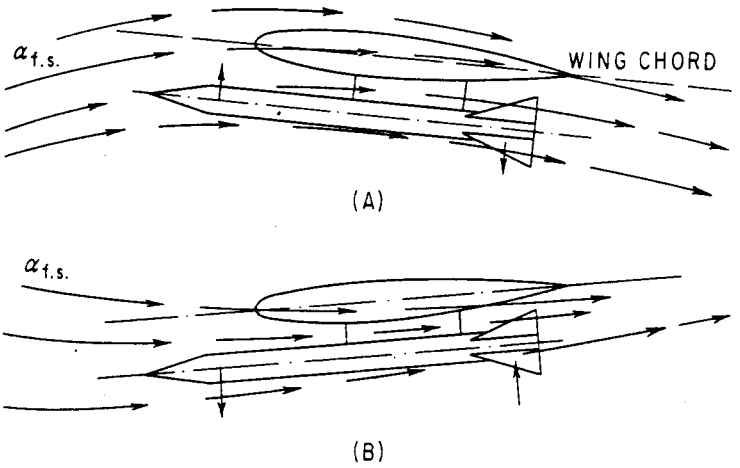

FIG. 11-1. Induced flow field in pitch of wing-pylon-missile combination. (*A*) Low-speed (high α) condition. (*B*) High-speed (low α) condition.

the effects of flow field induced by and on the missile-pylon-wing and missile-fuselage combinations. Numerous configurations have been investigated to provide the data to evaluate missile-launch dispersion characteristics. References 1 through 10 are but a partial list of unclassified reports on the subject of missile-aircraft flow interference. Many more reports that are available but classified should be consulted for a satisfactory solution to this launch problem.

A rather crude but informative representation of the nature of the flow field is shown in Figs. 11-1 and 11-2 for the sources of pitching, yawing, and rolling moments. As seen in Fig. 11-1, the flow field in pitch for a low-speed launch condition is typified by the flow about a wing at a relatively high angle of attack. In this attitude the missile is shown to be experiencing a positive angle of attack at the forebody section and a negative angle of attack at the aft section. Hence one would expect the missile to pitch upward upon launch. On the other hand, for the high-speed launch condition, the missile tends to pitch downward at launch. In addition to the pitching moments, adverse

yawing moments and side force may be of sufficient magnitude to cause the missile to veer into the parent aircraft at launch. The extremely long forebody on modern high-speed aircraft often presents a critical problem from the standpoint of missile-aircraft collision. Rolling moments also exist even in a rather simple straight-forward installation (straight wing, say). As a result the missile has a tendency to roll into the pylon upon separation. In the case where the rear fin of the missile "slaps on" the side of the pylon no particular harmful effect (from the aircraft-safety standpoint) is expected. However, if the missile rolls sufficiently to cause the leading edge of the tail fins of the missile to hit the trailing edge of the pylon, the damage can be extremely serious.

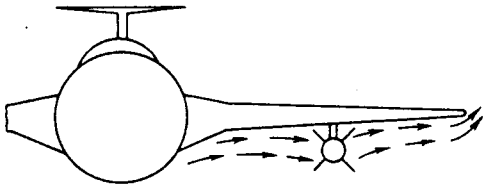

FIG. 11-2. Flow field induced by cross-flow phenomenon.

Another very important aspect of the flow field is its effect on the aerodynamic hinge moments of the movable surfaces on the missile. This is particularly critical at high subsonic speeds and above since local shock waves may be present and can have a strong effect on the center-of-pressure location and hinge-moment characteristics. Careful analysis should include experimental wind-tunnel tests or flight testing with the full-scale missile by utilizing a "captive-flight-balance system" to measure these induced forces and moments to make certain that the resultant aerodynamic hinge moments are within the capability of the servo system in the missile. Improper design or failure to account for the actual aerodynamic hinge moments in the "captive flight" or launch attitude could cause the servo to be overpowered, with the result that the missile would be launched with its control surfaces fully deflected.

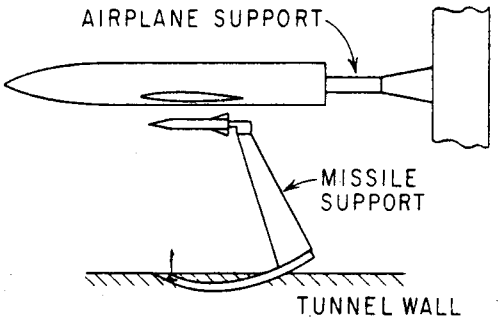

FIG. 11-3. Schema of test installation for measurement of airplane-missile mutual-interference effects.

The most commonly used method for determining the induced loads and mutual interference effects of the airplane-missile combination is scaled-model wind-tunnel testing. Separate sting mountings for the airplane and missile are used to measure the loads on the missile and airplane as shown in Fig. 11-3. Using this technique, data on the

effect of the missile on the parent aircraft may also be obtained in order to predict the performance degradation of the parent aircraft with the missile in the carried position. The effects of missile location in the immediate vicinity of the parent aircraft can also be determined by moving the complete missile-sting assembly relative to the airplane model.

Captive balance testing using a full-scale missile is also used to determine captive-flight loads on the missile as well as the effect of the missile on the launch aircraft. This particular technique has the advantage of obtaining full-scale-model test data. However, investigation of the various parameters such as spanwise and chordwise location and missile installation attitude is obviously extremely limited. Hence this test technique may be used to check the design installation based on scaled-model-test results obtained in the wind tunnel.

Control-system malfunction resulting from electrical- or hydraulic-system failure at launch may also cause the missile to be launched with its control surfaces deflected fully onto their physical stops. From the standpoint of safety of launch, this condition should be fully investigated. If results of calculations indicate the possibility of missile collision with the parent aircraft, proper design modification must be made. Such modification may consist of physically locking the control surfaces for a finite time after launch until the missile is sufficiently ahead of the aircraft.

The launch-dispersion characteristics in yaw may be determined by manual computation for one or two most adverse launch conditions. However, for detailed studies of the effects of individual parameters, such as missile stability margin and thrust malalignments, the computation procedure should be mechanized on the automatic computing machine. The basic equations of motion (in yaw) may be written as

$$\Sigma F_x = \frac{W}{g}\ddot{X} \tag{11-1}$$

$$\Sigma F_y = \frac{W}{g}\ddot{Y} \tag{11-2}$$

$$\Sigma M_z = I\ddot{\theta} \tag{11-3}$$

From Fig. 11-4, the right-hand side of Eqs. (11-1) and (11-2) may be expressed as

$$\Sigma F_x = F_A \cos\theta - F_N \sin\theta \tag{11-4}$$

and

$$\Sigma F_y = F_A \sin\theta + F_N \cos\theta \tag{11-5}$$

where

$$F_A = T - C_A qS \tag{11-6}$$

$$F_N = C_N qS \tag{11-7}$$

The summation of moments in yaw is

$$\Sigma M_z = M_\alpha \alpha + M_\delta \delta + M_{\dot\theta} \dot\theta + M_T + M_M + M_{\text{flow field}} \qquad (11\text{-}8)$$

where M_T = moment due to thrust malalignment
M_M = moment due to aerodynamic-surface malalignment

The flow-field effect should be determined for several points along the missile trajectory if a reasonably accurate answer is to be obtained. The values of C_A and C_N in Eqs. (11-6) and (11-7) should include the flow-field effect and can be determined from either wind-tunnel tests or captive-balance-flight-test results. For preliminary analysis, it is sufficient to assume a constant forward speed over the relatively short time interval to be studied. Using the iteration procedures similar to those described in Chap. 4, the above equations can be solved to determine the missile launch-dispersion characteristics.

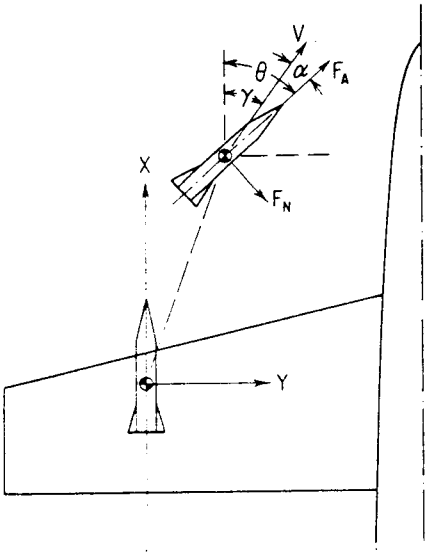

FIG. 11-4. Force diagram for missile-launch aircraft-collision study.

2. Missile Structural Failure. Another important consideration for parent-aircraft safety is the structural integrity of the missile during its captive flight and free flight in the immediate vicinity of the launch aircraft. The loads imposed by the flow-field effects must be carefully determined for a particular installation and speed condition in accordance with specification requirements. The missile airframe should then be designed to these captive-flight loads, which may in some cases be critical-design loads. The missile should also be designed to withstand the critical-flight loads under both normal and adverse flight conditions. Failure of the missile structure in flight in the vicinity of the launch aircraft is extremely hazardous and must be avoided by proper design.

11-3. LAUNCH BOUNDARIES—AIR LAUNCH

In addition to the problems of missile collision with the parent aircraft and missile structural break-up in front of the launch aircraft just discussed, additional consideration must be given to the safety of the launch aircraft. This takes the form of launch-aircraft boundaries

which would restrict the aircraft's "zone of operation" and hence provide a measure of safety against ground fire, blast effects from the missile and its warhead, etc. These launch boundaries are particularly meaningful for an air-to-surface missile weapon system which requires that the parent aircraft fly essentially the same path as the missile. Such a system may be a line-of-sight command guidance or a particular type of beam-rider system.

1. Launch-aircraft Trajectory. Figure 11-5 shows the pertinent parameters governing the flight path of the parent aircraft following missile launching. It is apparent that, from the kinematic standpoint, aircraft speed, maneuvering capability, missile flight time, and terrain clearance are the major governing factors in the determination of the launch boundaries. The launch boundaries may be readily determined by the following procedure.

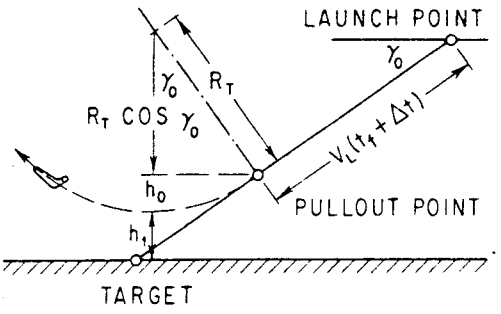

FIG. 11-5. Kinematics of launch boundary.

First, the kinematic or flight trajectory of the launch aircraft must be determined. The turn radius R_T in pitch may be calculated as

$$R_T = \frac{V_L^2}{g[n - (1 + \cos \gamma_0)/2]} \tag{11-9}$$

where V_L = launch velocity, fps, assumed to be constant throughout entire airplane trajectory
n = load-factor capability of airplane
γ_0 = initial launch angle which airplane and missile follow

The altitude required to turn from γ_0 to level attitude, designated as h_0 in Fig. 11-5, is shown to be

$$h_0 = R_T - R_T \cos \gamma_0 = R_T(1 - \cos \gamma_0) \tag{11-10}$$

Hence the distance S_0 shown in Fig. 11-5 may be determined as a function of h_0 and the terrain-clearance altitude h, as follows:

$$S_0 = \frac{h_0 + h_1}{\sin \gamma_0} \tag{11-11}$$

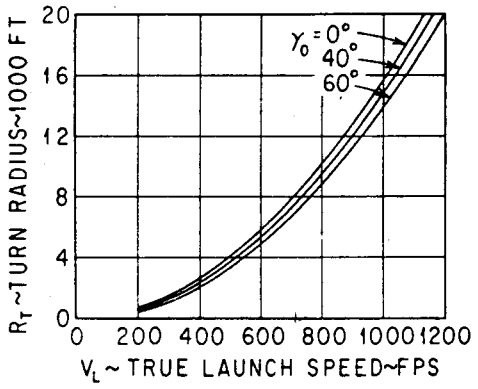

FIG. 11-6. R_T vs. V_L for various γ_0's ($n = 3$).

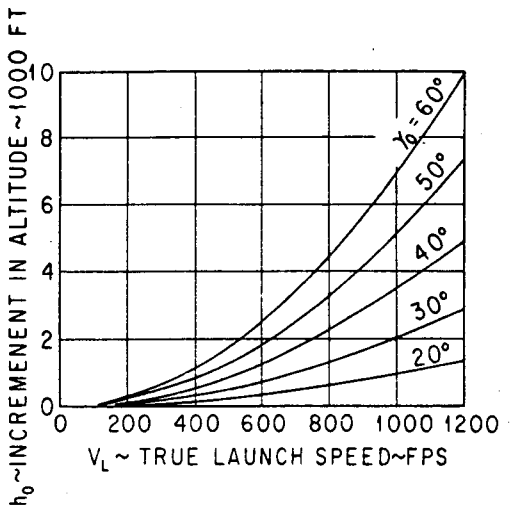

FIG. 11-7. h_0 vs. V_L for various γ_0's ($n = 3$).

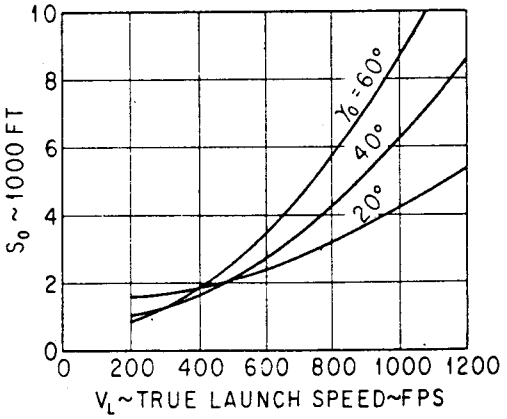

FIG. 11-8. S_0 vs. V_L for various γ_0's ($n = 3$, $h_1 = 500$ ft).

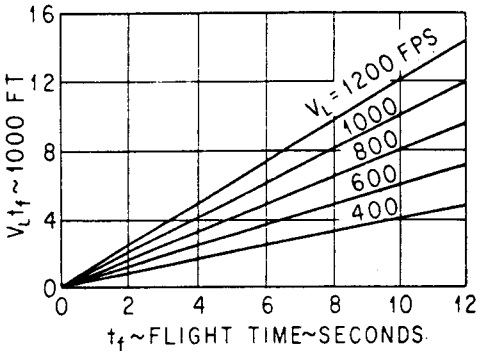

FIG. 11-9. $V_L t_f$ vs. t_f.

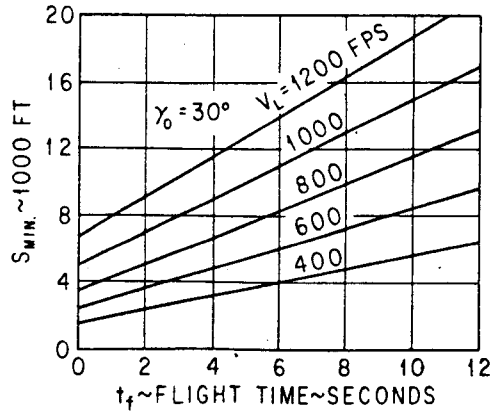

FIG. 11-10. $S_{\min}$ vs. t_f ($\gamma_0 = 30°$, $n = 3$, $h_1 = 500$ ft).

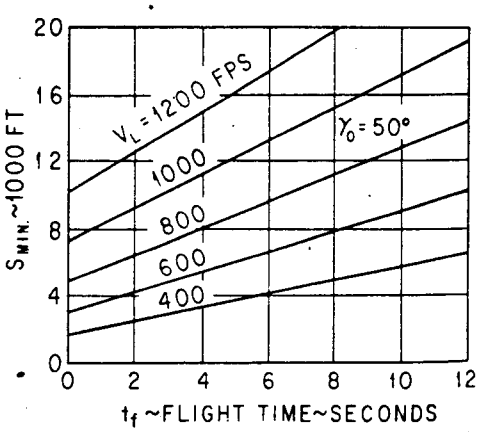

FIG. 11-11. $S_{\min}$ vs. t_f ($\gamma_0 = 50°$, $n = 3$, $h_1 = 500$ ft).

The value of h_1 may also represent the altitude clearance required from the standpoint of enemy ground fire, blast effect from the warhead of the missile, etc. Thus the trajectory of the launch aircraft written in terms of $S_{\min}$ may be summarized as

$$S_{\min} = S_0 + V_L(t_f + \Delta t) \tag{11-12}$$

$$S_{\min} = \frac{h_0 + h_1}{\sin \gamma_0} + V_L(t_f + \Delta t) \tag{11-12a}$$

$$S_{\min} = \frac{R_T(1 - \cos \gamma_0) + h_1}{\sin \gamma_0} + V_L(t_f + \Delta t) \tag{11-12b}$$

where t_f = flight time of missile

Δt = time lag from missile impact to commencement of aircraft-pull-out maneuver

Assuming a typical aircraft load-factor capability of 3 g's and a terrain-clearance requirement of 500 ft, values of the pertinent trajectory parameters R_T, h_0, S_0, and $V_L t_f$ have been calculated from Eqs. (11-9) through (11-11) and presented in Figs. 11-6 through 11-9. The values of $S_{\min}$ for two typical launch angles (30 and 50°) are shown in Figs. 11-10 and 11-11 for a range of launch speeds.

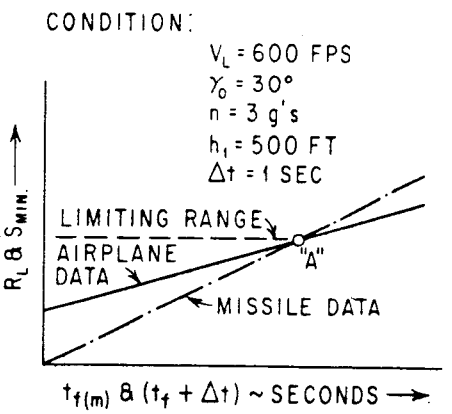

FIG. 11-12. Determination of launch boundary.

2. Missile Trajectory. Next, missile trajectory must be calculated before the launch boundaries of the parent aircraft can be determined. This may be done by calculating the missile trajectory and flight time for three different slant ranges S_L at a given initial launch angle and calculating speed by the methods outlined in Chap. 4. The resultant trajectory data may then be plotted as missile slant range vs. missile flight time $t_{f(m)}$, as shown in Fig. 11-12.

3. Launch-boundary Determination. The actual launch boundary of the parent aircraft may be determined by matching the trajectory data of the parent aircraft and missile previously described. This may be done readily by superimposing the trajectory information of the parent aircraft in Fig. 11-12 in terms of $S_{\min}$ as a function of $(t_f + \Delta t)$ from Eq. (11-12b). The intersection of the two curves establishes

the limiting range for the given condition of launch speed and dive angle. This range is defined as the minimum range from which the parent aircraft can launch the missile, follow the missile toward the target, pull out at (or very shortly after) missile impact, and clear the ground by the desired height h_1. Limiting range for other launch conditions can also be determined by the methods just described. Typical launch boundaries for two launch speeds are shown in Fig. 11-13.

From the standpoint of guidance accuracy, the missile must also be designed to fly within a certain boundary during launch. This boundary represents the maximum launch dispersion permissible before the degradation to the delivery accuracy of the missile becomes unacceptable. As previously mentioned, the beam-riding missile must stay within the beam width of the guidance system in order to achieve "lock-on" for the remainder of its flight trajectory. For command control (particularly in the case of visual line-of-sight command), the missile must not disperse out of the pilot's normal field of view or too far off the normal intended flight path for the missile to return within the flight duration of the missile. Quite frequently, finite-length rail launchers are used to "guide" the missile through the adverse-flow-field region in order to minimize missile dispersion at launch. These launching rails are mostly used in cases where the parent aircraft are "retrofitted" for missile launching. In cases where the parent aircraft and missile are designed initially as an integrated weapon system, the requirements for finite length rail launchers are minimized.

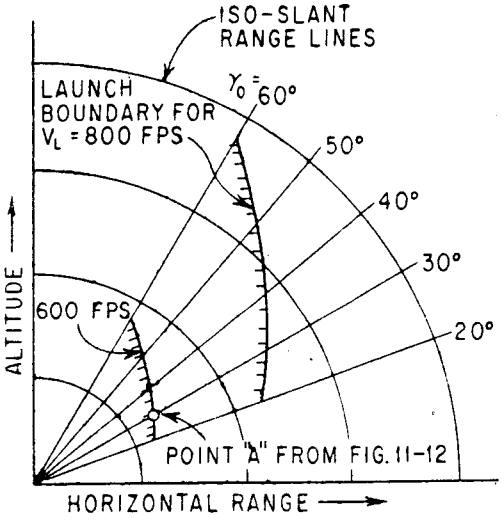

FIG. 11-13. Typical launch boundaries.

11-4. CONSIDERATION TO PARENT-AIRCRAFT PERFORMANCE

Consideration should be given by both the missile and aircraft designers to minimizing the performance degradation of the parent aircraft with external missile installation. Since selection of the spanwise and chordwise locations is generally limited by wing-bending and

aircraft center-of-gravity considerations, the designer must exercise extreme care in selecting the most favorable installation within this limited range. The final selected installation should represent the best compromise from the standpoint of the effect of the launch aircraft on the missile and the effect of the missile installation on the aircraft. The importance of the latter effect is readily apparent when one considers the fact that severe performance degradation may be realized with an improper missile installation. The resultant loss in range and in high-speed capability of the launch aircraft with its store of externally carried missiles is obviously undesirable from a tactical standpoint.

The problem of designing a missile-aircraft system with the least detrimental mutual effect is a challenging one that requires additional research and experimental work. Much experimental work has already been done on the various types of missiles or external-store installations. Measurements of loads on the missile as well as on the parent aircraft have been made in the wind tunnel, as previously mentioned. In the calculation of the performance degradation of the parent aircraft, the two most important pieces of information required are (1) basic performance curves of the parent aircraft and (2) a good correlation of installation drag of the missile. The former information consists basically of the thrust and drag variation with speed (see Fig. 4-8) and other engine data such as fuel-flow data. The latter may be obtained only after extensive study of the flow-field problem has been conducted or data from experimental tests of the configuration are available. It is emphasized here that item 1 is extremely important in that one must know exactly in what region of the drag curve the airplane is operating before any reasonable (let alone accurate) estimates of the performance degradation can be made. Hence it is important that the airplane and missile engineers work closely in this area to assure aircraft-missile compatibility. Once the above required data are made available, the performance degradation of the parent aircraft can be determined by the methods outlined in Chap. 4.

It should be remembered that, even with a well-designed installation, the penalty involved in externally carried missiles can be very high. Often a fairly respectable high-supersonic fighter becomes merely another high-subsonic aircraft when carrying several missiles externally. The present trend is toward internal stowage. Consequently much work is now in progress to study the aerodynamics of very-low-aspect-ratio wings for future design considerations, for both internal- and external-stowage considerations.

11-5. GROUND LAUNCH

The problem of launching missiles from the ground may be divided broadly into two general categories: (1) effects of the launching phase on the missile and (2) effects of the missile on the launcher and surrounding areas. The former effects are studied from the standpoint of missile-guidance and missile-component operation, while the latter effects are concerned primarily with the safety of the launching crew and surrounding areas. The latter problem is the topic of discussion in Sec. 11-6. This section is primarily concerned with the effects of the launching environment on the missile and its operation.

From the standpoint of missile guidance, several potential sources of detrimental effects causing excessive missile dispersion at launch are present. These include launcher deflection, missile tip-off from the launcher, thrust and fin malalignments, and atmospheric disturbances such as tail wind, cross wind, and gusts. Each of these factors affecting missile launch dispersion is discussed below.

1. Launcher Deflection. One of the most common factors present, particularly with mobile launchers, is the launcher deflection which results from ignition shock and sudden high thrust build-up from the booster. This motion can have a detrimental effect on the missile flight in that the initial heading of the booster configuration is different from that set previously. The missile will therefore fly a new flight path as the result of this pitching rate just as the missile leaves the launcher. This problem can be solved by (1) designing a stiffer launcher, (2) accounting for this motion in setting the launcher, or (3) a combination of both. For long-range ballistic missiles, which are generally launched vertically from rugged launching pads, this problem is virtually nonexistent.

2. Tip-off. Another common factor arises if the supporting shoes on the missile do not leave the supporting rail or rails simultaneously. Such a case may be one in which the two shoes (one forward and one aft) ride on the same rail. When this happens, the missile will tilt downward under the force of gravity and cause the missile to fly a new flight path. With simultaneous shoe release, the missile would have a simple translational instead of combined translational and rotational motion immediately upon leaving the launcher. This translational motion is not so detrimental to the dispersion as the rotational motion.

3. Thrust and Fin Malalignment. Turning moment due to thrust and aerodynamic surface malalignments is another important cause of missile dispersion during launch. The dispersion resulting

from this source can be very serious for missiles flying on "open loop" (i.e., without guidance or control) during their early phase of launch. In this case, a relatively large static stability margin (see Sec. 5-3 or 5-7) is required to minimize the dispersion due to these malalignments. This may be realized by incorporating relatively large tail surfaces on the missile (or large fins at the aft section of external droppable boosters). It will be shown in Chap. 12 that excessive static stability margin may prove to be undesirable when the missile is launched in a cross wind. Another method of minimizing missile dispersion at launch due to thrust and fin malalignment is spinning the missile immediately off the launcher. This technique is commonly used on uncontrolled and unguided ballistic missiles designed for relatively short ranges (i.e., less than 50 miles). For missiles which are controlled from the instant of launch, thrust and fin malalignment effects are of secondary importance.

Intentional thrust misalignment is used on certain types of cruise missile to counteract the effect of gravity during boost. In this case, the thrust vector is aligned below the center of gravity of the missile-booster combination. If the underalignment is too great, the missile may attained a large angle of attack, possibly resulting in stalling the missile at the end of its boost phase. On the other hand, insufficient underalignment may result in an angle of attack which is too low to sustain missile weight, causing an undesirable loss in flying altitude before the missile can attain sufficient speed under its own power.

4. Wind. Since it is tactically impractical always to launch into the wind, one must contend with the problem of wind blowing from any direction. Depending upon the application, sometimes the tail wind and sometimes the side wind may result in the critical design point. One of the main points to remember is that the static stability of the missile should not be so large that the configuration weathercocks into the relative wind, resulting in flight-path dispersion under conditions of uncontrolled flight. For missiles which are being controlled from the instant of launch, sufficient aerodynamic control effectiveness must be provided to maintain the missile on the desired flight path during launch.

Special consideration should be given to the effect of wind on long-range ballistic missiles, which lift off vertically from their launching pads. Strong cross winds could cause sufficient force to topple the missile over its base unless some tie-down provisions are made. In addition, loads induced by vortex effects at or near the tip of the missile may be sufficiently critical to cause structural failure of the missile on

the launch pad. These ground wind-induced loads are particularly critical for a missile with large length-to-diameter ratio and its attendant low structural strength and natural cantilever mode frequencies. The latter is conducive to a condition of resonance with the wind-induced load frequency. Modification of the nose geometry may be necessary to alleviate or alter the nature of the loads induced by the forebody vortices. Detail analysis including wind-tunnel tests on structural or dynamically similar models is required to determine the severity of this wind-induced loading problem for each missile design.

11-6. RANGE SAFETY

The advent of atomic- and nuclear-warhead-carrying missiles poses an extremely serious problem of safety not only to the large cities and their populations in the case of area-defense missiles but also to friendly troops and installations for the front-line tactical missiles. For the very-short-range tactical ballistic missiles which fly essentially a zero-lift trajectory, the problem of safety is not particularly severe since the missile is aimed and should fly into the general direction of the target. However, proper warhead arming and fusing must be provided to prevent premature warhead detonation at or near the launch site. For all other types of missiles which generally fly a prescribed lifting trajectory (including the long-range ballistic missiles), the flight path and resultant impact point can be extremely erratic if guidance- and control system failures occur. Hence reliability of the components as well as a proper arming system are prime requisites in any missile weapon system.

Since it is practically impossible to attain 100 per cent reliability for the over-all missile system, the problem of range safety must be analyzed from a realistic standpoint. For example, a multiple compound failure of components, which may be an extremely remote possibility, should not be used in the determination of the maximum missile impact area. On the other hand, simple failure or realizable compound failure of certain components should be taken into consideration to determine the severity of the range safety problem and consequently the requirement for a destructive system in the missile. Perhaps one of the most common failures is one which results in fully deflected controls causing the missile to turn in azimuth, or backward toward the launching area. The maximum area surrounding the launch site within which the missile can impact (when a component malfunctions) should be calculated to determine the need of the destructive system.

11-7. SHIPBOARD AND UNDERWATER LAUNCHES

Two very important design aspects in designing missiles for launching from ships or submarines are (1) space limitation and (2) motions of the ship during both check-out and launching. In addition to these, protection to both the ship and personnel from rocket-motor blast effects must be provided. For a particular type of missile configuration (airplane type where large wings are used to maintain sufficiently high lift-to-drag ratio L/D for long-range flights) extreme care must be exercised to assure a successful launch. The motions (pitch in particular) of the ship or submarine must be taken into account (if the launching platform is not stabilized) in order to determine the exact attitude of the missile at the end of the boost phase. This is particularly critical, since most missiles which fall into this category generally fly close to their maximum C_L. A slight change in attitude as the result of ship motions could mean an aborted flight.

Experience and test results on launching ballistic missiles from underwater are presently extremely limited. One of the main problems associated with underwater launch is to assure that the missile emerges from the water at an attitude compatible with the capabilities of the guidance and control system of the missile. In addition, aerodynamic stability and control must be provided in order to steer the missile back to the desired flight path. Extensive systematic tests must be made with dynamically similar models to determine such obvious effects as launch speed, attitude, and depth of the launching submarine on the attitude of the missile when it emerges from the surface of the water. The effect of sea state (roughness of the sea) should also be studied since it may be a major factor in determining the trajectory of the emerging missile. Rocket-motor ignition for an underwater-launched ballistic missile occurs when the missile has attained sufficient clearance from the surface of water to assure that the rocket motor experiences no adverse back pressure such as would be the case if the rocket motor were ignited while in the water. Ignition of the rocket motor in this mode of launch may be achieved effectively with a timer.

SYMBOLS

C_A	axial-force coefficient
C_L	lift coefficient
C_N	normal-force coefficient

F	force
M	moment
M_M	moment due to aerodynamic surface malalignment
M_T	moment due to thrust
R_T	turn radius
S	reference area
S_L	slant range
$S_{\min}$	minimum slant range for launch boundary
S_0	distance used in launch-boundary determination
T	thrust
V_L	launch velocity
W	weight
X	distance along X axis shown in Fig. 11-4
Y	distance along Y axis shown in Fig. 11-4
h_0	altitude required to turn
h_1	terrain-clearance altitude
n	load factor
q	dynamic pressure
t_f, $t_{f(m)}$	missile flight time
Δt	time lag between missile impact and commencement of aircraft pull-out maneuver
α	angle of attack
γ_0	initial launch angle
θ	missile attitude

Subscripts

A	axial direction
N	normal direction
fs	free stream
x, y, z	about the X, Y, Z axis system

REFERENCES

1. Alford, W. J., Jr., and H. N. Silver: Investigation at High Subsonic Speeds of Finned and Unfinned Bodies Mounted at Various Locations from the Wings of Unswept- and Swept-wing Fuselage Models, Including Measurements of Body Loads, *NACA Research Mem.* L54B18, Apr. 1, 1954.

2. Margolis, K., F. S. Malvestuto, Jr., and P. J. Maxie, Jr.: Theoretical Calculations of Supersonic Wave Drag at Zero Lift for a Particular Store Arrangement, *NACA Tech. Note* 4120, June, 1958.

3. O'Bryan, T. C.: Flight Measurement of Aerodynamic Loads and Moments on an External Store Mounted under the Wing of a Swept-wing Fighter-type Airplane, *NACA Research Mem.* L53G22, Nov. 25, 1953.

4. Silvers, H. N., and K. P. Spreeman: Wind-tunnel Investigation of a Wing-fuselage Combination with External Stores, *NACA Research Mem.* L7K20, July 9, 1948.

5. Silvers, H. N., and T. C. O'Brien: Some Notes on the Aerodynamic Loads Associated with External-store Installations, *NACA Research Mem.* L53E06A, June 22, 1953.

6. Silvers, H. N., T. J. King, Jr., and W. J. Alford, Jr.: Wind-tunnel Investigation at High Subsonic Speeds of the Effects of Wing-mounted External Stores on the Loading and Aerodynamic Characteristics in Pitch of a 45° Sweptback Wing Combined with a Fuselage, *NACA Research Mem.* L54A21, Mar. 23, 1954.

7. Spreeman, K. P., and W. J. Alford, Jr.: Investigation of the Effects of Geometric Changes in an Underwing Pylon-suspended External-store Installation on the Aerodynamic Characteristics of a 45° Sweptback Wing at High Subsonic Speeds, *NACA Research Mem.* L50L12, Mar. 5, 1951.

8. Alford, W. J., Jr., N. H. Silvers and T. J. King, Jr.: Preliminary Low-speed Wind Tunnel Investigation of Some Aspects of the Aerodynamic Problems Associated with Missiles Carried Externally in Positions Near Aircraft Wings, *NACA Research Mem.* L54J20, December, 1954.

9. Alford, W. J., Jr.: Theoretical and Experimental Investigation of the Subsonic Flow Fields beneath Swept and Unswept Wings with Tables of Vortex-induced Velocities, *NACA Rept.* 1327, 1957 (supersedes *Tech. Note* 3738).

10. Alford, W. J., Jr., H. N. Silvers, and T. J. King, Jr.: Experimental Aerodynamic Forces and Moments at Low Speed of a Missile Model during Simulated Launching from the Midsemispan Location of a 45° Sweptback Wing-fuselage Combination, *NACA Research Mem.* L54K11a, Feb. 4, 1955.

CHAPTER 12

FREE-FLIGHT DISPERSIONS

12-1. INTRODUCTION

In addition to the range safety considerations mentioned in Chap. 11, the dispersion characteristics of the missile during free flight are of considerable importance from the standpoint of delivery accuracy of the missile weapon system. In the case of the free-flight (uncontrolled) short-range ballistic missile, the total dispersion results primarily from the free-flight portion of its trajectory (the other causes are launcher-aiming error, target-location error, etc.). In the case of a reentry body of a long-range ballistic missile, the dispersion resulting from its free-flight or terminal phase must be kept low in order to minimize the requirements for an extremely accurate and expensive guidance system to steer the missile (and its reentry body) to the prescribed point in space prior to separation of the reentry body and its warhead. Even in cases where terminal guidance is employed, the missile may fly a limited uncontrolled or unguided trajectory just prior to impact. Such occurrences may take place as a result of loss of guidance due to component malfunction, ground clutter, enemy countermeasures, etc. Hence the dispersion characteristics of the missile during free flight must be carefully analyzed before the effectiveness of the missile weapon system can be accurately determined.

The following sections in this chapter deal with the problems of dispersion of short-range free ballistics during launch or boosting phase. The problem of drift (dispersion) due to cross wind is treated in detail to show the pronounced effect of the external-configuration design. In addition, the dispersion-sensitivity factors for vacuum-flight conditions simulating very-high-altitude reentry are discussed. Finally, reentry body-design considerations are discussed from the standpoint of minimizing free-flight dispersion as well as other pertinent design considerations.

12-2. BOOST PHASE

The primary sources of dispersion during the launch or boost phase of flight for a free-flight ballistic missile consist of the following: (1) launcher dynamics (i.e., launcher deflection, tip-off effects, etc.), (2) launcher setting or aiming error, (3) variation in rocket-motor performance, (4) thrust and fin malalignments, and (5) cross-wind effects. Each of these effects will be treated in the following sections.

1. Launcher Dynamics. As discussed in Sec. 11-5, the launcher may deflect under the influence of rocket-motor ignition shock and sudden thrust build-up. Since the launcher is generally considered by the dynamics engineers as a complex structural system, particularly one which is integral with a mobile vehicle, the exact nature and magnitude of the launcher deflection are extremely difficult to calculate. Hence experimental test data must be obtained by high-speed-camera coverage of several actual missile launchings to determine the amount of the launch deflection under operating conditions. This information can then be fed back into the analysis of the missile delivery accuracy. Should the deflection prove to be intolerable, the launcher must be modified or "beefed up" to reduce the magnitude of the deflection. Since finite-length rail launchers are commonly used on unguided free-flight missiles and rockets, missile tip-off off the launcher may occur if the front shoe leaves the rail prior to the aft shoe. The consequent rotation under the force of gravity is undesirable and may be eliminated by designing equal launch rails with simultaneous fore- and aft-shoe releases.

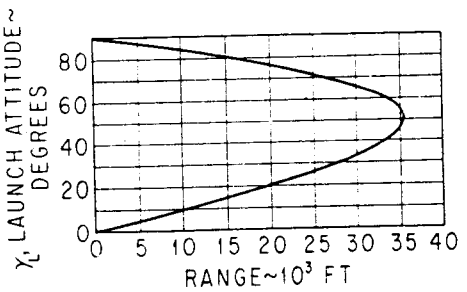

FIG. 12-1. Typical variation of launch attitude with range.

2. Launcher Setting. Since it is physically impossible to set the launcher precisely at the desired angle, error in launcher setting is always present. The severity of the error in launcher setting increases at launch angles below and above the launch angle for maximum range. This is readily apparent from Fig. 12-1, which shows the range variation with launch attitude. For most short-range (i.e., say, less than 30 miles) applications, the optimum launch attitude γ_{opt} is closer to 50° than to 45° obtained from drag-free consideration. For somewhat greater range applications where the ratio of total rocket-motor

impulse to burnout weight is in excess of about 100, the angle for maximum range increases from 50 to approximately 65°, as shown in Fig. 12-2. In either case, however, the (down-range) dispersion sensitivity due to launcher-setting error, defined as $\partial X/\partial \gamma_L$, is zero at γ_L for maximum range and increases (negatively) above and below this optimum angle, as shown in Fig. 12-3. The down-range dispersion ΔX_γ due to launcher-setting is thus

$$\Delta X\gamma = \frac{\partial X}{\partial \gamma_L} \Delta \gamma_p \qquad (12\text{-}1)$$

where $\Delta\gamma_p$ is the error in launcher setting in pitch. The azimuth dispersion $\Delta\gamma_y$ (due to azimuth launch-setting error) is simply

$$\Delta Y\gamma = X\, \Delta\gamma_y \qquad (12\text{-}2)$$

where X is total range and $\Delta\gamma_y$ is the error in launcher setting in the azimuth plane.

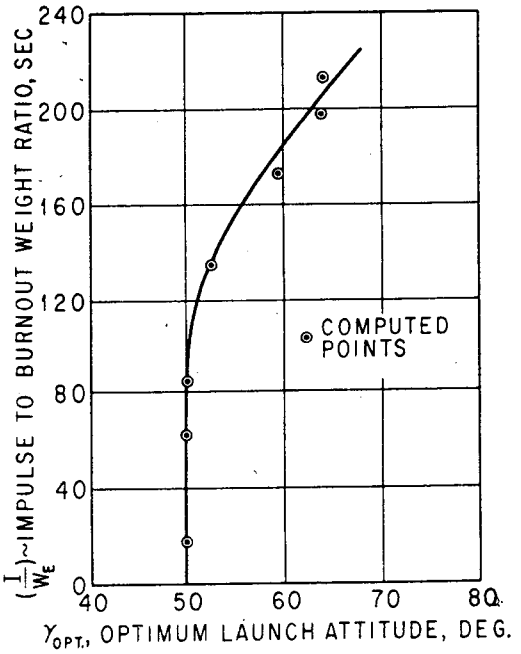

FIG. 12-2. Effect of ratio I/W_E on γ_{opt}.

3. Variation in Rocket-motor Performance. Because of the tolerances in rocket-motor design, propellant properties, manufacturing, etc., the total impulse of the rocket motor may vary over a range of a fraction of a per cent to several per cent depending on the operating environment. Variation of rocket-motor performance due to temperature variation in the propellant (particularly in the case of most solid-propellant rocket motors) may be partially accounted for by measuring the temperature inside the rocket motor prior to launch. The uncertainty in temperature measurement constitutes a source of dispersion. Perhaps the easiest method of determining this dispersion is to (1) first calculate the effect on range due to variation in total

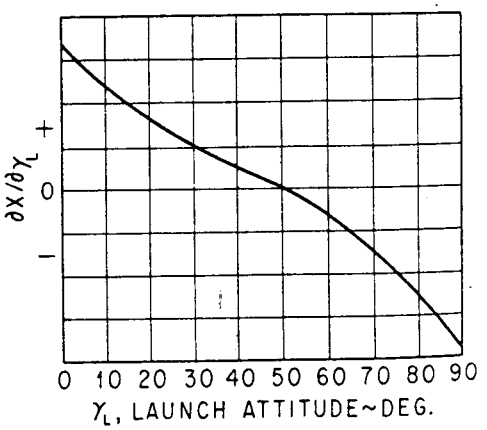

FIG. 12-3. Typical variation of range-sensitivity factor with range.

rocket-motor impulse I, (2) determine the range-sensitivity factor $\partial X/\partial I$, and (3) evaluate the effect of temperature on total impulse. The latter is generally furnished by the rocket-motor manufacturer. With the above data, the range dispersion due to impulse variation ΔX_I may be calculated as follows:

$$\Delta X_I = \frac{\partial X}{\partial I} \Delta I \tag{12-3}$$

where ΔI is the impulse variation. Equation (12-3) may also be written in terms of propellant-temperature error as

$$X_T = \frac{\partial X}{\partial I} \frac{\partial I}{\partial T} \Delta T \tag{12-4}$$

where $\partial I/\partial T$ is determined from the rocket-motor basic performance data shown in Fig. 12-4. In addition to the effect of temperature variation, the rocket-motor impulse may vary from one motor to the next for a given propellant-temperature condition. The range dispersion due to this basic inherent tolerance may also be calculated by Eq. (12-3) above.

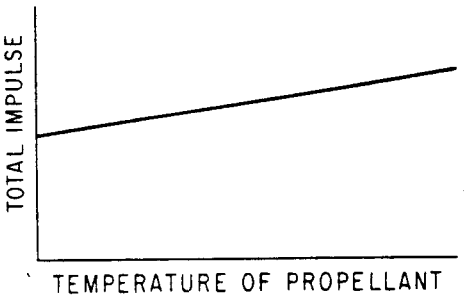

FIG. 12-4. Effect of propellant temperature on total impulse.

4. Thrust and Fin Malalignment. Perhaps the most difficult parameter to determine is the malalignment of the thrust vector and/or aerodynamic surfaces. Results from static firings from many rocket motors must be obtained in order to evaluate the magnitude and nature of the thrust malalignment. In addition, numerous measurements must be made on the aerodynamic fins to get a representative statistical average of the fin malalignments. Since the direction of these malalignments is generally random in nature, the dispersion resulting from these malalignments is also random. Since no method of compensating the effects of thrust or fin malalignments is available, the designer must resort to methods of minimizing the dispersion due to these effects. One obvious method is to hold the tolerances on the rocket-motor and fin designs to an absolute miminum. However, such design practice is generally extremely costly and hence is not adhered to. Another method involves designing a missile with very large static stability margin for the launch condition. This may be realized by either locating the center of gravity relatively far forward

of the center of pressure or putting large stabilizing fins at the aft end of the missile. While the missile with this large static stability margin is more resilient to any thrust or fin malalignment effects, it is also more conducive to dispersion due to cross-wind effects since its weather-cocking tendency is greatly increased, as discussed in a subsequent section.

A practical method of partially nullifying the effects of thrust and fin malalignments is by imparting a spin to the missile at the instant of launch and throughout its boost phase. This initial spin may be produced either by spin-jet rockets mounted on the missile or by using helical-rail launchers. Spin rate or rolling velocity for the remainder of the powered (or unpowered) flight may be obtained by canting the aerodynamic stabilizing fins. The effectiveness of the initial spin on reducing the dispersion due to thrust and fin malalignments is readily apparent from the following sample calculations:

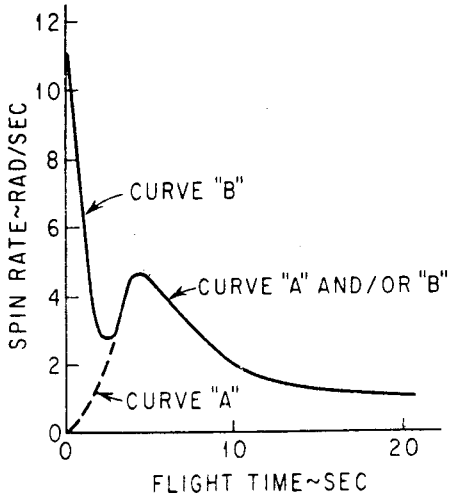

FIG. 12-5. Spin rate vs. time.

Example: $\gamma_L = 20°$, $X = 13{,}500$ yd.

a. Lateral-thrust malalignment = $\frac{1}{8}$ in. from center of gravity

b. Angular-thrust malalignment = 0.00176 radian

c. Fin malalignment = $\frac{1}{2}°$ (in pitch)

d. Fin intentionally canted to produce spin rate as shown by curve *A* in Fig. 12-5.

The range and azimuth dispersions Δx and Δy for the missile launched without initial spin (curve *A* in Fig. 12-5) are 1,300 and 125 yd, respectively. The resultant dispersion is thus $[(1{,}300)^2 + (125)^2]^{\frac{1}{2}} = 1{,}305$ yd. However, by imparting an initial spin rate of 11 radians/sec through the use of a helical-rail launcher (shown by curve *B* in Fig. 12-5), the corresponding dispersions are reduced to 425 and 185 yd, respectively. The resultant dispersion is hence reduced to 463 yd, corresponding to a reduction of approximately 65 per cent.

5. Surface Winds. In launching free-flight ballistic rockets, the magnitude and direction of the surface winds as well as winds aloft (the latter are generally called ballistic winds) must be taken into account. This is done by properly canting the launcher in elevation or in the azimuth plane depending on the presence of either a head or tail wind

or a cross wind. Since it is impractical to obtain an accurate wind measurement at or near the launch site, the inaccuracy in such measurements results in an incomplete compensation for the presence of surface winds; hence dispersion due to surface-wind effects is realized.

From the standpoint of dispersion due to surface-wind effects, it is desirable to design the missile with zero (or even a slightly negative) stability margin (i.e., neutral stability). A highly statically stable missile is undesirable since it has a very strong tendency to weathercock into the relative wind and hence is more conducive to dispersion due to surface winds. References 1 to 5 are recommended to the readers for the mathematical and quantitative treatments of the general effects of wind and malalignments, as well as a discussion on the optimization of these two effects on dispersion.

12-3. POWER-OFF FLIGHT

During the power-off trajectory of a free-flight ballistic missile, dispersions may be caused by several factors which are discussed below.

1. Variation in Missile Characteristics. Since it is generally impractical to maintain the exact missile characteristics on all missiles coming off the assembly line, the range of each missile will vary somewhat from the nominal range calculated for an "average" or "datum" missile configuration. Hence this variation may be considered as a dispersion over the nominal condition. Since the weight from one missile to another may vary from a few to many pounds, the range variation or dispersion may be readily calculated by getting a statistical average of this weight variation by the following relationship:

$$\Delta X_W = \frac{\partial X}{\partial W} \Delta W \tag{12-5}$$

where ΔX_W = range dispersion due to weight variation
$\partial X/\partial W$ = range-sensitivity factor due to weight variation
ΔW = statistical average weight variation

Because of aerodynamic smoothness tolerances as well as rough-handling effects in the field, the drag of the missile may also vary from one missile to the next. This variation in drag characteristic may be significant for the relatively long range flight conditions (i.e., near γ_{opt} launch attitudes). This factor is rather difficult to assess. Hence

intelligent guesses must be made; they should be based on past experience or data on this subject. Consequently the dispersion resulting from this factor may be conveniently calculated as follows:

$$\Delta X_D = \frac{\partial X}{\partial C_D} \Delta C_D \tag{12-6}$$

where ΔX_D = range dispersion due to C_D variation
$\partial X/\partial C_D$ = range-sensitivity factor due to C_D
ΔC_D = variation in drag coefficient

2. Variation in Atmospheric Density. During its power-off free-flight phase, the missile trajectory is primarily a function of its drag and mass characteristics (assuming still-air condition). Since the drag of the missile is the product of $C_D \frac{1}{2} \rho V^2$, the density of the atmosphere must be known or assumed. Meteorological data taken prior to launch may be subject to (1) error due to inaccuracy in the basic instrumentation and (2) changes in atmospheric condition between the time the data were recorded and the time of launch. Hence the error in the determination of atmospheric density results in a range dispersion which may be calculated as

$$\Delta X_\rho = \frac{\partial X}{\partial (\%\rho)} \Delta (\%\rho) \tag{12-7}$$

where ΔX_ρ = range dispersion due to density variation
$\partial X/\partial(\%\rho)$ = range sensitivity due to density variation (generally expressed as per cent density error)
$\Delta(\%\rho)$ = per cent density error

3. Drift Due to Cross Wind. The problem of evaluating the missile dynamic response in the presence of cross winds during its power-off (ballistic) flight trajectory may be conveniently divided into two phases. A qualitative analysis will be presented first to clarify the nature of its response characteristics. Then an analytical method will be derived in order to evaluate this cross-wind effect quantitatively.

a. Qualitative Analysis. The mechanics of missile response (or drift) due to cross winds may be conveniently illustrated by means of Fig. 12-6. A constant forward velocity is assumed for the moment. Figure 12-6*A* shows the plan view of the normal attitude of the missile during its power-off flight. As it encounters a cross wind, shown in Fig. 12-6*B*, it weathercocks into the relative wind as shown in Fig. 12-6*C*. The rapidity with which the missile weathercocks of course depends on the static stability margin of the missile in this flight condition (positive static stability margin is assumed throughout this

analysis, i.e., the missile is statically stable at all times during its trajectory). It is seen from Fig. 12-6*C* that, at this instant, the missile will be accelerated in the azimuth direction by the drag component $D_0 \sin \beta_0$. Thus it is clear that, as time elapses, the missile drift rate $\dot{y}_D$ develops, as indicated in Fig. 12-6*D*, and consequently reduces β. For a reasonably long flight trajectory, a steady-state condition will be attained wherein the missile will be drifting at the velocity of the cross wind, as shown in Fig. 12-6*E*. Obviously, in this steady-state condition, the missile will experience no unbalance of forces in the azimuth direction and hence no acceleration in that direction. The above simplified qualitative analysis may be summarized in terms of acceleration $\ddot{y}_D$ and drift rate $\dot{y}_D$ with a time history as presented in Fig. 12-7. The corresponding "instants" of conditions described above are included in Fig. 12-7 for clarification.

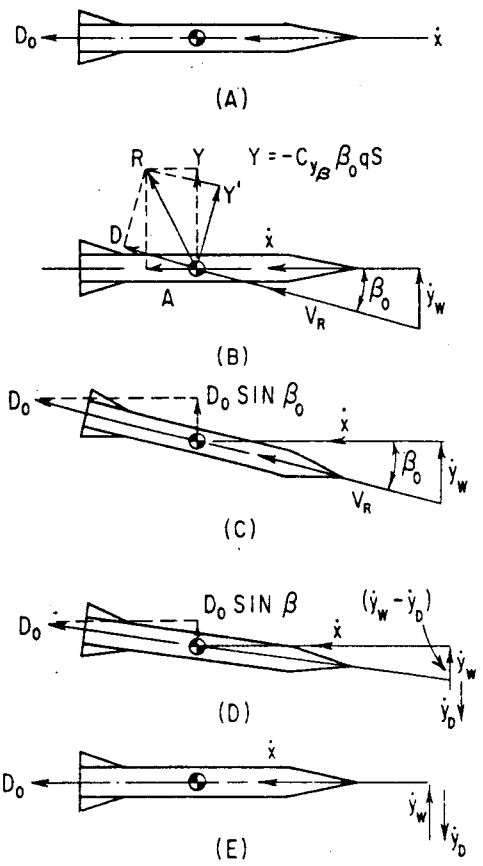

FIG. 12-6. Mechanics of drift due to cross wind. (*A*) Undisturbed-flight condition. (*B*) Instant of cross-wind occurrence. (*C*) Missile has weathercocked into resultant velocity V_R. (*D*) Shortly after occurrence of cross wind. (*E*) Steady-state condition (i.e., missile drifting with velocity of cross wind $Y_D = Y_W$).

As the result of the above discussion, it is clear that a single-body-mounted lateral accelerometer will not sense acceleration in the azimuth direction since the only external driving force in the azimuth direction is the aerodynamic drag (component) which lies in the insensitive axis of this accelerometer. Hence a single accelerometer mounted rigidly within the missile airframe cannot be employed as a device to detect or compensate for cross-wind effects.

b. Quantitative Analysis. The above section presented the qualitative behavior of the missile flying in the cross-wind condition. A quantitative evaluation of the missile response is presented below for calculating the drift dispersion due to cross winds.

In the development of the method for calculating drift due to cross winds, it is convenient to assume that the missile has already weather-cocked and commenced to drift, as shown in Fig. 12-6*D*. From Fig. 12-6*D*, the acceleration of the missile in the azimuth direction $\ddot{y}_D$ may be written as

$$F_Y = m\ddot{y}_D = D_0 \sin \beta \quad (12\text{-}8)$$

Since $D_0 = C_{D_0} \frac{1}{2} \rho V^2 S$, Eq. (12-8) becomes

$$\ddot{y}_D = \frac{C_{D_0} \frac{1}{2} \rho V^2 S \sin \beta}{2m} \quad (12\text{-}9)$$

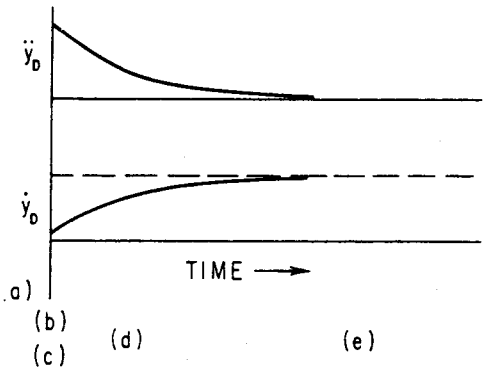

FIG. 12-7. Summary of missile dynamic response to cross wind.

$$\text{But} \quad \beta = \sin^{-1} \frac{\dot{y}_W - \dot{y}_D}{V_R} \quad (12\text{-}10)$$

where $\dot{y}_D$ is the drift rate of the missile and V_R the resultant velocity defined as

$$V_R = \sqrt{\dot{x}^2 + (\dot{y}_W - \dot{y}_D)^2} = \sqrt{\dot{x}^2 + \dot{y}_W{}^2 + \dot{y}_D{}^2 - 2\dot{y}_W\dot{y}_D} \quad (12\text{-}11)$$

For most applications, β is small and may be written as

$$\beta \cong \frac{(\dot{y}_W - \dot{y}_D)}{V_R} \quad (12\text{-}12)$$

Hence Eq. (12-9) may be expressed as

$$\ddot{y}_D = \frac{C_{D_0} \rho S V_R (\dot{y}_W - \dot{y}_D)}{2m} \quad (12\text{-}13)$$

Since $V_R \cong \dot{x}$, the forward speed of the missile, Eq. (12-13) becomes

$$\ddot{y}_D = \frac{C_{D_0} \rho S \dot{x} (\dot{y}_W - \dot{y}_D)}{2m} \quad (12\text{-}14)$$

Integrating $\ddot{y}_D$ from the limits of $(\dot{y}_D)_0$ to $\dot{y}_D$,

$$\int_{(\dot{y}_D)_0}^{\dot{y}_D} \frac{d\dot{y}_D}{\dot{y}_W - \dot{y}_D} = \frac{S}{2m} \int_0^t (C_{D_0} \rho \dot{x})\, dt \quad (12\text{-}15)$$

we get

$$-\ln (\dot{y}_W - \dot{y}_D) - \ln [\dot{y}_W - (\dot{y}_D)_0] = \frac{S}{2m} \int_0^t (C_{D_0} \rho \dot{x})\, dt \quad (12\text{-}16)$$

or

$$\ln \left[\frac{\dot{y}_W - (\dot{y}_D)_0}{\dot{y}_W - \dot{y}_D} \right] = \frac{S}{2m} \int_0^t (C_{D_0} \rho \dot{x})\, dt \quad (12\text{-}17)$$

or
$$\frac{\dot{y}_W - (\dot{y}_D)_0}{\dot{y}_W - \dot{y}_D} = e^{\frac{S}{2m}\int_0^t (C_{D_0}\rho\dot{x})\,dt} \tag{12-18}$$

In order to evaluate the missile drift rate $\dot{y}_D$, the values of $\int_0^t (C_{D_0}\rho\dot{x})\,dt$ and $(\dot{y}_D)_0$ must be determined first. In most cases, however, ideal-trajectory data (standard atmospheric trajectories with no wind or malalignments) are available since these are basic data with which the designer commences his design and analyses. Hence plots of $(C_{D_0}\rho\dot{x})$ vs. time, such as shown in Fig. 12-8, can be readily made for most of

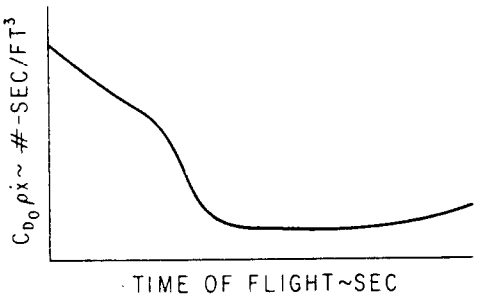

FIG. 12-8. Variation of $C_{D_0}\rho\dot{x}$ with time.

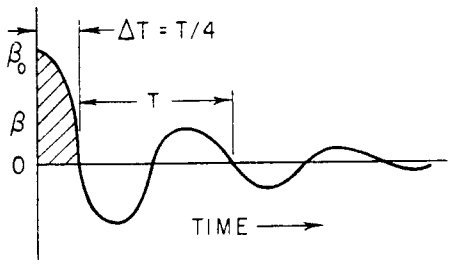

FIG. 12-9. Initial transient response of a typical statically stable missile.

the flight conditions for which the drift dispersions are desired. By simple graphical integration of the $(C_{D_0}\rho\dot{x})$ vs. time curve (Fig. 12-8), the value of $[\dot{y}_W - (\dot{y}_D)_0]/(\dot{y}_W - \dot{y}_D)$ may be calculated vs. flight time of the missile.

The only remaining term that needs to be determined in order to calculate the missile drift rate $\dot{y}_D$ is $(\dot{y}_D)_0$. The term $(\dot{y}_D)_0$ represents the initial drift rate of the missile from initial missile transient due to cross wind. Schematically, the initial transient-response characteristics of a typical stable missile are shown in Fig. 12-9. Again, for a statically stable missile with a reasonably high degree of damping, the value of $(\dot{y}_D)_0$ may be approximated by the first quarter cycle of the initial transient response as shown in Fig. 12-9. During this small time interval Δt the Mach number, q, and density can be assumed to be constant. Hence the impulse due to this initial transient (from Fig. 12-6B) is

$$Y\,\Delta t = m\,\Delta\dot{y}_D = C_{Y_\beta}\beta_0 \tfrac{1}{2}\rho V_R^2 S\,\Delta t \tag{12-19}$$

Since
$$\beta_0 \cong \frac{\dot{y}_W}{V_R}$$

Eq. (12-19) becomes

$$m\,\Delta\dot{y}_D = C_{Y_\beta}\dot{y}_W{}^{1}\!/_{2}\rho V_R S\,\frac{2}{\pi}\,\frac{T}{4} = m(\dot{y}_D)_0 \tag{12-20}$$

where $2/\pi$ is the ratio of the area under a cosine curve to that for a constant β_0 over the time interval Δt (or $T/4$). The period T shown in Fig. 12-9 is related to the yawing-moment derivative C_{n_β}, as

$$T = 2\pi\sqrt{\frac{I_z}{C_{n_\beta}qSd}} \tag{12-21}$$

Hence the value of $(\dot{y}_D)_0$ may be expressed as

$$(\dot{y}_D)_0 = \frac{C_{Y_\beta}\dot{y}_W\dot{x}\rho S}{2m}\sqrt{\frac{I_z}{C_{n_\beta}qSd}} \tag{12-22}$$

Therefore, once the initial conditions in which the cross wind is assumed to occur are known, the value of $(\dot{y}_D)_0$ can be readily calculated by Eq. (12-22). Consequently the drift rate of the missile $\dot{y}_D$,

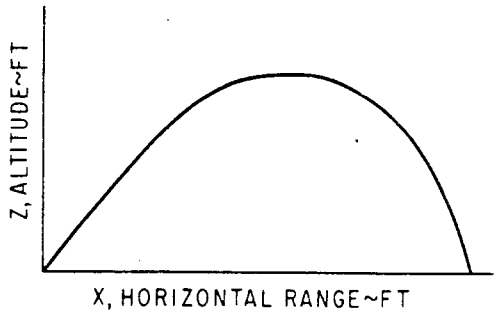

FIG. 12-10. Ideal trajectory (no wind).

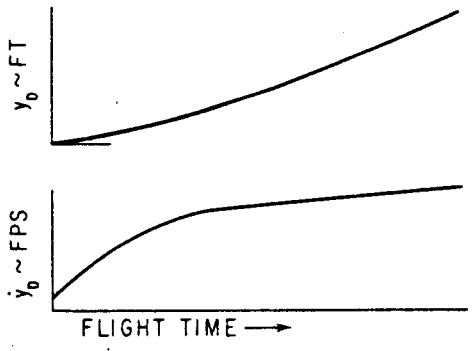

FIG. 12-11. Variation of $\dot{y}_D$ and y_D with time.

may be readily calculated from Eq. (12-18) for the entire trajectory for any cross-wind conditions. The drift dispersion y_D is merely the integral of the $\dot{y}_D$ vs. time curve previously calculated.

A sample calculation is presented in Table 12-1 for clarification, as well as to facilitate future application of the method developed here. The sample presented assumes a cross wind of constant magnitude throughout the entire altitude range of the missile trajectory shown in Fig. 12-10. For cross winds which vary with altitude, Eq. (12-18) is still applicable if incremental altitudes and the average cross-wind for these altitude intervals are used. The drift rate and drift dispersion due to a constant cross wind of 20 fps (occurring at 4 sec after launch) for this sample problem are shown in Fig. 12-11.

4. Determination of Over-all Free-flight Dispersion. In general, the dispersion of a free-flight ballistic missile is of the elliptical pattern. The elliptical probable error is the probability that 50 per cent of all missiles fired will fall within an ellipse defined by

$$\frac{x^2}{\sigma_x^2} + \frac{y^2}{\sigma_y^2} = 1.386 \tag{12-23}$$

where σ_x and σ_y are the standard deviations of error in the x and y direction and may be expressed as

$$\sigma_x = \sqrt{\sigma_{x_1}^2 + \sigma_{x_2}^2 + \sigma_{x_3}^2 + \cdots} \tag{12-24}$$

$$\sigma_y = \sqrt{\sigma_{y_1}^2 + \sigma_{y_2}^2 + \sigma_{y_3}^2 + \cdots} \tag{12-25}$$

where σ_{x_1}, σ_{y_1}, etc., are the standard deviations of error in the x and y direction caused by launcher setting, wind, malalignment effects, etc. When the values of σ_x and σ_y are approximately equal, the error between the elliptical probable error and the circular probable error in defining the area in which 50 per cent of the missiles will fall is negligible. The circular probable error (CEP) is defined as

$$\text{CEP} = 1.18\sqrt{\sigma_x \sigma_y} \tag{12-26}$$

12-4. DISPERSION-SENSITIVITY FACTORS IN VACUUM

Heretofore discussion has been focused on the free-flight dispersion characteristics associated with atmospheric trajectories. This presupposes that trajectory data are available in order to assess these dispersion characteristics. However, for some cases where no trajectory data are available, it is desirable to estimate the order of magnitude of the dispersions resulting from errors in several of the missile trajectory parameters. In addition, it is important to determine the relative importance of these trajectory parameters in order that proper emphasis may be placed on the more important components of the missile system during its early preliminary-design phase. In the following paragraphs, the dispersion-sensitivity factors in vacuum condition are derived and are based on (1) a flat earth, rectilinear coordinate system and (2) a spherical earth, nonrectilinear coordinate system.

TABLE 12-1. SAMPLE CALCULATION ON MISSILE DISPERSION DUE TO CROSS WIND DURING POWER-OFF FLIGHT

Given:	$m = 11.54$ slugs	$\dot{x} = 1{,}770$ fps	$d = 1.0$ ft
	$C_{Y_\beta} = -0.283$ per deg	$\rho = 0.0022$ slug/ft^3	$I_z = 60$ slug/ft^2
	$C_{n_\beta} = 0.549$ per deg	$S = 0.786$ ft^2	$\dot{y}_W = 20$ fps at $t = 4$ sec after launch
	$q = 3{,}468$ psf		

Using Eq. (12-22),

$$(\dot{y}_D)_0 = \frac{(0.283 \times 57.3)(20)(1{,}770)(0.0022)(0.786)}{2(11.54)} \sqrt{\frac{60}{(0.549)(57.3)(3{,}468)(0.786)(1)}}$$

$$= 1.13 \text{ fps}$$

No Wind—Ideal-Trajectory Data

1 t sec	2 ρ	3 $\dot{x}$	4 C_{D_0}	5 $C_{D_0}\rho\dot{x}$	6 t	7 $(C_{D_0}\rho\dot{x})_{av}$	8 $\int_0^t C_{D_0}\rho\dot{x}$	9 $\Sigma(8)$	10 $\frac{s}{2m}$ (9)	11 $\ln\left\{\frac{\dot{y}_W-(\dot{y}_D)_0}{\dot{y}_W-\dot{y}_D}\right\}$	12 $\dot{y}_W-\dot{y}_D$	13 $\dot{y}_D$	14 Δy_D	15 Σy_D, ft
4.00	0.00220	1,777	0.4225	1.650	4	1.46	0	0	0	1.0	18.87	1.13	0	0
5.02	0.00214	1,664	0.4354	1.556	8	1.22	5.84	5.84	0.1985	1.220	15.45	4.55	11.36	11.36
6.62	0.00206	1,511	0.4552	1.416	12	0.74	4.88	10.72	0.3645	1.440	13.10	6.90	22.90	34.26
8.98	0.00197	1,323	0.4914	1.283	16	0.37	2.96	13.68	0.4650	1.594	11.82	8.18	30.16	64.42
10.33	0.00192	1,232	0.5036	1.190	20	0.24	1.48	15.16	0.5150	1.675	11.25	8.75	33.86	98.28
11.13	0.00190	1,183	0.5097	1.142	24	0.24	0.96	16.12	0.5485	1.730	10.90	9.10	35.70	133.98
11.93	0.00188	1,138	0.5137	1.096	28	0.245	0.96	17.08	0.5800	1.786	10.57	9.43	37.06	171.04
12.77	0.00186	1,095	0.4905	0.996	32	0.25	0.98	18.06	0.6140	1.850	10.20	9.80	38.46	209.50
13.65	0.00184	1,055	0.4297	0.830	36	0.26	1.00	19.06	0.6480	1.912	9.86	10.14	39.88	249.38
14.53	0.00182	1,023	0.3397	0.632	40	0.29	1.04	20.10	0.6840	1.983	9.51	10.49	41.26	290.64
15.49	0.00181	996	0.2429	0.438	44	0.33	1.16	21.26	0.7240	2.063	9.13	10.87	42.72	333.36
16.41	0.00179	977	0.1731	0.303	48	0.39	1.32	22.58	0.7680	2.158	8.74	11.26	44.26	377.62
17.47	0.00178	959	0.1542	0.263	50.4*		0.94	23.52	0.7990	2.225	8.48	11.52	27.35	404.97
20.83	0.00175	914	0.1550	0.247										
24.67	0.00174	881	0.1556	0.239										
30.59	0.00178	864	0.1560	0.240										
34.79	0.00184	876	0.1558	0.252										
38.51	0.00193	899	0.1555	0.269										
42.87	0.00206	937	0.1549	0.299										
46.87	0.00222	978	0.1543	0.335										
49.79	0.00235	1,009	0.1727	0.409										

Notes: Total drift dispersion $y_D = 404.97$ ft at end of flight. Columns 1 through 5 from digital computation. Columns 6 through 7 from faired curve (i.e., Fig. 12-8). Column 8 = column 7 $\times \Delta t$. Column 11: see Eq. (12-17).

* End of flight.

1. Flat Earth, Rectilinear Coordinate System. For relatively short range flights whereby a flat earth, rectilinear coordinate system may be assumed, the equations of motion of a point mass in a vacuum are readily expressed from Fig. 12-12.

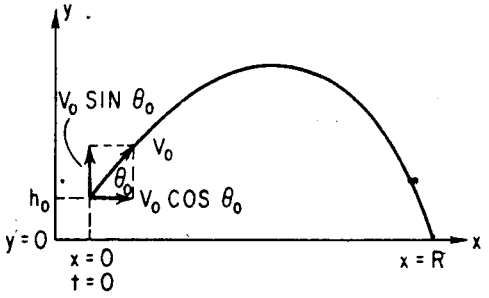

FIG. 12-12. Definition of terms for sensitivity-factor determination (flat earth).

$$\dot{x} = V_0 \cos \theta_0 \tag{12-27}$$

$$\dot{y} = V_0 \sin \theta_0 - gt \tag{12-28}$$

Integrating Eqs. (12-27) and (12-28), we get

$$x = V_0 \cos \theta_0 t + C_1 \tag{12-29}$$

$$y = V_0 \sin \theta_0 t - \frac{gt^2}{2} + C_2 \tag{12-30}$$

From the boundary conditions,

$$t = 0,\ y = h_0 \qquad \text{then } C_2 = h_0$$

$$t = 0,\ x = 0 \qquad \text{then } C_1 = 0$$

Substituting the values of C_1 and C_2 and Eq. (12-29) into (12-30), we get

$$y = x \tan \theta_0 - \frac{gx^2}{2V_0^2 \cos^2 \theta_0} + h_0 \tag{12-31}$$

Since $x = R$ at $y = 0$, Eq. (12-31) becomes

$$0 = R \tan \theta_0 - \frac{gR^2}{2V_0^2 \cos^2 \theta_0} + h_0 \tag{12-32}$$

$$R^2 - \frac{(2V_0^2 \sin \theta_0 \cos \theta_0)R}{g} - \frac{2V_0^2 h_0 \cos^2 \theta_0}{g} = 0 \tag{12-33}$$

hence

$$R = \frac{V_0^2 \sin 2\theta_0}{2g} \pm \frac{V_0}{g} \cos \theta_0 \sqrt{V_0^2 \sin^2 \theta_0 + 2gh_0} \tag{12-34}$$

Since R is positive for $\theta_0 = 0°$ (i.e., $R = V_0\sqrt{2h_0/g}$), the negative sign in the second term of Eq. (12-34) may be neglected. Thus Eq. (12-34) becomes

$$R = \frac{V_0^2 \sin 2\theta_0}{2g} + \frac{V_0 \cos \theta_0}{g} \sqrt{V_0^2 \sin^2 \theta_0 + 2gh_0} \tag{12-35}$$

The dispersion-sensitivity factors due to errors in velocity, altitude, and missile attitude at missile cutoff, $\partial R/\partial V_0$, $\partial R/\partial h_0$, and $\partial R/\partial \theta_0$, respectively, may be obtained by taking the partial derivative of R with respect to V_0, h_0, and θ_0 in Eq. (12-35). These dispersion-sensitivity factors are

$$\frac{\partial R}{\partial V_0} = \frac{V_0 \sin 2\theta_0}{g} + \frac{2 \cos \theta_0 (V_0^2 \sin^2 \theta_0 + g h_0)}{g\sqrt{V_0^2 \sin^2 \theta_0 + 2g h_0}} \tag{12-36}$$

$$\frac{\partial R}{\partial h_0} = \frac{V_0 \cos \theta_0}{\sqrt{V_0^2 \sin^2 \theta_0 + 2g h_0}} \tag{12-37}$$

and

$$\frac{\partial R}{\partial \theta_0} = \frac{V_0^2 \cos 2\theta_0}{g}\left(1 + \frac{V_0 \sin \theta_0}{\sqrt{V_0^2 \sin^2 \theta_0 + 2g h_0}}\right) - \frac{2 h_0 V_0 \sin \theta_0}{\sqrt{V_0^2 \sin^2 \theta_0 + 2g h_0}} \tag{12-38}$$

For $\theta_0 = 0°$ (i.e., free flight commencing at the apogee) condition, the above expressions can be simplified as

$$R = V_0\sqrt{\frac{2h_0}{g}} \tag{12-39}$$

$$\frac{\partial R}{\partial V_0} = \sqrt{\frac{2h_0}{g}} \tag{12-40}$$

$$\frac{\partial R}{\partial h_0} = \frac{V_0}{\sqrt{2g h_0}} \tag{12-41}$$

$$\frac{\partial R}{\partial \theta_0} = \frac{V_0^2}{g} \tag{12-42}$$

Although the above expressions are applicable only for the vacuum (drag-free) flight condition, they are useful in that the order of magnitude of the dispersions as well as the relative importance of the various trajectory parameters (i.e., V_0, h_0, and θ_0) may be readily determined. The range and sensitivity factors for two actual flight conditions using the drag of a typical missile configuration have been computed and

compared with the values derived from Eqs. (12-39) through (12-42) below.

$V_0 = 1{,}000$ fps, $h_0 = 5{,}000$ ft	$V_0 = 1{,}000$ fps, $h_0 = 10{,}000$ ft
$R = 16{,}500$ ft (actual condition)	$R = 23{,}000$ ft (actual)
$= 17{,}700$ ft (vacuum condition)	$= 25{,}000$ ft (vacuum)
$\frac{\partial R}{\partial h_0}$ = 1.60 ft/ft (actual)	= 1.10 ft/ft (actual)
$\frac{\partial R}{\partial h_0}$ = 1.77 ft/ft (vacuum)	= 1.25 ft/ft (vacuum)
$\frac{\partial R}{\partial V_0}$ = 13.0 ft/fps (actual)	= 17.8 ft/fps (actual)
$\frac{\partial R}{\partial V_0}$ = 17.7 ft/fps (vacuum)	= 25.0 ft/fps (vacuum)
$\frac{\partial R}{\partial \theta_0}$ = 26.4 ft/mil (actual)	= 25.4 ft/mil (actual)
$\frac{\partial R}{\partial \theta_0}$ = 31.0 ft/mil (vacuum)	= 31.0 ft/mil (vacuum)

2. Spherical Earth, Nonrectilinear Coordinate System. For long-range ballistic flight trajectories such as those of the ICBM's, the dispersion-sensitivity factors for a vacuum (drag-free) flight condition may be readily determined from the simplified expression for the range[6] [Eq. (4-43)] shown below.

$$R = 2r_0 \tan^{-1} \frac{\sin \theta_f \cos \theta_f}{1/\bar{V}_f^2 - \cos^2 \theta_f} \tag{12-43}$$

where $\bar{V}_f = V_f/V_s$ = ratio of cutoff velocity to satellite velocity
θ_f = angle of incidence as shown in Fig. 4-16

Substituting V_f/V_s for $\bar{V}_f$ and deleting the subscript f in θ, Eq. (12-43) becomes

$$R = 2r_0 \tan^{-1} \frac{\sin \theta \cos \theta}{(V_s/V_f)^2 - \cos^2 \theta} \tag{12-44}$$

Taking the partial derivative of R with respect to V and θ, the dispersion-sensitivity factors become

$$\frac{\partial R}{\partial V} = 4r_0 \frac{\sin \theta \cos \theta (V_s^2/V^3)}{\left\{1 + \left[\frac{\sin \theta \cos \theta}{(V_s/V)^2 - \cos^2 \theta}\right]^2\right\}\left[\left(\frac{V_s}{V}\right)^2 - \cos^2 \theta\right]^2} \tag{12-45}$$

and

$$\frac{\partial R}{\partial \theta} = \frac{2r_0}{\left\{1 + \left[\frac{\sin \theta \cos \theta}{(V_s/V)^2 - \cos^2 \theta}\right]^2\right\}} \left\{\frac{(\cos^2 \theta - \sin^2 \theta)}{\left[\left(\frac{V_s}{V}\right)^2 - \cos^2 \theta\right]} - \frac{2 \sin^2 \theta \cos^2 \theta}{\left[\left(\frac{V_s}{V}\right)^2 - \cos^2 \theta\right]^2}\right\} \tag{12-46}$$

The values of the above sensitivity factors have been computed for

the optimum cutoff attitude (see Fig. 4-14*b*) for ranges of 2,000- and 4,000-nautical-mile ballistic-missile flight conditions. These values are shown below to indicate the order of magnitude of these sensitivity factors.

$R = 2{,}000$ nautical miles	$R = 4{,}000$ nautical miles
$\theta = 37°$	$\theta = 28.5°$
$V = 17{,}300$ fps	$V = 21{,}700$ fps
$V_s = 25{,}900$ fps	$V_s = 25{,}900$ fps
$h_0 = 0$ ft	$h_0 = 0$ ft
$r_0 = 20.9 \times 10^6$ ft	$r_0 = 20.9 \times 10^6$ ft
$\frac{\partial R}{\partial V} = 1{,}558$ ft/fps	$\frac{\partial R}{\partial V} = 3{,}293$ ft/fps
$\frac{\partial R}{\partial \theta} = -2{,}990$ ft/mil	$\frac{\partial R}{\partial \theta} = -2{,}470$ ft/mil

12-5. REENTRY-BODY DESIGN CONSIDERATIONS

One of the most important subsystems of a long-range ballistic-missile system is the reentry body. In view of the order of magnitude of the dispersion-sensitivity factors due to errors in cutoff velocity and missile attitude, $\partial R/\partial V$ and $\partial R/\partial \theta$ discussed in the previous section, it is of paramount importance that the reentry-body configuration must be designed which will result in the lowest possible free-flight dispersion. On the other hand, it must also be optimized from other design considerations, i.e., aerodynamic heating, minimum structural weight, reliability, etc.

In general, it is desirable to avoid the use of a guidance system in the reentry body in order to minimize the cost of the missile as well as to improve the reliability of the reentry-body subsystem. Hence, the reentry-body configuration must be carefully designed in order that its free-flight dispersion resulting from atmospheric disturbances, i.e., wind shears, cross winds, etc., is within the specification limits. From the discussion in Sec. 12-3, it is apparent that a low-drag configuration is desirable from the standpoint of minimum free-flight drift dispersion due to cross winds. Specifically, it is desirable to make the value of $C_D S/m$, commonly known as the "ballistic factor," as low as possible to achieve low free-flight dispersion due to wind effects. A low value of ballistic factor has the added advantage that the impact Mach number for a given flight range is greater; hence the vulnerability to enemy countermeasures is reduced. In addition, a reentry-body configuration with a low ballistic factor minimizes the separation problem since

the force required to separate the reentry body from its last-stage booster is decreased or may be completely eliminated. In the latter case, separation is achieved by the force of gravity simply by releasing a clamp which holds the structures of the two bodies together during their exit flight.

While a low drag or ballistic factor is desirable from the standpoints of free-flight dispersion, vulnerability, etc., the problems associated with aerodynamic heating become more severe. Hence a severe weight penalty may be imposed by the added material required to protect the reentry body during its terminal flight. At the present, the two most feasible techniques used in combating this heating problem are (1) the heat-sink method and (2) ablation. The former method involves using a material which absorbs most of the heat generated while the latter method involves using a material which melts or ablates off during reentry. Other methods such as cooling the surface by a liquid, alteration of the flow over the body by protruding spikes, or magnetohydrodynamic are being investigated for possible future applications. The selection of the best method can be made only after a thorough analysis of the magnitude and rate of heat transfer, the cost and availability of materials, etc.

In addition to the problems associated with the dispersion and aerodynamic heating, consideration must be given to the dynamic-response characteristics of the reentry body during its critical terminal flight. In general, a reentry body without a control or guidance system must be statically and dynamically stable. Static stability is required in order to prevent the reentry body from tumbling during its entire terminal flight. Adequate damping is desirable since it reduces the induced drag and hence its dispersion during its flight in the sensible atmosphere. In addition, good damping characteristics decrease the severity of the aerodynamic loading and heating during reentry. Spinning the reentry body prior to its terminal flight into the atmosphere may be used to obtain stability and to nullify the detrimental effects of aerodynamic out of trim. Readers are referred to the partial list of reports (refs. 7 through 18) for detailed treatments of many of the important aspects of reentry-body design.

SYMBOLS

C_D drag coefficient
C_n yawing-moment coefficient
C_y side force

C_1, C_2	constants of integration
D	drag
D_0	drag at zero lift or normal force
F	force
I	rocket-motor impulse
I_x, I_z	moment of inertia about the X and Z axis
R	range of the missile
S	reference area
T	period of oscillation
V	forward velocity
V_f	cutoff velocity
$\overline{V}_f$	ratio of V_f to V_s
V_R	resultant forward velocity
V_s	satellite velocity
W	weight of missile
W_E	burnout weight of missile
X	range of missile
Y	side force
Z	altitude
d	body diameter
h	altitude
m	mass
$C_D S/m$	"ballistic factor"
q	dynamic pressure
r_0	radius of earth
t	(flight) time
x	down-range (in X direction)
y	distance in the azimuth direction
$\dot{y}_D$	drift rate
$\dot{y}_W$	wind velocity
β	angle of sideslip
γ_L	launch attitude
ρ	air density
θ_f	angle of incidence as shown in Fig. 4-16
σ_x, σ_y	standard deviations of error in the x and y direction

Subscripts

D	drift
p	pitch setting
y	azimuth setting
0	initial condition

REFERENCES

1. Rosser, J. B., R. R. Newton, and G. L. Gross: "Mathematical Theory of Rocket Flight," McGraw-Hill Book Company, Inc., New York, 1947.

2. Davis, L., Jr., J. W. Follin, Jr., and L. Blitzer: "The Exterior Ballistics of Rockets," D. Van Nostrand Company, Inc., Princeton, N.J., 1958.

3. Hunter, M. W., A. Shef, and D. V. Black: Some Recent Aerodynamic Techniques in Design of Fin-stabilized Free-flight Missiles for Minimum Dispersion, *J. Aeronaut. Sci.*, vol. 23, no. 6, pp. 571–577, June, 1956.

4. Oswald, T. W.: Dynamic Behavior during Accelerated Flight with Particular Application to Missile Launching, *J. Aeronaut. Sci.*, vol. 23, no. 6, pp. 781–791, August, 1956.

5. Whitehurst, J. W.: "Some Aspects of Missile Launch Dispersion," The Catholic University of America 1959 First Award Papers, IAS Regional Student Conferences, 6th annual ed., The Minta Martin Aeronautical Student Fund.

6. Eggers, A. J., H. J. Allen, and S. E. Niece: A Comparative Analysis of the Performance of Long-range Hypervelocity Vehicles, *NACA Tech. Note* 4046, October, 1957.

7. Allen, H. J., and A. J. Eggers, Jr.: A Study of the Motion and Aerodynamic Heating of Missiles Entering the Earth's Atmosphere at High Supersonic Speeds, *NACA Tech. Note* 4047, October, 1957.

8. Allen, H. J.: Motion of a Ballistic Missile Angularly Misaligned with the Flight Path upon Entering the Atmosphere and Its Effects upon Aerodynamic Heating, Aerodynamic Loads, and Miss Distance, *NACA Tech. Note* 4048, October, 1957.

9. Tobak, M., and W. R. Wehrend: Stability Derivatives of Cones at Supersonic Speeds, *NACA Tech. Note* 3788, September, 1956.

10. Nelson, R. L.: The Motions of Rolling Symmetrical Missiles Referred to a Body-axis System, *NACA Tech. Note* 3737, November, 1956.

11. Charters, A. C.: The Linearized Equations of Motion Underlying the Dynamic Stability of Aircraft, Spinning Projectiles, and Symmetrical Missiles, *NACA Tech. Note* 3350, January, 1955.

12. Philips, W. H.: Effect of Steady Rolling on Longitudinal and Directional Stability, *NACA Tech. Note* 1627, June, 1958.

13. Bolz, R. E.: Dynamic Stability of a Missile in Rolling Flight, *J. Aeronaut. Sci.*, vol. 19, no. 6, pp. 395–403, June, 1952.

14. Laitone, E. V.: Dynamic Longitudinal Stability Equations for the Re-entry Ballistic Missile, *J. Aeronaut. Sci.*, vol. 26, no. 2, pp. 94–98, February, 1959.

15. Bogdonoff, S. M., and I. E. Vas: Preliminary Investigations of Spiked Bodies at Hypersonic Speeds, *J. Aeronaut. Sci.*, vol. 26, no. 2, pp. 65–74, February, 1959.

16. Allen, H. J.: Hypersonic Flight and the Re-entry Problem (Twenty-first Wright Brothers Lecture), *J. Aeronaut. Sci.*, vol. 25, no. 4, pp. 217–227, April, 1958.

17. Singer, S. F., and R. C. Wentworth: A Method for Calculating Impact Points of Ballistic Rockets, *Jet Propulsion*, vol. 27, no. 4, pp. 407–409, April, 1957.

18. Robertson, R. E.: Impact Points of Ballistic Rockets, *Jet Propulsion*, vol. 27, no. 12, p. 1256, December, 1957.

CHAPTER 13

POWER-PLANT-DESIGN CONSIDERATIONS

13-1. INTRODUCTION

Heretofore the discussion on missile configuration design has been focused primarily from the aerodynamic standpoint. Since the power plant constitutes a major component of the over-all configuration of the missile, it is well to discuss some of its more important design aspects and how it affects the configuration of the missile. The type of power plant selected is primarily dictated by the type of mission the missile is designed to accomplish. The selected power plant may be one of the many which will be described in a later section. Its installation must then be optimized from the standpoint of the over-all efficiency of the external configuration. It may be installed as an integral part of the main body of the missile, as in the case of a solid-propellant or prepackaged-liquid rocket motor, or it may be pylon-mounted, particularly in the case of air-breathing power plants. For certain missions, it may be advantageous to use a combination of an integral rocket or pylon-mounted power plant and an external droppable booster. The optimum installation can be made only after a thorough analysis of the problems involved has been made.

13-2. TYPES OF POWER PLANT

There are a great variety of propulsive devices ranging from the time-tested, reliable reciprocating engine to the more recently developed air turbo rocket. Each of these power plants has its advantages and disadvantages as well as limitations regarding its applications. Categorically speaking, it can be said that all air-breathing engines are limited to operation in the lower atmosphere whereas rocket engines, which carry their own oxidizer, may be used at all altitudes. Thus, for altitudes below approximately 20 miles, both rockets and air-breathing engines may be used whereas, above this altitude, only rockets may be

considered. From the standpoint of efficient operation, the velocity ranges are considered for the following types of power plant:

Mach No. range	*Propulsion system*
0 to 0.7	Piston engine and propeller
0.5 to 0.8	Turboprop
0.7 to 2.5	Turbojet
2.0 and 4.0	Ram jet, air turbo rocket, rocket
4.0 and up	Rocket

1. Reciprocating Engine. The four-stroke-cycle spark-ignition engine is probably the simplest in principle of all prime movers.

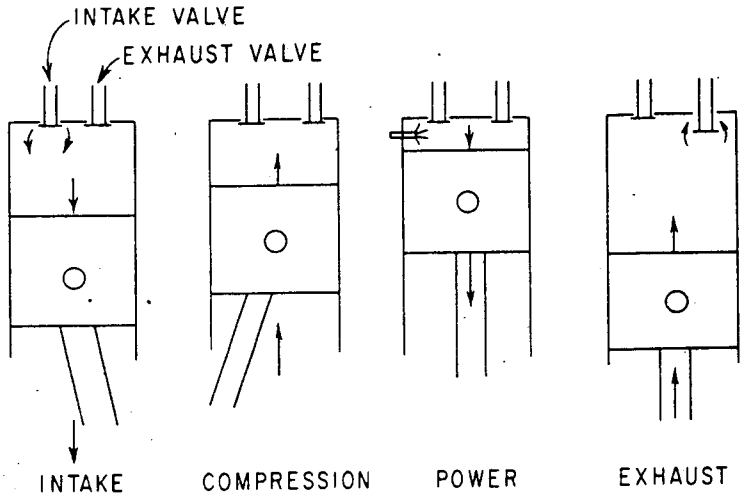

FIG. 13-1. Four-stroke-cycle reciprocating engine.

As shown in Fig. 13-1, a piston reciprocating in a cylinder draws a mixture of fuel and air in through the intake valve during its downward stroke and compresses the mixture on its subsequent upward stroke. An electric spark then occurs, which ignites the gas mixture, releasing chemical energy in the form of heat, which in turn causes a substantial increase in pressure. This increased pressure forces the piston downward, delivering mechanical power to the crankshaft. When the piston reaches the bottom of the cylinder, the exhaust valve opens to allow the burned gases to push out on the exhaust stroke. Figure 13-2 shows the pressure and temperature characteristics of the fuel-air mixture as a function of piston travel.

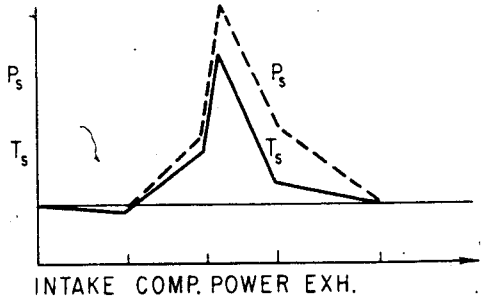

FIG. 13-2. Pressure and temperature as function of stroke—four-cycle reciprocating engine.

The reciprocating engine has the advantage of very low specific fuel consumption and relatively high static power. These favorable characteristics make this type of engine far superior to any other type of engine for relatively low speed and low altitude operation.

2. Turbojet. The major components of a turbojet engine are the compressor, combustion chamber, and the turbine to drive the compressor as shown schematically in Fig. 13-3. Atmospheric air enters the diffuser, where it is partially compressed to reduce its velocity. As it passes through the compressor, its pressure is raised to several times

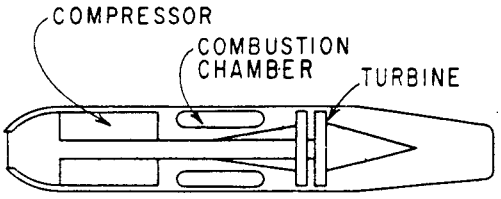

FIG. 13-3. Schema of a turbojet.

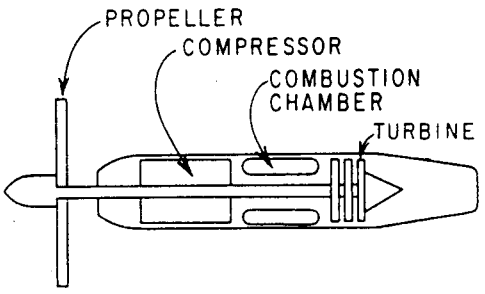

FIG. 13-4. Schema of a turboprop.

its original value. The temperature also increases appreciably. Between the compressor outlet and the combustion chamber, the air undergoes a slight diffusion. In the combustion chamber, heat is added to raise the energy level of the gases. Although the process of combustion is essentially a constant-pressure process, a slight pressure loss occurs because of friction and momentum changes. From the combustion chamber, the hot gases are expanded through the turbine, which extracts just enough energy to drive the compressor and to overcome bearing friction. The gases then flow through the exhaust nozzle to increase the kinetic energy and obtain thrust.

3. Turboprop. This engine is practically identical to the turbojet. The differences are primarily due to the manner in which the generated power is used. Where the principal function of the turbojet is to produce thrust in the form of an exhaust jet, the turboprop uses most of the energy of the gases to drive a propeller, as shown in Fig. 13-4.

4. Air Turbo Rocket. This type of engine, which combines the essential features of both the turbojet and rocket, is in the development stage. A gas generator, using ethylene oxide as a monopropellant, produces gas which exhausts through a turbine, which in turn drives a single-stage axial-flow compressor as shown in Fig. 13-5. JP-4 fuel is

introduced and burned downstream in what is essentially an afterburner. Thrust is obtained from both the JP-4 air mixture and the gases from the ethylene oxide reaction. This engine would have the advantage of being capable of operating at very high Mach numbers (up to 4.0) and yet producing a high thrust at static sea-level condition. The chief disadvantages are (1) very high fuel consumption and (2) high vapor pressure.

5. Ram Jet. The most important feature of a ram-jet engine is that it has no moving parts in the engine proper. For this reason, it

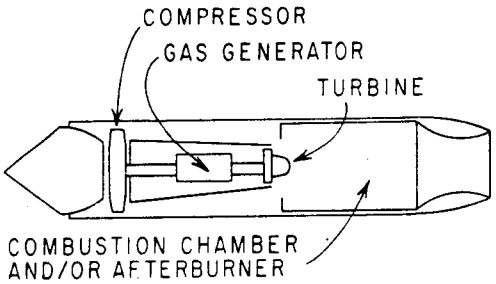

FIG. 13-5. Schema of an air turbo-rocket.

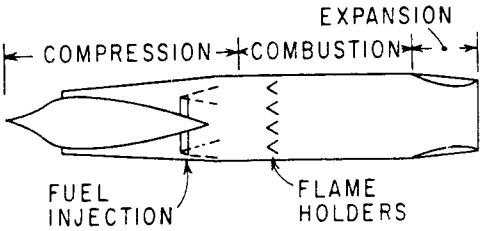

FIG. 13-6. Schema of a ramjet.

is simple, easily fabricated, and relatively inexpensive. The basic components, as shown schematically in Fig. 13-6, are an inlet, a combustion chamber, and a nozzle. The operating cycle is basically similar to other jet engines, i.e., compression, burning, and expansion. Entering air is diffused as it flows to the burner section. Fuel is injected and burned. The hot gases are then expelled at high velocity through the nozzle to develop thrust. This type of engine is a continuing burning device operating with a continuous flow of air. Hence a ram-jet-powered vehicle must have an initial velocity before the ram jet can operate. Since the compression ratio and hence power output increase with speed, the ram jet is generally used only for flights at relatively high supersonic speeds.

6. Rocket. The rocket is technically a jet engine. It differs from the air-breathing type in that it does not depend upon the atmospheric air as an oxidizing agent. Both the fuel or propellant(s) and the oxidizing agent are carried within the rocket motor. The propelling action is derived from the generation of large quantities of gases by the chemical reaction of propellants within the combustion chamber. These gases are expelled with supersonic velocity.

For sustained or intermittent operation over relatively long periods of time, the liquid-propellant rocket is generally used. The duration

depends primarily on the quantity of fuel available. The operating pressures are lower than those employed by the solid-propellant units (300 to 750 psi as compared with 1,500 to 3,000 psi). Because of their reliability and handling characteristics, etc., the solid-propellant units are becoming more "popular" in filling the bill that has normally been filled by the liquid-propellant rockets. Design considerations for both liquid- and solid-propellant rockets will be presented in a later section of this chapter.

13-3. FUNDAMENTALS OF ROCKET ENGINES

1. Principles of Rocket Propulsion. Rocket propulsion is one form of jet propulsion which involves forward thrust or motion due to rearward ejection of high-velocity gases or fluid jet. The principle of jet propulsion is based on Newton's third law of motion, which states that for every action there is an equal and opposite reaction. In a rocket engine, the force of the momentum of the rearward ejection of hot gases imparts a reverse or forward thrust to the engine.

2. General Equations. In the quantitative analysis of the performance of a rocket engine, it is generally assumed that the chemical reactions in the combustion chamber are in the state of thermochemical equilibrium. This assumption appears to be quite valid except where high-energy fuels are considered. For the latter type of fuel, the exact nature of their thermochemical reactions has not been completely determined. Because of the strong possibility of ionization and recombination in the products of combustion in the nozzle and downstream of the nozzle, an exact determination of the performance of a rocket motor using these high-energy fuels cannot be easily made by theoretical analysis. Hence experimental means involving static firings, etc., must be employed. Another important assumption made is that the flow within the rocket engine is isentropic. This assumption is generally valid as long as the nozzle is designed so that the gases undergo a full or underexpansion at the exit of the nozzle. A condition of full expansion is one in which the gases have been expanded from a high pressure from the combustion chamber to a pressure at the nozzle exit equal to the ambient. A condition of underexpansion is one in which the exit pressure of the gases is higher than the ambient pressure. The assumption of isentropic flow for a condition of overexpansion (exit pressure less than ambient pressure) may be completely unjustifiable, particularly when the ambient pressure is very much greater than the exit pressure of the gases because of flow separation

and shock formation within the nozzle. However, with careful design practices, the above assumptions may be used in the quantitative prediction of the performance of the rocket engine.

The thrust of a rocket engine is the resultant pressure of forces acting upon its outer and inner surfaces and may be expressed as

$$T = \int_{A_o} p_o \, dA_x + \int_{A_i} p_i \, dA_x \tag{13-1}$$

where T = thrust
p_o = outside or ambient pressure
p_i = inside pressure
A_x = axial or x component of wall of rocket engine

From Fig. 13-7, the value of the first integral is

$$\int_{A_o} p_o \, dA_x = -p_o A_e \tag{13-2}$$

where A_e is the exit area of the nozzle. From the momentum theorem, which states that the integral of all the pressure forces acting on a mathematical closed surface is equal to the momentum flux through the surface, the second integral may be written as

$$\int_i p \, dA_x - \int_e p_e \, dA_x = M_x \tag{13-3}$$

where p_e = pressure at the nozzle exit
M_x = momentum flux in the axial direction and may be written as

$$\int_e \rho V_x^2 \, dA_x$$

Hence Eq. (13-1) becomes

$$T = \int_e \rho V_x^2 \, dA_x + \int_e p_e \, dA_x - p_o A_e \tag{13-4}$$

Since

$$\int_e \rho V_x^2 \, dA_x = \frac{\dot{W}_p}{g} V_j \tag{13-5}$$

and

$$\int_e p_e \, dA_x = p_e A_e \tag{13-6}$$

Equation (13-4) becomes

$$T = \frac{\dot{W}_p V_j}{g} + (p_e - p_o) A_e \tag{13-7}$$

where $\dot{W}_p$ = propellant-weight flow rate
V_j = exit velocity of exhaust gas

In the above derivation it was assumed that the exit velocity is parallel to the direction of the thrust. For nozzles with a large divergence angle α as shown in Fig. 13-8, a divergence coefficient λ must be applied. The value of λ is defined as[1,*]

$$\lambda = \frac{1 - \cos 2\alpha}{4(1 - \cos \alpha)} = \tfrac{1}{2} + \tfrac{1}{2} \cos \alpha \tag{13-8}$$

and is plotted in Fig. 13-8. Hence Eq. (13-7) becomes

$$T = \lambda \frac{\dot{W}_p V_j}{g} + (p_e - p_o)A_e \tag{13-9}$$

From Eq. (13-9), it is seen that for a fully expanded (or design) condition the term $(p_e - p_o)$ is equal to zero. For underexpansion, the

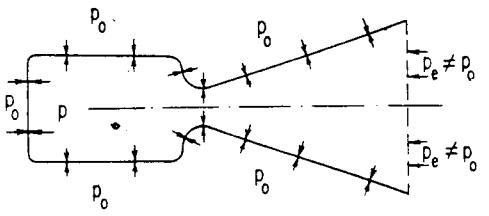

FIG. 13-7. Pressure forces.

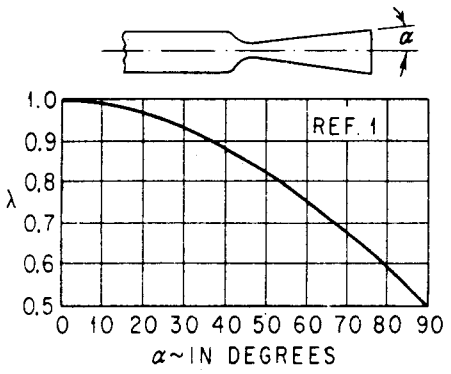

FIG. 13-8. Divergent coefficient vs. divergence angle.

value of thrust is increased by the amount $(p_e - p_o)A_e$. Thus, for operation at altitudes above the design altitude, the nozzle and hence the rocket engine becomes more efficient. Conversely, below design altitudes, the rocket engine is less efficient.

The thrust coefficient is often used as a measure of performance of the nozzle or the expansion process in the nozzle and is used as follows:

$$T = C_T p_c A_t \tag{13-10}$$

where C_T = thrust coefficient
p_c = chamber pressure
A_t = throat area of nozzle

* Superscript numbers indicate references listed at the end of the chapter.

From relationships derived for isentropic flow through a converging-diverging (DeLaval-type) nozzle, the thrust coefficient may also be expressed as

$$C_T = \sqrt{\frac{2\gamma^2}{\gamma - 1}\left(\frac{2}{\gamma + 1}\right)^{(\gamma+1)/\gamma(-1)}\left[1 - \left(\frac{p_e}{p_c}\right)^{(\gamma-1)/\gamma}\right]} + \frac{p_e - p_o}{p_c}\frac{A_e}{A_t} \qquad (13\text{-}11)$$

The values of C_T for condition of full expansion ($p_e = p_o$) for various values of γ and p_c/p_e have been calculated and are presented in Fig. 13-9.

Another useful expression involves the area ratio (defined as ratio of throat area to exit area of the nozzle) required for complete or full

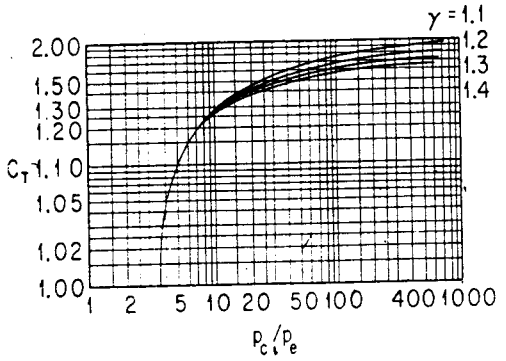

FIG. 13-9. Thrust coefficient vs. p_c/p_e for various γ's—full-expansion condition.

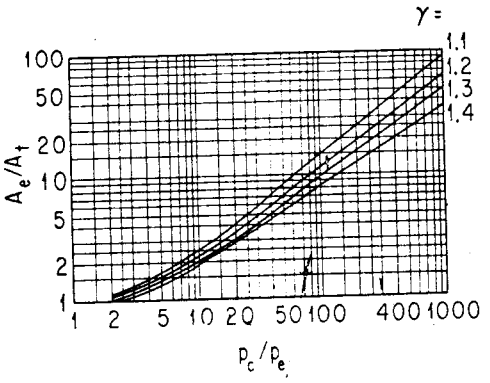

FIG. 13-10. Variation of A_e/A_t with p_c/p_e for various γ's—full-expansion condition.

expansion. This ratio may be expressed as a function of γ and p_e/p_c as follows:

$$\frac{A_t}{A_e} = \left(\frac{\gamma + 1}{2}\right)^{1/(\gamma-1)}\left\{\left(\frac{p_e}{p_c}\right)^{1/\gamma}\sqrt{\frac{\gamma + 1}{\gamma - 1}\left[1 - \left(\frac{p_e}{p_c}\right)^{(\gamma-1)/\gamma}\right]}\right\} \qquad (13\text{-}12)$$

Values of A_t/A_e for various values of γ and p_c/p_e are shown in Fig. 13-10

Other equations and definitions which are useful in rocket-motor performance analysis are (1) fuel specific impulse, (2) over-all specific impulse, (3) total impulse, and (4) characteristic velocity. The fuel specific impulse I_{sp} is defined as the ratio of total impulse to fuel weight and may be expressed as

$$I_{sp} = \frac{\int_0^{t_b} T\,dt}{W_p} = \frac{I}{W_p} \quad \text{sec} \qquad (13\text{-}13)$$

where t_b = total burning time of rocket motor

It may also be expressed as

$$I_{sp} = \frac{T}{\dot{W}_p} \qquad \text{sec} \tag{13-13a}$$

The over-all specific impulse I_o is defined as the ratio of total impulse to total motor weight and is expressed as

$$I_o = \frac{\int_0^{t_b} T\,dt}{W_m} \qquad \text{sec} \tag{13-14}$$

where W_m = total rocket-motor weight (propellant plus inert weights)
The total impulse I is defined as the integral of the thrust vs. burning-time curve and is expressed as

$$I = \int_0^{t_b} T\,dt \qquad \text{lb-sec} \tag{13-15}$$

The characteristic velocity C^* is a measure of the efficiency of the propellant of the rocket motor and is defined as

$$C^* = \frac{V_j}{C_T} = \frac{gp_cA_t}{\dot{W}_p} \tag{13-16}$$

13-4. ROCKET-MOTOR-DESIGN CONSIDERATIONS

The selection of either a liquid- or solid-propellant rocket motor is perhaps one of the most complex problems a designer must solve before an optimum missile configuration and weapon system can be realized. Each type has its advantages and disadvantages which the designer must consider in detail before a compromise can be made. The following sections are devoted to a discussion of some of the various design aspects associated with each type in order to provide a fuller appreciation of the problems involved.

1. Liquid-propellant Rocket Motor. Until recently, liquid propellant rockets have been used exclusively to propel such vehicles as ballistic missiles, high-altitude-research vehicles, and ICBM's. The employment of liquid rockets was long undisputed because:

a. It was the only type of propulsion system far along in its development that could ensure, with some degree of reliability, long duration of sustained or intermittent operation.

b. It can provide thrust-vector control with relative ease by gimbaling of the thrust chamber.

However, with the advent of solid-propellant rocketry in recent years, parts of the above which used to be characteristic of liquid rockets have been largely nullified. The details of solid rockets are discussed in subsequent paragraphs.

A liquid-propellant rocket system generally consists of the following:

a. One or more tanks to store the propellants—depending on the type of propellants used (monopropellants or bipropellants)

b. A feed mechanism for forcing the liquids into the thrust chamber

c. A power source to furnish the energy required by the feed mechanism

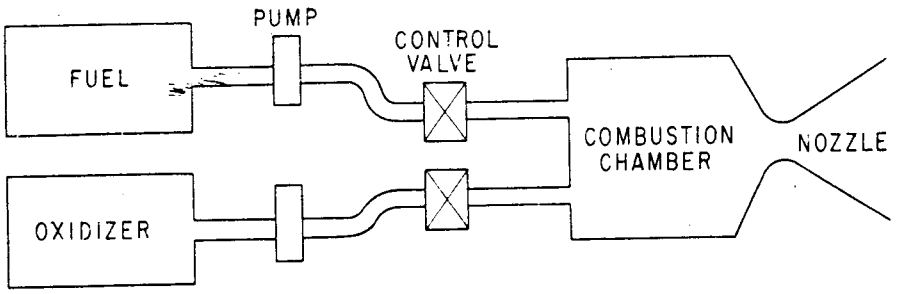

FIG. 13-11. Schema of a liquid-propellant rocket motor.

d. A control device for regulating the propellant flow rates

e. A chamber for combustion

f. An expansion nozzle

A typical liquid system is schematically shown in Fig. 13-11.

One of the most attractive features of a liquid-propellant rocket motor is that the motor may be throttled, stopped, and restarted during missile flight. Hence it is relatively simple to program the thrust desired for a given mission. In addition, the specific impulse of liquid propellant is generally higher than that of a solid propellant. Gimbaled nozzles and thrust chambers are practical on this type of motor for thrust-vector control. Another attribute of a liquid-propellant rocket motor is that regenerative cooling of the nozzle using its own fuel supply is feasible and practical. Liquid-propellant rocket motors also offer good (range) growth potential by increasing the volume of the fuel tanks.

Because of the more complex nature of a liquid-propellant rocket-motor system, it is inherently less reliable and generally more costly. Despite the higher values of fuel specific impulse, the additional weight due to auxiliary devices such as pumps, valves, and fuel lines may result in an over-all specific impulse equal to or less than that realized on

a solid-propellant rocket motor. Sloshing of the liquid fuel may create a dynamic problem unless suitable baffles or pressurization are provided. Finally, the fuel-handling problems including the toxic effects on personnel and the long count-down to get the missile to firing status may be highly undesirable for most missile weapon systems. This undesirable feature is presently amelioriated through the development of "prepackaged" liquid-propellant rocket motors[2] which eliminate the long count-down and can be stored in the "ready" state.

Presently, "prepackaged" liquid-propellant rocket motors have been restricted to total impulses in the neighborhood of 50,000 lb-sec and below. Additional development is necessary to prove their design feasibility for the higher total impulse required for long-range ballistic missiles. The "prepackaged" liquid-propellant rocket motor is relatively simple since it requires no pumps, valves, etc., which are required for other liquid-propellant units. A solid-charge propellant gas generator within the motor provides the pressurization which forces the liquid propellant into the combustion chamber.

2. Solid-propellant Rocket Motor. A typical solid-propellant rocket motor is schematically shown in Fig. 13-12. The principal components of this type of motor are:

a. Propellant grain
b. Chamber
c. Nozzle
d. Igniter

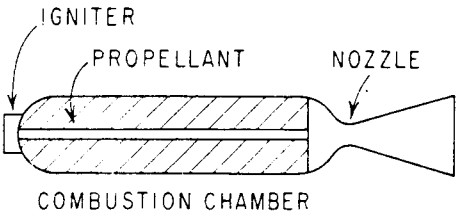

FIG. 13-12. Schema of a solid-propellant rocket motor.

The grain configuration of internal burning varies greatly and is governed by the desired thrust-time history. In general, regressive burning (thrust decreases with time) is desired to keep the axial g of a missile to a minimum. However, many other factors are involved in the final selection of the thrust-time history or grain configuration. Some typical grain configurations used are shown in Fig. 13-13 for various thrust-time histories.

Solid propellants are composed of solid mixtures of an oxidizer and a combustible fuel. Presently, there are two general types of propellants: double-base and composite. Double-base propellants consist essentially of nitrocellulose colloided with nitroglycerin. The composite propellants consist principally of crystalline oxidizer (an inorganic salt such as potassium perchlorate, ammonium perchlorate, or ammonium nitrate) and a polymeric binder such as synthetic rubber,

plastic, or polystyrene. These propellants may be either mechanically extruded or cast into the proper grain geometry such as those shown in Fig. 13-13.

The art of designing solid-propellant units has been significantly advanced over the past decade, so that this type of rocket motor is now highly competitive with liquid-propellant units. Development in solid propellants together with technological advances in high-strength materials result in the attainment of very high values of fuel specific

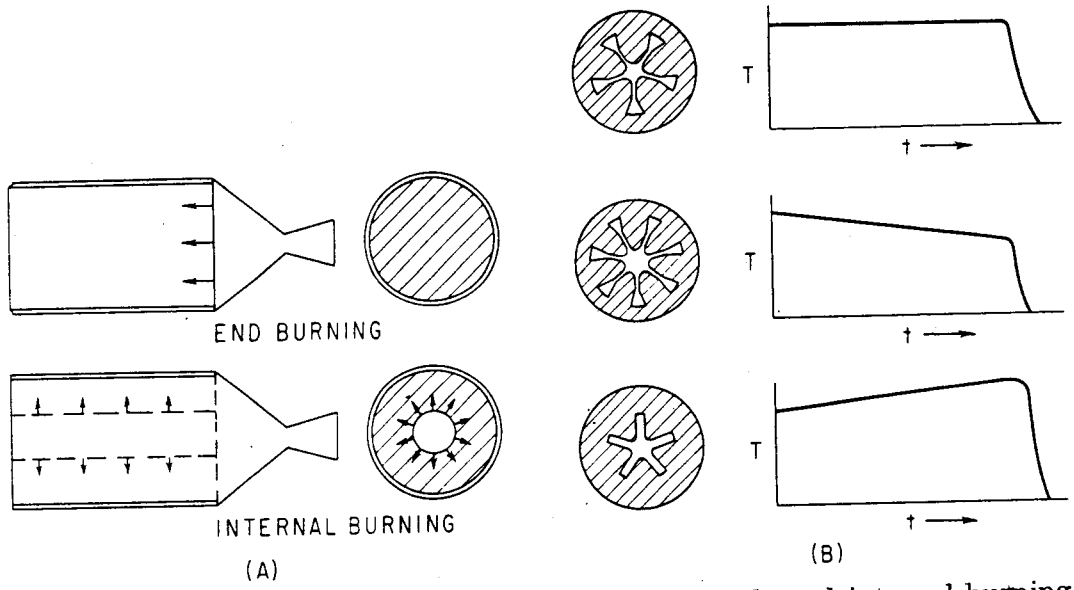

FIG. 13-13. Propellant grain configurations. (*A*) End- and internal-burning motors. (*B*) Various thrust histories.

impulse and motor mass fraction or over-all specific impulse. Furthermore, with the inherent simplicity due to the elimination of moving parts such as pumps and valves, solid-propellant rocket motors have been considered and used on practically all types of missiles. Logistics is another consideration which favors this type of rocket motor very heavily.

Recent development has indicated that thrust termination can be effected by nozzle blow-out or by blowing out ports in the forward section of the combustion chamber. By this means the chamber pressure can be reduced below that required for sustained burning and hence terminate the thrust. Careful design must be made in order that random reignition does not occur once burning is stopped. The accomplishment of thrust termination and vector control (jet vanes and jetavators) paves the way for application of this type of motor to ballistic missiles which require thrust cutoff for different range

missions. It has been shown (see Sec. 12-4) that an error in the burnout velocity has a large detrimental effect on the accuracy of the ballistic missile. Hence it is important that thrust termination of the propellant unit be accurately accomplished and with a good degree of repeatability from one motor to another.

Several undesirable features are present in the solid-propellant rocket motors. One of the most outstanding of these is that the unit cannot be throttled or restarted once it has been shut off. Another undesirable feature is that for certain types of solid propellants the temperature sensitivity may be very high. Since most missile weapon systems are designed to operate over a wide range of temperature conditions (usually from -65 to $+160°F$), the propellant must withstand the stresses imposed by temperature changes without cracking. In addition, the rocket motor must ignite and fire successfully within these temperature limits. High temperature sensitivity leads to unduly high chamber pressure at elevated propellant-grain temperatures and hence results in heavier motor casing. In general, the low-temperature conditions result in the most critical operating condition wherein the propellant grain may crack and cause erratic burning or explosion. Consequently heating blankets are frequently used on units using propellants with undesirably high temperature sensitivity.

Another poor feature in the use of solid-propellant rocket motors is that they generally incur a relatively large shift in missile center-of-gravity location between the launch and burnout condition. This may be undesirable for those missiles which require high maneuverability after motor burnout. One such example may be a short-range air-to-air missile which uses a solid-propellant unit to accelerate to speed and then coasts the remainder of the way toward the target. Since a forward center-of-gravity movement increases the static stability margin of the missile, the maneuverability of the missile is decreased (see Sec. 6-4). The large center-of-gravity shift between launch and burnout condition may be minimized to some extent by locating the main part of the rocket motor as close to the missile center of gravity as possible. In such an arrangement, a blast tube connecting the main combustion chamber and nozzle is required and incurs both a weight penalty and loss in motor efficiency. In many cases, it may be necessary to attach the propulsion unit at the aft end of the missile. In these cases, the large center-of-gravity shift may dictate a configuration which is statically unstable at launch in order that sufficient maneuverability can be obtained for the burnout center-of-gravity condition.

In preliminary design, it is often desirable to lay out the approximate dimensions of the rocket motor in order to determine the over-all dimensions of the complete missile configuration. The pertinent data involved are the value of total impulse and thrust level required for the missile system.

a. Determination of Propellant Weight. The propellant weight is determined by Eq. (13-13) or

$$W_p = \frac{I}{I_{sp}} \tag{13-13b}$$

The value of fuel specific impulse depends upon the type of solid propellant selected. The propellant chosen must be compatible with the following requirements: (1) desired value of I_{sp}, (2) burning rate, (3) temperature sensitivity, (4) operating pressure, and (5) cost and availability (see Table 13-1).

b. Determination of Propellant Length. For an end-burning (cigarette-type) grain design (see Fig. 13-13*a*), the length of the propellant may be calculated as follows:

$$l_e = \frac{4W_p}{\pi d^2 \rho} \tag{13-17}$$

where l_e = length of propellant for end-burning grain design
d = diameter of propellant (may be assumed to be diameter of missile if rocket motor is integral part of missile)
ρ = density of propellant (approximately 0.06 lb/cu in. for most propellants)

The volumetric loading, defined as the ratio of propellant volume to total combustion-chamber volume for this end-burning grain design, is one. For an internal-burning grain design such as that shown in Fig. 13-13*a*, the volumetric loading is less than unity. The exact value is a function of many variables, including chamber pressure, type of propellant, and velocity of gas flow past the propellant surface. For preliminary analysis the value of 0.85 appears to be reasonable. Hence the length of the propellant for the internal-burning grain design may be approximated as

$$l_i = \frac{l_e}{0.85} \tag{13-17a}$$

where l_i = length of propellant for an internal-burning grain design

The variation of propellant length with propellant weight for various missile diameters is shown in Fig. 13-14.

c. Determination of Nozzle Length. The length of the nozzle is a function of several variables including thrust level, chamber pressure, and design operating altitude (or expansion ratio). As a first crude approximation, the length of the nozzle may be assumed to be between 30 and 35 per cent of the propellant length. For a more accurate

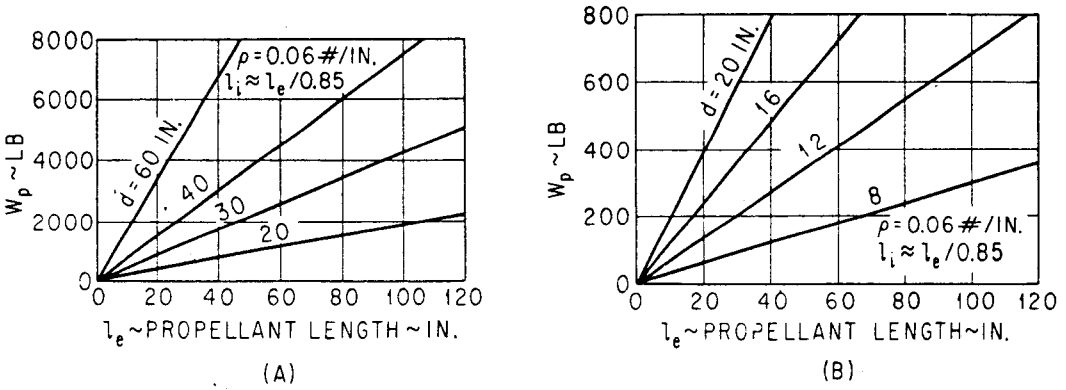

FIG. 13-14. Variation of propellant length with propellant weight. (*A*) Large motors. (*B*) Small motors.

approximation, the length of the nozzle may be determined analytically. To determine the nozzle length analytically, certain assumptions must be made. These are:

1. Chamber pressure p_c
2. Specific-heat ratio of the propellant γ
3. Exit pressure of the nozzle p_e
4. Half convergence angle β
5. Half divergence angle α

If the type of propellant is not specified in the preliminary design study, a low operating pressure should be chosen in order to minimize the weight of the thrust chamber. On the other hand, if too low a pressure is assumed, the fuel specific impulse may be unduly compromised. For motor casings which must carry large external loadings (such as those from aerodynamic wing or tail surfaces) the thickness of these motor cases will be governed by the external loading conditions. In such cases a high chamber pressure should be used in order to realize higher values of fuel specific impulse. The specific-heat ratio γ varies from propellant to propellant depending upon composition. However, the value of γ varies from 1.10 to 1.25 for most propellants. For optimum efficiency, the nozzle exit pressure p_e is assumed to be equal to the ambient pressure p_o at the design altitude.

Fuel	Oxidizer	Best oxidizer fuel mixture ratio (by weight)	Theoretical combustion temperature deg. F	Ratio of specific heats	Average molecular weight of combustion products	Bulk density at 80°F propellant combination temperature g/cm³	Specific impulse at 400 psia (sea-level expansion, sec)
Ammonia	Chlorine trifluoride	3	4980	1.32	22	1.26	238
Ammonia	Fluorine	3	7270	1.33	19	1.16	300
Ammonia	Fluorine (50%) and nitrogen trifluoride (50%)	2.8	6540	1.32	19	1.15	290
Ammonia	ON 7030[5]	2.1	4900	1.23	21	1.03	
Ammonia	Oxygen	1.3	4940	1.23	19	0.88	255
Ammonia	RFNA (22% NO_2)	2.15	4220	1.24	21	1.12	230
Butyl mercaptan	Nitric acid (95%)	4	4780	1.22	27	1.28	220
Diborane	Fluorine	5	7880	1.3	21	1.07	270
Diethylenetriamine	Oxygen	1.5	6500	1.24	21	1.06	245
Diethylenetriamine and hydrazine	Oxygen	2.5	6000	1.22	22		245
Diethylenetriamine (80%) and methylamine (20%)	RFNA (22% NO_2)	3	5250	1.23	24	1.33	240
Ethyl alcohol (92.5%, obsolescent)	Oxygen	1.5	5400	1.21	23	0.98	232
Ethyl alcohol (75%) and water (obsolescent)	Oxygen	1.3	5150	1.22	23	0.99	225
Ethylene diamine	Oxygen	1.4	6000	1.23	19	1.04	250
Ethylene oxide	ON 7030[5]	2	5730	1.24	24	1.14	
Ethylene oxide	Oxygen	1.1	5750	1.24	22	0.99	215
Hydrazine (anhydrous)	Chlorine trifluoride	2.5	6000	1.33	23	1.46	255
Hydrazine (anhydrous)	Fluorine	2	7740	1.33	19	1.3	290
Hydrazine (anhydrous)	H_2O_2 (90%)	1.5	4170	1.25	18	1.2	245
Hydrazine (anhydrous)	H_2O_2 (99.6%)	1.7	4690	1.22	19	1.24	255
Hydrazine (anhydrous)	Nitrogen tetroxide	1.1	4950	1.26	19	1.2	250
Hydrazine (anhydrous)	Oxygen	0.75	5370	1.25	18	1.06	265
Hydrazine (anhydrous)	Oxygen difluoride	1.1	6380	1.28	18	1.23	260
Hydrazine (anhydrous)	RFNA (15% NO_2)	1.3	4980	1.25	20	1.26	247
Hydrazine (anhydrous)	Tetranitromethane	1.4	5250	1.27	20	1.29	228
Hydrogen (max Isp)	Fluorine	9.42[7]	8100	1.31	10	0.46	380
Hydrogen (max Isp)[8]	Oxygen	3.8	4600	1.30	7.8	0.27	360
		8[7]	5870	1.22	16	0.43	360
		3.5	4500	1.26	9	0.26	348
JP-4	Fluorine	2.9	7100	1.22	24	1.19	275
JP-4	H_2O_2 (99.6%)	6.5	4830	1.2	22	1.28	238
JP-4 (C/H = 6.85)	Oxygen	2.2	5880	1.24	22	0.98	240
JP-4 (C/H = 6)	Oxygen	2.3	5770	1.24	22	0.98	247
JP-4	Oxygen (70%) and ozone (30%)	2.3	5950	1.24	22	1.04	252
JP-4	Oxygen (30%) and ozone (70%)	2.3	6180	1.25	21	1.08	257
JP-4	Ozone	2.4	6380	1.25	21	1.14	260
JP-4	RFNA (22% NO_2)	4.1	5150	1.23	25	1.3	228
Kerosene	H_2O_2 (54%), ammonium nitrate (40%), and H_2O (6%)	9	4270	1.21	22	1.34	228
Kerosene	Oxygen	2.2–2.5	5200	1.24	22	0.99	240
Methyl acetylene	Oxygen	2	6180	1.27	22	0.93	237
Methylamine	Oxygen			1.22	20	0.91	248

PROPELLANTS

Cost per lb		Ideal use	Handling hazard[1]		Coolant qualities		Best container material[2]		Storability[3]	
Fuel	Oxidizer		Fuel	Oxidizer	Fuel	Oxidizer	Fuel	Oxidizer	Fuel	Oxidizer
$0.04	$3.50	Small, high-performance research rockets	Some	Dangerous	Fair to poor	Unknown	All	Mild S, SS 347	Fair to poor	Fair to poor
0.04	6.00[4]	Superperformance vehicle	Some	Dangerous	Fair to poor	Very poor	All	Al, SS 347	Fair to poor	Fair to poor
0.04		Superperformance vehicle	Some	Dangerous	Fair to poor	Unknown	All	Al, SS 347	Fair to poor	Fair to poor
0.04			Some		Fair to poor		All		Fair to poor	
0.04	0.05	Rocket aircraft, small missile	Some	Some	Fair to poor		All	Al, mild S, SS 347	Fair to poor	Fair to poor
0.04	0.11	IRBM, rocket aircraft	Some	Dangerous	Fair to poor	Good	All	Al, SS 347	Fair to poor	Good
$0.20	$0.10		Some	Dangerous	Unknown	Good	SS 347	Al, SS 347	Good	Good
	$6.00[4]	Long-range medium-size rocket	Dangerous		Fair to poor	Very poor	All	Al, SS 347	Good	Fair to poor
0.18	0.05	Large nonproduction missile	None	Some	Good	Very poor[6]	All	Al, mild S, SS 347	Good	Fair to poor
		Short-range liquid rockets	None	Some	Good	Very poor	All	Al, mild S	Good	Fair to poor
0.18	0.11	Gas generator	None	Dangerous	Good	Good	All	Al, SS 347	Good	Good
$0.15	$0.05	Rocket aircraft, general-purpose	None	Some	Good	Very poor[6]	All	Al, mild S, SS 347	Good	Fair to poor
0.12	0.05	High-altitude rocket (Viking)	None	Some	Good		All	Al, mild S, SS 347	Good	Fair to poor
0.25	0.05	Superperformance vehicle	Unknown	Some	Good	Very poor	All	Al, mild S, SS 347	Good	Fair to poor
0.20			Some		Good		All		Fair to poor	
0.20	0.05	Auxiliary power generators	Some	Some	Good	Very poor[6]	All	Al, mild S, SS 347	Good	Fair to poor
$2.00	$0.50	High-performance vehicle	Some	Dangerous	Good	Unknown	All	Mild S, SS 347	Good	Fair to poor
2.00	6.00[4]	Superperformance vehicle (satellite)	Some	Dangerous	Good	Very poor	All	Al, mild S, SS 347	Good	Fair to poor
2.00	0.55	Rocket aircraft	Some	Some	Good	Good	All	Al, SS 347	Good	Good
2.00	1.20	Rocket aircraft	Some	Some	Good	Good	All	Al, SS 347	Good	Fair to poor
2.00	0.08	Small vehicle (A-A)	Some	Dangerous	Good	Unknown	All	SS 347	Good	Fair to poor
2.20	0.05		Some	Some	Good	Very poor[6]	All	Al, mild S, SS 347	Good	Fair to poor
2.00			Some	Dangerous	Good	Unknown	All	Al, mild S, SS 347	Good	Fair to poor
2.00	0.10	Air-ground rockets	Some	Dangerous	Good	Good	All	Al, SS 347	Good	Good
2.20	0.30	Rocket aircraft	Some	Some	Good	Good	All	all	Good	Good
7.00	6.00	Superperformance vehicle (space flight)	Dangerous	Dangerous	Good	Very poor	All	Al, SS 347	Fair to poor	Fair to poor
7.00	6.00	Superperformance vehicle (space flight)	Dangerous	Dangerous	Good	Very poor	Al, mild S, SS 347	Al, SS 347	Fair to poor	Fair to poor
7.00	0.05	Superperformance vehicles	Dangerous	Some	Good	Very poor	Al, mild S, SS 347	Al, mild S, SS 347	Fair to poor	Fair to poor
7.00	0.05	Superperformance vehicles	Dangerous	Some	Good	Very poor	Al, mild S, SS 347	Al, mild S, SS 347	Fair to poor	Fair to poor
$0.015	$6.00[4]	Superperformance vehicle	None	Dangerous	Good	Very poor	All	Al, SS 347	Good	Fair to poor
0.015	1.20	Gas generator	Some	Some	Good	Good	All	Al, SS 347	Good	Fair to poor
0.015	0.05	IRBM	None	Some	Good	Very poor[6]	All	Al, mild S, SS 347	Good	Fair to poor
0.015	0.05	IRBM	None	Some	Good	Very poor[6]	All	Al, mild S, SS 347	Good	Fair to poor
0.015		Superperformance vehicle	None	Some	Good	Very poor	All	Al, SS 347	Good	Fair to poor
0.015		Superperformance vehicle	None	Dangerous	Good	Very poor	All	Al, SS 347	Good	Fair to poor
0.015		Superperformance vehicle	None	Dangerous	Good	Very poor	All	Al, SS 347	Good	Fair to poor
0.015	0.11	Small missile (A-A)		Dangerous	Good	Good	All	Al, SS 347	Good	Good
$0.015	$0.75	Rocket aircraft	None	Some	Good	Good	All	All	Good	Good
0.013	0.05	IRBM, ICBM	None	Some	Good	Very poor	All	Al, SS 347	Good	Fair to poor
$0.17	$0.05	Liquid JATO	Some	Some	Unknown	Very poor	Al, mild S, SS 347	Al, mild S, SS 347	Fair to poor	Fair to poor
0.35	0.05	Gas generator	None	[illegible]	[illegible]	Very poor	All	Al, mild S, SS 347	Good	Fair to poor

LIQUID

Fuel	Oxidizer	Best oxidizer fuel mixture ratio (by weight)	Theoretical combustion temperature deg. F	Ratio of specific heats	Average molecular weight of combustion products	Bulk density at 80°F propellant combination temperature g/cm³	Specific impulse at 400 psia (sea level expansion, sec)
n-Octane	Oxygen	2.4	5790	1.23	22	0.96	250
n-Octane	Oxygen difluoride	3.8	7340	1.33	20	1.22	Unknown
n-Octane	RFNA (6.5% NO_2)	4.5	5100	1.24	24	1.26	226
Nitroethane	Oxygen	0.65	5570	1.23	23	1.09	215
Nitropropane	Oxygen	0.9	5620	1.23	23	1.06	210
Polyethylene	RFNA (22% NO_2)	4.5	5320	1.22	25	1.4	Unknown
Propylene oxide	Oxygen	1.6	5900	1.23	23	1	230
Propylene oxide (69.5%) and ethylene oxide (30.5%)	Oxygen	1.5	5900	1.23	23	1	Unknown
Triethylamine (63%) and orthotoluidine (37%)[9]	ON 7030[5]	3.7	5800	1.24	25	1.19	
Triethyl-trithiophosphite[9]	ON 7030[5]	2.5	6000	1.23	30	1.28	
Triethyl-trithiophosphite[9]	RFNA (22% NO_2)	3	5520	1.21	30	1.43	230
Turpentine[9]	Nitric acid	4.4	4950	1.22	25	1.32	244
Turpentine[9]	Oxygen	2.4	5880	1.23	22	1.04	240
Turpentine[9]	RFNA (22% NO_2)	4.2	5400	1.22	26	1.36	241
Unsymmetrical dimethyl hydrazine	Oxygen	1.4	5650	1.24	20	0.96	249
Unsymmetrical dimethyl hydrazine	RFNA (22% NO_2)[10]	2.6	5200	1.23	22	1.23	241
Unsymmetrical dimethyl hydrazine	WFNA[11]	2.7	5100	1.23	22	1.22	240

SOLID

Fuel and oxidizer[12]	Type	Pressure range, psi	Low-pressure limit, psi	Specific impulse at 300 psi, sec	Burning-rate exponent	Burning rate, ips	Ignition sensitivity
Amino ethanes[13]	Composite	300–2000	80	200		0.3–0.6	Medium
Ballistite[13]	Double-base	1000–3000	200	200	0.85		Low
Black powder[13]	Composite	100–1000	15	70	0.5–0.8	0.1–0.5	Low
Buna and sulfo rubbers[13]	Composite	100–800	30	210		0.4	Very low
Cordite[13]	Double-base	1000–3000	300	180	0.77		Low
GALCIT 161[13]	Composite	1300–3700	700	190	0.75	1.4–1.5	High
Hydrogen peroxide and polyethylene	Liquid-solid	100–300	75	160			Very low
Lox-rubber	Liquid-solid	100–500	15	225			
NDRC EJA[13]	Composite	600–1000		180	0.45	0.2–1	Low
Polymethane[13]	Composite	500–2000		215			Low
WASAG DEGN	Homogeneous	700–4000	700	180	0.73	0.2–0.8	Medium
Polyurethane[14]	Composite						Low

[1] "Some" hazard means slightly toxic and corrosive; "dangerous" hazard means toxic, corrosive, and explosive.

[2] "Al" means aluminum alloys; "all", all normal metals and plastics; "mild S", mild steels; "SS", stainless steels.

[3] "Good" storability means liquid can be stored in ordinary vessels or tanks over long periods and at many temperatures without decomposition or change of state.

[4] Liquid.

[5] Nitrogen tetroxide (70 per cent) and nitric oxide (30 per cent).

[6] Except at high coolant pressure.

[7] Mixture ratio yielding the highest loading density, or mass ratio.

[8] The combination of hydrogen and oxygen is rapidly becoming a favorite and will be widely used in the future. The hydrogen is used as the engine coolant.

[9] Little used; mostly of academic interest.

[10] Hydrogen fluoride is often added to reduce the corrosive effect of nitric acid.

[11] A little worse than RFNA.

[12] Ammonium nitrate, ammonium perchlorate, and potassium nitrate are oxidizers used with such fuels as Thiokol and the sulfo rubbers.

[13] Various light metal powders are added to some of the composite and double-base propellants to increase the specific impulse.

[14] A favorite for long-range vehicles.

PROPELLANTS

Cost per lb		Ideal use	Handling hazard[1]		Coolant qualities		Best container material[2]		Storability[3]	
Fuel	Oxidizer		Fuel	Oxidizer	Fuel	Oxidizer	Fuel	Oxidizer	Fuel	Oxidizer
$0.07	$0.05	Precision rocket chamber	None	Some	Good	Very poor	All	Al, mild S, SS 347	Good	Fair to poor
0.07			None	Dangerous	Good	Unknown	All	Al, SS 347	Good	Fair to poor
0.07	0.08	Precision research rocket testing	None	Dangerous	Good	Good	All	Al, SS 347	Good	Good
1.00	0.05		Dangerous	Some	Unknown	Very poor	All	Al, mild S, SS 347	Fair to poor	Fair to poor
	0.05	Auxiliary power pack	Dangerous	Some	Unknown	Very poor	All	Al, mild S, SS 347	Fair to poor	Fair to poor
	$0.11		None	Dangerous		Good		Al, SS 347		Good
	0.05		Some	Some	Unknown	Very poor	All	Al, mild S, SS 347	Fair to poor	Fair to poor
$0.10	0.05		Some	Some	Unknown	Very poor	All	Al, mild S, SS 347	Fair to poor	Fair to poor
$1.50			None		Good		All		Good	
3.80			Some		Unknown		Mild S, SS 347		Good	
3.80	$0.11	Starting liquid for large engines	Some	Dangerous	Unknown	Good	Mild S, SS 347	Al, SS 347	Good	Good
0.11	0.12	Small storable rockets	None	Dangerous	Fair to poor	Good	All	Al, SS 347	Good	Good
0.10	0.05	Gas generator, auxiliary power unit	None	Some	Fair to poor	Very poor	All	Al, mild S, SS 347	Good	Fair to poor
0.10	0.11		None	Dangerous	Fair to poor	Good	All	Al, SS 347	Good	Good
$1.50	$0.05	ICBM, IRBM	Some	Some	Good	Very poor[6]	All	Al, mild S, SS 347	Good	Fair to poor
1.50	0.11	Rocket aircraft, small missiles	Some	Dangerous	Good	Good	All	Al, SS 347	Good	Good
1.50	0.15		Some	Dangerous	Good	Good	All	Al, SS 347 and 410	Good	Good

PROPELLANTS

Pressure sensitivity to temperature, %/°F	Weight, lb/cu ft	Storability	Ideal use	Cost per lb	Hygroscopicity	Exhaust
	90 (approx)	Good	Very large booster		Negligible	
0.5–1.3	75–105	Fair	Small ordnance	$5–$10	Low	High flash, black smoke
	75–130	Good	Igniters	0.50–1.00	Low	Gray smoke
	70 (approx)	Medium	Medium-size high-performance units (when case-bonded)		Low	
0.7		Fair	Ordnance		Negligible	High flash, black smoke
0.23	110	Very good	JATO	0.75–1.00	Negligible	White smoke
		Very good (for polyethylene)	Start-stop or throttling solids			Almost invisible
						Smokeless
0.2–0.3		Good	JATO		Very low	Gray smoke
		Good	Super boosters		Low	
		Good	High-performance boosters	2.00–5.00		High flash, black smoke
		Very good	High-performance boosters		Low	

Additives

	Application	Remarks
Ammonium nitrate	Depresses freezing point of nitric acid	Difficult to mix with acid in small amounts
Hydrogen fluoride	Inhibits corrosive effect of RFNA and WFNA	Action not well understood; believed to react with Al in tanks and chamber
Aluminum	Increases specific impulse or combustion temperature of solid propellants	Affects exhaust products; coats exhaust nozzle
Silicon monoxide	With hydrocarbon fuels (in very small amounts)	Deposits out as protective film on thrust chamber wall; may reduce burn-through
Diboranes and boron hydrides	With kerosene and JP fuels for turbojets; not yet ready for rockets	Raises combustion temperature (and impulse) considerably; usually added

Monopropellants

	Specific impulse at 300 psia, sec	Application	Remarks
Hydrogen peroxide (95–98%)	150	Gas generator for pumps; auxiliary for rocket-vehicle control	Difficult handling; needs pure Al or SS 347; clean
Nitromethane	180	Small, simple ordnance rockets	Dangerous handling (can detonate unexpectedly)
Hydrazine	195–220 (?)	Gas generator; small rocket	Difficult handling; poisonous fumes; can break up at high temperature
[illegible]	160	Gas generator; small rocket	Safe handling; dangerous and very smoky exhaust fumes

With the assumptions on the operating pressure, propellant specific-heat ratio, and exit pressure made, the thrust coefficient C_T can be calculated by Eq. (13-11). Hence

$$C_T = \sqrt{\frac{2\gamma^2}{\gamma - 1}\left(\frac{2}{\gamma + 1}\right)^{(\gamma+1)/\gamma-1}\left[1 - \left(\frac{p_e}{p_c}\right)^{(\gamma-1)/\gamma}\right]} \tag{13-18}$$

With C_T known, the nozzle throat area A_t can be readily determined from Eq. (13-10). In actual practice, Eq. (13-10), which is applicable for an ideal condition, must be modified by the nozzle divergence coefficient λ [Eq. (13-8)], nozzle discharge coefficient C_d, and nozzle velocity coefficient φ. For a well-designed nozzle, the value of C_d and φ approaches unity. Hence

$$A_t = \frac{T}{C_T p_c C_d \varphi} \tag{13-19}$$

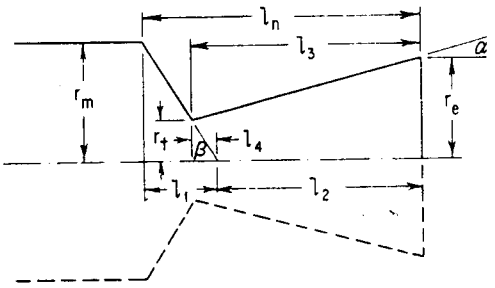

FIG. 13-15. Nozzle geometry.

Since it is assumed that the nozzle will be designed for full expansion (i.e., $p_e = p_o$), the nozzle exit area A_e may be determined from Eq. (13-12) or Fig. 13-10. Finally, the length of the nozzle may be calculated by assuming the value of the half convergence and divergence angle. From Fig. 13-15, the length of the nozzle l_n can be derived as follows:

$$l_n = l_1 + l_2 \tag{13-20}$$

where

$$l_1 = r_m \cot \beta \tag{13-20a}$$

$$l_2 = l_3 - l_4$$
$$= (r_e - r_t) \cot \alpha - r_t \cot \beta \tag{13-20b}$$

Hence

$$l_n = (r_m - r_t) \cot \beta + (r_e - r_t) \cot \alpha \tag{13-20c}$$

d. Determination of Rocket-motor Weight. Without going into a detailed stress analysis of the combustion chamber and nozzle, the weight of the total (loaded) rocket motor may be estimated by assuming a value for either the over-all specific impulse I_o or rocket-motor mass ratio ζ. The latter is defined as

$$\zeta = \frac{W_p}{W_m} \tag{13-21}$$

From Eqs. (13-13), (13-14), and (13-15), Eq. (13-21) may be written as

$$\zeta = \frac{I_o}{I_{sp}} \tag{13-21a}$$

The value of ζ varies from approximately 0.75 for small motors with high operating pressure (i.e., 1,000 psi and above) and large external loads to 0.90 for the larger units used on long-range ballistic missiles. For the latter applications, the operating pressure is generally relatively low (i.e., between 300 to 600 psi). Furthermore, because of the near zero lift trajectory (i.e., gravity turn), the aerodynamic loading for long-range ballistic missiles is kept to a minimum. Hence, with the assumed value of ζ, the total rocket-motor weight may be determined from Eq. (13-21).

SYMBOLS

A_e	exit area of nozzle
A_t	throat area of nozzle
A_x	axial or x component of the wall area of the nozzle
C^*	characteristic velocity
C_d	nozzle discharge coefficient
C_T	thrust coefficient
I	rocket-motor impulse
I_o	over-all specific impulse
I_{sp}	fuel specific impulse
M_x	momentum flux in the axial direction
P_s	stagnation pressure
T	thrust
T_s	stagnation temperature
V_j	exit velocity of the exhaust gas
W_m	total rocket-motor weight
W_p	weight of propellant
l_e	length of propellant for an end-burning grain design
l_i	length of propellant for an internal-burning grain design
l_n	nozzle length
l_1, l_2, l_3, l_4	nozzle dimensions (see Fig. 13-15)
p	pressure forces
p_c	chamber pressure
p_i	pressure forces acting upon the inner surfaces of the rocket
p_o	pressure forces acting upon the outer surfaces of the rocket
r_m	radius of rocket motor
r_t	radius of nozzle throat
α	half divergence angle of nozzle
β	half convergence angle of nozzle
γ	specific-heat ratio of propellant

ζ rocket-motor mass ratio
λ divergence coefficient
ρ propellant density
φ nozzle velocity coefficient

REFERENCES

1. Malina, F. J.: Characteristics of Rocket Motor Unit Based on Theory of Perfect Gases, *J. Franklin Inst.*, vol. 230, no. 4, October, 1940.

2. Kaprielyan, S. P., and J. P. Kushnerick: Liquid-prepack Engines, *Aircraft and Missiles*, vol. 2, no. 11, pp. 6–10, November, 1959.

3. Wimpress, R. N.: "Internal Ballistics of Solid Fuel Rockets," McGraw-Hill Book Company, Inc., New York, 1950.

4. Bonney, A. E., M. J. Zucrow, and C. W. Besserer: "Aerodynamics Propulsion—Structures and Design Practice," D. Van Nostrand Company, Inc., Princeton, N.J., 1956.

5. Sutton, G. P.: "Rocket Propulsion Elements," John Wiley & Sons, Inc., New York, 1956.

6. Zucrow, M. J.: "Principles of Jet Propulsion and Gas Turbines," John Wiley & Sons, Inc., New York, 1948.

7. Geckler, R. D., and R. E. Davis: Modern Developments in Solid-propellant Rocket Engineering, *Aeronaut. Eng. Rev.*, vol. 16, no. 8, August, 1957.

8. Marsel, C. J.: Rocket Propulsion, *Astronautics*, vol. 4, no. 4 (pt. 2 of 2 parts), pp. 7–11, April, 1959.

9. Warren, F. A.: "Rocket Propellants," Reinhold Publishing Corporation, New York, 1958.

10. Geckler, R. D.: "The Mechanism of Combustion of Solid Propellants," p. 289, Selected Combustion Problems, AGARD, 1954.

11. Vandenkerckhove, J. A.: Recent Advances in Solid Propellant Grain Design, *ARS J.*, vol. 29, no. 7, pp. 483–491, July, 1959.

12. Shafer, J. I.: "Solid Rocket Propulsion," John Wiley & Sons, Inc., New York, 1959.

13. Newman, R. S.: The Dual-thrust Solid Propellant Rocket Engine, *Astronautics*, vol. 3, no. 3, March, 1958.

14. Stone, M. W.: A Practical Mathematical Approach to Grain Design, *Jet Propulsion*, vol. 28, no. 4, pp. 236–244, April, 1958.

15. Mayer, E.: Vaporization Rate Limited Combustion in Bipropellant Rocket Motors, *ARS J.*, vol. 29, no. 7, pp. 505–513, July, 1959.

16. Gerstein, Melvin: Correlation and Prediction of Flame Properties with Special Reference to Liquid Hydrazine, *ARS J.*, vol. 29, no. 7, pp. 514–516, July, 1959.

17. Dugger, G. L.: Recent Advances in Ramjet Combustion, *ARS J.*, vol. 29, no. 11, pp. 819–827, November, 1959.

CHAPTER 14

STRUCTURAL-DESIGN CONSIDERATIONS

14-1. INTRODUCTION

In most preliminary missile configuration designs, detailed structural-design analysis is not made. This arises primarily from the fact that the exact magnitude of the air loads and inertia loads is not available. However, the designer should bear in mind that a simple efficient external configuration can also lead to a more efficient and lighter structural configuration. In addition, the designer should be aware of the fact that structural weight can have a pronounced and detrimental effect on the performance of the missile system. For example, in the case of a long-range ballistic missile, each additional pound of "excess" inert weight requires an addition of as much as 100 lb of propellant weight to achieve a given design range. Or, as another aspect of this, an increase of 1 lb of inert weight decreases the range of the missile by several miles. Hence proper emphasis must be placed on the structural design aspects during the early design phase of a given missile weapon system. With proper structural design practices, the resultant missile configuration and hence the over-all missile weapon system will be lighter in weight, easier to manufacture, and hence generally lower in per unit cost.

The primary function of the structural-design engineer is manyfold: (1) to provide structural adequacy of the missile airframe under its operating environment, (2) to investigate the most suitable materials to meet the loadings and their associated operating environmental conditions in the missile weapon system, and (3) to analyze and select the most optimum type of construction for the type of configuration from the standpoint of ease of manufacturing, cost per unit, and interchangeability of parts, which is a stringent requirement for certain missile systems. The purpose of this chapter is to present some of the more important structural-design considerations involved in the design of missile configurations.

14-2. FUNDAMENTAL STRUCTURAL CONCEPTS

Before a detailed discussion on design loads and structural analysis is presented, a brief summary of some of the fundamental structural concepts is given in the subsequent paragraphs.

1. Dynamic Equilibrium. Newton's third law of motion states that for every action there is an equal and opposite reaction. In the case of a body of a missile which is accelerated in the direction of an external load or force, the reaction in the opposite direction consists of the inertia force of the body. The application of the inertia forces to oppose the external resultant force is known as D'Alembert's principle. This principle states that "the impressed forces acting on any body are in dynamic equilibrium with the inertial forces of the particles of the body." Since a body must be placed in equilibrium before the internal shears and bending moments can be determined, it follows that accelerating bodies must be placed in equilibrium by applying the necessary inertia forces in accordance with D'Alembert's principle. The following paragraphs outline the procedure for determining the magnitude of the forces. Note that the inertia-load factors always act in a direction opposite to that of the acceleration which produces them.

2. Linear Acceleration Due to Translation. When the missile is flying in its trimmed condition (i.e., condition B as described in Sec. 10-2, Fig. 10-2), it experiences a linear acceleration as the result of pure translational motion. The magnitude of the force normal to the missile longitudinal axis is determined by

$$F = N = C_{N_{TR}} q S_\pi \tag{14-1}$$

where $C_{N_{TR}}$ is the trimmed normal-force coefficient as defined in Sec. 5-5 (Fig. 5-6). In dealing with the inertia of a missile, it is more convenient to express the magnitude of the forces (those due to external aerodynamic loading and inertia loading) in terms of gravitational units rather than in terms of mass and acceleration. Hence, from Newton's equation, $F = ma$ or $(W/g)a$, the magnitude of F is expressed as

$$F = nW \tag{14-1a}$$

where n is equal to a/g and is the load factor expressed in g's, and F is the force expressed in gravitational units. For example, a force of 1,000 lb acting on a 500-lb missile results in a magnitude of F of 2 g's.

3. Linear Component of Angular Acceleration. In addition to the linear acceleration due to pure translational motion, the missile experiences an angular acceleration as the result of any unbalanced external aerodynamic loads. These angular accelerations may be considered as transient conditions such as those discussed in Chap. 10 (i.e., condition A, C, D, and E described in Sec. 10-2). The magnitude of these angular accelerations may be determined as

$$\ddot{\theta} = \frac{M}{I} \tag{14-2}$$

where $\ddot{\theta}$ = angular acceleration, radians/sec
M = external rotational moment due to external unbalanced forces, ft-lb
I = moment of inertia of the missile, slug-ft^2

The magnitude of the moment may be determined from the aerodynamic derivatives or plots of moment coefficient vs. angle of attack for various control-surface deflections (i.e., Figs. 10-2 and 10-3). Hence

$$M = (C_{m_\alpha}\alpha + C_{m_\delta}\delta)qS_\pi d \tag{14-3}$$

or

$$M = C_m qS_\pi d \tag{14-3a}$$

The magnitude of the moment of inertia of the missile may be calculated by summing the moment of inertia of the various component parts about their respective centers of gravity and then transferring to the missile center-of-gravity location. Mathematically, it can be expressed as

$$I = \Sigma\left(I_0 + \frac{W}{g}x^2\right) \tag{14-4}$$

where I_0 = moment of inertia of a given mass about its own center of gravity
x = distance from missile center of gravity to any mass W/g

The linear component of angular acceleration Δn is expressed as

$$\Delta n = \frac{\ddot{\theta}l}{g} \tag{14-5}$$

where l is any distance from the center of gravity of the missile (positive when measured forward of the center of gravity). From Eq. (14-5) it is apparent that the incremental load factor due to angular acceleration varies linearly with distance from the missile center of gravity as

illustrated in Fig. 14-1. Hence the total linear acceleration of the missile is the sum of the linear acceleration due to pure translation and the linear component due to angular acceleration and can be expressed as

$$(n_Z)_{\text{total}} = \frac{F}{W} \pm \frac{\ddot{\theta} l}{g} \tag{14-6}$$

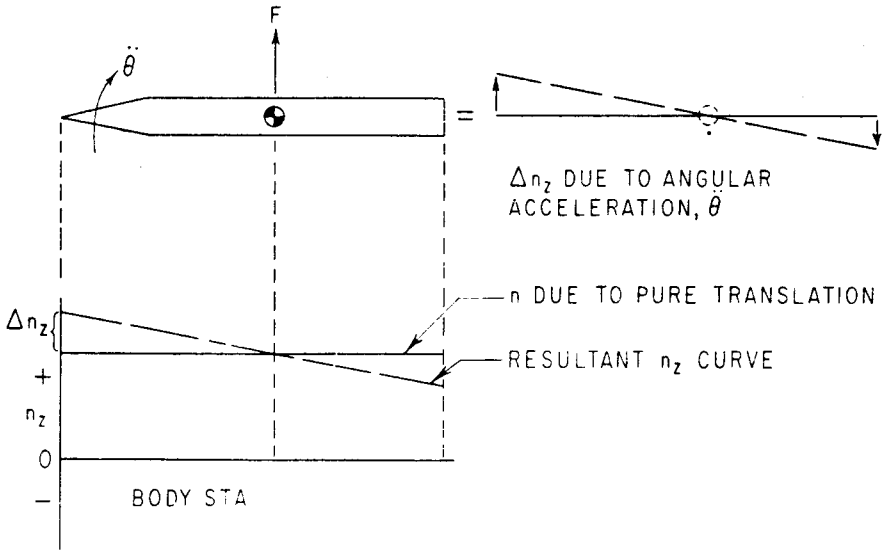

FIG. 14-1. Linear components of acceleration.

4. Missile-loading Concept. In order to facilitate the determination of critical structural-loading conditions on the body of the missile, the simple beam analogy is used. In this technique, the body of the missile is replaced by a simple beam supported at the center-of-gravity location of the missile as shown in Fig. 14-2. The external load distribution on the body is next superimposed on the beam. For simplicity, the wing and tail loadings are replaced by concentrated loads at their respective centers of pressure. For the purpose of illustration (see Fig. 14-2), the missile is assumed to be in trimmed level flight ($1g$) condition. Hence the summation of moments about the center of gravity or beam support due to the external loads acting on the missile is equal to zero. Since there is no unbalanced external moment, the missile undergoes no angular acceleration. Hence the resultant force is acting at the missile center of gravity against the acceleration of gravity. It is also assumed that the internal body weight distribution takes the simple form shown in Fig. 14-2.

With both external and internal loadings known, the missile is placed in dynamic equilibrium by opposing the external upward-acting

force (of $1g$) by $1g$ of missile dead weight or inertia force acting downward. A shear diagram is then constructed by simply summing the external and inertia loads on the missile starting from the nose aft and from the aft end of the missile forward to the missile center of gravity as shown in Fig. 14-2. Finally, the moment diagram is made by taking the summation of the moment of the shear forces about the missile

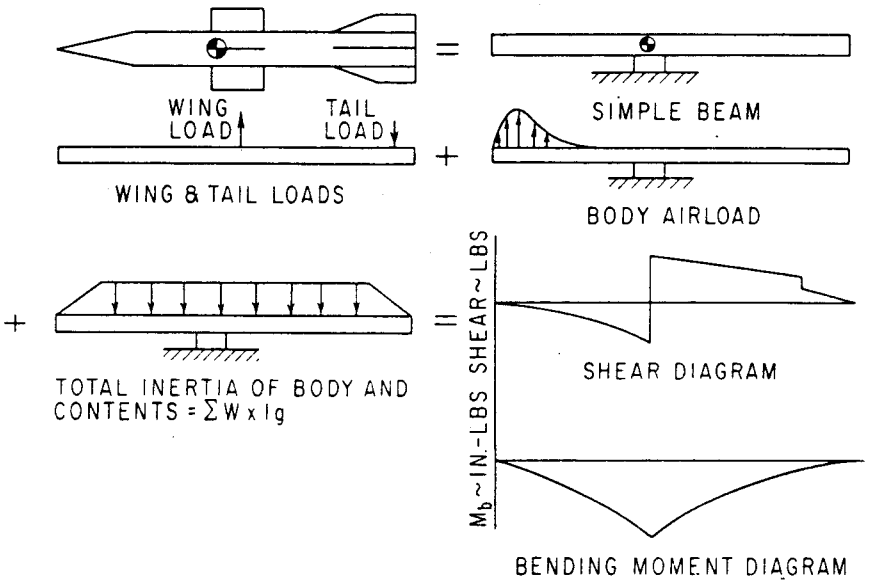

FIG. 14-2. Missile-loading concept.

center of gravity. Mathematically, the shear and moment may be expressed as

$$S = \int w\,dx \qquad \text{and} \qquad M_b = \int S\,dx = \int\int w\,dx\,dx$$

where S = shear force
M_b = bending moment
w = running load as illustrated in Fig. 14-3
x = any station along beam or body of missile

From the moment diagram, the change in bending moment between any two stations may be readily determined.

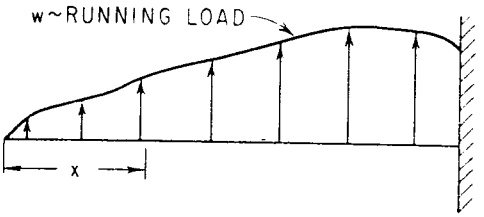

FIG. 14-3. General loading for the determination of shear and moment diagrams.

14-3. DESIGN LOADS

There are many types of external and internal loads imposed on the

missile structures and components. In general, these loads may be divided into two classes: flight loads and ground loads. In practical design, critical structural-design conditions arise from both classes of load. Hence the designer must consider these loadings with equal care.

1. Flight Loads. The flight loads may be subdivided into two categories: free-flight loads and captive-flight loads. Free-flight loads arise primarily from aerodynamic and thermal forces and internal pressure forces such as those present in a rocket motor or propulsion system. Captive-flight loads arise primarily from the aerodynamic loads induced on the missile during its carried condition by the parent aircraft. The missile structure must be adequate to withstand the most critical loadings imposed during flight on each component of the missile. The air loads on the missile for various conditions of flight may be determined by the methods outlined in Chap. 10. These air loads when combined with the missile inertia forces result in the net structural loads on the missile as discussed in Sec. 14-2.

2. Ground Loads. The basic ground loads consist of those which the missile experiences during transportation and preparation for launching. Many data have been gathered over the past several years on the environmental conditions of all modes of transportation.[1,2]* These environmental loads, which are generally expressed in terms of amplitude and frequency (i.e., 30 g's at 150 cps), may have a detrimental effect on the missile, particularly on its internal electronic components. Hence proper design such as shock mounting must be incorporated to minimize the effects of these environmental loads. In addition, proper design must be incorporated in missile shipping containers to withstand the loads encountered during transportation and ground handling.

The ground-handling loads must also be carefully analyzed to assure that the structural design of the missile and the ground-support equipment (i.e., missile launcher, erector, etc.) are satisfactory. The magnitude of these loads can be determined only after the complete concept and details of the ground-support system have been established.

3. Factors of Safety. Factors of safety are applied to the limit or actual flight or ground-handling loads to assure that all stresses are below the ultimate or yield strength of the material from which the missile structural components are fabricated. This procedure prevents the structure from attaining any appreciable permanent deformation

* Superscript numbers indicate references listed at the end of the chapter.

under the actual load and from failing at ultimate load. The magnitude of the factor of safety to be used in the design of each missile component must be carefully selected to preclude undue weight penalties in the missile. As previously noted, each pound of "excess" inert or structural weight added may have a large detrimental effect on the performance of the missile. On the other hand, the structural design should be realistic and adequate to satisfy the over-all mission requirements of the weapon system.

The factors of safety which are currently considered in the structural design of missiles are:

a. 1.5 × limit (actual) stress for design conditions which involve a safety hazard to personnel, for example, a missile-launching condition in which failure of a structural component could endanger the lives of the handling personnel

b. 1.25 × limit stress (actual) for design conditions which do not involve hazard to personnel, for example, a terminal dive on target

c. 1 × limit stress for all other design conditions

Margins of Safety. The margin of safety is defined as a ratio of the excess strength to the required strength and is expressed as

$$\text{Margin of safety MS} = \frac{\sigma_{\text{allowable}}}{\sigma} - 1 \tag{14-7}$$

where $\sigma_{\text{allowable}}$ = ultimate or yield strength of material, psi (physical property of material)

σ = stress in member

Two values of margin of safety are generally computed for each missile structural component analyzed. These are based on the yield strength and ultimate strength of the material. Hence

$$\text{MS}_{\text{yield}} = \frac{\sigma_{\text{allowable yield}}}{\sigma_{\text{limit or actual}} \times \text{factor of safety (generally} = 1)} - 1 \tag{14-8}$$

$$\text{MS}_{\text{ultimate}} = \frac{\sigma_{\text{allowable ultimate}}}{\sigma_{\text{limit or actual}} \times \text{factor of safety (1.25 or 1.50)}} - 1 \tag{14-9}$$

The margin of safety should never be negative but should be zero or a small positive value. The margin of safety for each member should be clearly indicated in the stress analysis. If it is later desired to increase

the load on any member or to decrease the size of the member, the margin of safety gives an immediate indication of the permissible load increase.

14-4. OVER-ALL STRUCTURAL ANALYSIS

In the structural-load analysis, the net load or shear force the structure has to support is of primary interest. This net load is the difference between the external loads and the inertia loads for a given missile flight condition. Theoretically, if the inertia load distribution is exactly equal and opposite to the external load distribution (i.e., zero net force along the entire missile), the shear forces and bending moments are nonexistent. Hence, for this idealized condition, the structural weight of the missile approaches the theoretical minimum value from the standpoint of loads. Therefore, it is apparent that the configuration design engineer should carefully consider the general internal component weight distribution in an effort to minimize the magnitude of this net force. The critical design condition for a given portion of the structure is defined as that which results in a maximum net load or shear force on that portion of the structure.

After the critical structural-design conditions are determined, the structural components of the missile are analyzed. For simple structural members, the classic equation for beam bending may be used to determine the stresses produced by the design bending moments such as those shown in Fig. 14-2.

$$\sigma = \frac{M_b c}{I_a} \tag{14-10}$$

where σ = tensile or compressive stress, psi
M_b = applied bending moment, in.-lb
c = distance from neutral axis to element in which stress is to be determined, in.
I_a = area moment of inertia of cross section of structural member, in.^{4}

In the case of circular, unstiffened, thin-walled cylinders (monocoque construction) which are frequently used for small missile bodies, Eq. (14-10) becomes

$$\sigma_{\max} = \frac{M_b r}{\pi r^3 t} = \frac{M_b}{\pi r^2 t} \tag{14-11}$$

where r = radius of tube
t = wall thickness of cylinder

For a solid rectangular cross section which is similar to the airfoil section of a small missile (see Fig. 14-4*a*), Eq. (14-10) becomes

$$\sigma_{max} = \frac{M_b(t_1/2)}{(bt_1^3/12)} = \frac{6M_b}{bt_1^2} \tag{14-12}$$

where b = chord of section
t_1 = thickness of section

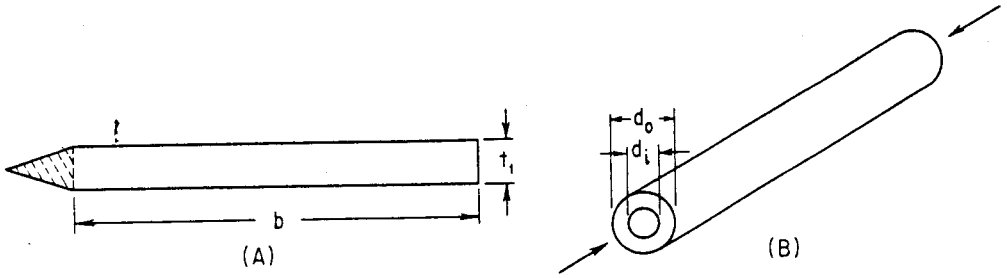

FIG. 14-4. Notations for structural analysis. (*A*) Airfoil cross section. (*B*) Circular cylinder.

The axial stress of a structural member which is axially loaded may be calculated by the following simple equation:

$$\sigma_{axial} = \frac{P}{A} \tag{14-13}$$

where P = magnitude of the axial load, lb
A = effective cross-sectional area of structural member in plane normal to direction of applied load, in.^{2}

For a cylinder subjected to a compressive load P (see Fig. 14-4*b*), the axial stress is

$$\sigma_{axial} = \frac{P}{A} = \frac{4P}{\pi(d_o^2 - d_i^2)} \tag{14-14}$$

where d_o = outside diameter of cylinder, in.
d_i = inside diameter of cylinder, in.

The critical axial-loading condition generally occurs during the boost phase wherein the missile is subjected to high acceleration in the axial direction. For example, if a 10g axial acceleration is imposed on the missile, this force is opposed or reacted by a 10g inertia load acting

on each weight increment of the missile. The dead-weight distribution of the missile produces a corresponding axial-load distribution along the body axis of the missile as shown in Fig. 14-5. The axial stresses produced by this loading are then combined with the previously determined bending stresses to obtain the total stresses for the given design condition. Hence

$$\sigma_{\text{total}} = \sigma_{\text{bending}} \pm \sigma_{\text{axial}} = \frac{M_b c}{I_a} \pm \frac{P}{A} \tag{14-15}$$

The above simplified analysis is applicable for relatively simple structural members such as those previously described. However, in

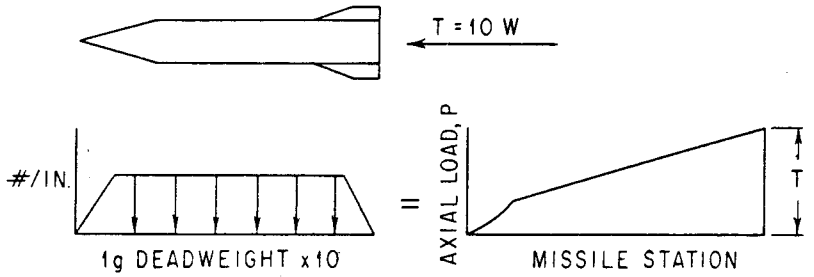

FIG. 14-5. Axial-load distribution.

most missile designs, particularly those associated with the larger missiles, many complex structural configurations are encountered. For these designs, much more elaborated analysis must be conducted. In cases where the most involved analysis is inadequate to predict accurately the stress on the structure, a relatively large factor of safety should be incorporated until results of static tests become available.

14-5. MATERIAL

The materials in general usage for the construction of missiles are aluminum, steel, magnesium, and titanium. Because of the high temperatures encountered by missiles flying at high supersonic and hypersonic speeds, other types of materials are coming into more common usage. These include molybdenum, beryllium, plastic, and graphite compounds. Since the designer has a wide variety of choice of these basic metals and many of their alloys, he must conduct a thorough analysis of their many advantages and disadvantages before he can select the best for his particular design. The following factors are

some of the most important of those which required careful consideration:

1. Material strength and density
2. Structural temperature expected in operation
3. Stiffness or deformation requirements
4. Corrosion resistance
5. Availability of materials
6. Fabrication limitations
7. Cost, both basic material and manufactured cost

For detailed discussion and data on material properties, the reader should consult any of the published literature on this subject (i.e., refs. 6, 10, and 12).

14-6. WEIGHT AND COST

In general, missile structural design permits more latitude in the selection of economic manufacturing processes and materials than manned aircraft. This is due primarily to the human-safety considerations involved in aircraft design. Adequate strength with minimum structural weight is generally the designer's aim for manned aircraft and cruise-type missiles. In short-range missiles, however, the unit cost vs. structural weight trade-off for each component must be closely examined. Structural weight can become less significant than manufactured cost of the component. However, for long-range ballistic missiles, it is mandatory to keep the structural weight as low as permissible without incurring unduly high cost for the material or its fabrication. Therefore, the designer should become more fully aware of the weight and cost interrelationship, particularly during the early design stages, in order to arrive at a more optimum design.

14-7. TYPES OF CONSTRUCTION

1. Body. The body of the missile can be constructed as a monocoque or semimonocoque structure. The monocoque structure consists of an unstiffened shell with very few transverse frames. This type of structure is relatively simple to manufacture with a minimum of detail parts and few manufacturing operations. This type of construction is used on ballistic missiles as well as for small missiles (up to approximately 24 in. outside diameter). The semimonocoque structure consists of a shell which is stiffened longitudinally by stringers and

transversely by bulkheads. This type of construction, which is generally used in the fabrication of manned aircraft, is also used in the construction of large ballistic missiles as well as cruise missiles. A large number of detail parts and assembly operations are required to produce this type of structure.

2. Aerodynamic Surfaces. Aerodynamic surfaces can be fabricated by a variety of methods. Small thin surfaces can feature solid, hollow-cast, or built-up honeycomb cross sections, depending perhaps upon the most economic means of fabrication. As the surfaces get larger and thicker, the use of solid sections becomes prohibitive from a weight standpoint and honeycomb or hollow-cast sections become more attractive. Casting materials have generally featured low material allowable strengths with the associated weight penalty but castings can be cheap in quantity production and require few final machining operations. Recent modifications to casting alloys have considerably improved their strength properties. Honeycomb construction permits the use of higher material allowables but obviously involves a multiplicity of detail parts (core, inserts, edge members, attachment fittings) and assembly operations. Again, the designer must carefully analyze the many factors involved including cost, weight, strength, etc., before he can select the optimum type of construction. An improper selection in the early stage of the missile design may require costly as well as time-consuming tooling and fabrication modifications for the final production design. However, the designer must also consider these changes in the event of subsequent technological advances. If proper foresight is used in selecting the type of construction during the early design stage, subsequent changes and modifications dictated by technological advances and other missile design requirements will be minimized.

SYMBOLS

A	effective cross-sectional area
C_m	moment coefficient
$C_{N_{TR}}$	trim normal-force coefficient
F	(normal) force
I	moment of inertia
I_a	area moment of inertia
I_0	moment of inertia of a given mass about its own center of gravity
M	moment

M_b	applied bending moment
MS	margin of safety
N	normal force
P	compressive or axial load
S	shear force
S_π	body frontal (reference) area
W	weight
c	distance from the neutral axis to the element in which the stress is to be determined
d	body diameter
d_i	inside diameter of the cylinder
d_o	outside diameter of the cylinder
l	distance from missile center of gravity
n	load factor
n_Z	linear acceleration (in the normal direction)
q	dynamic pressure
r	radius of the tube (or cylinder)
t	wall thickness of the cylinder
t_1	thickness of the section
w	running load
x	any station along the beam or body of the missile
$\ddot{\theta}$	angular acceleration
σ	stress in member

REFERENCES

1. Firmage, D. A.: "Transportation Shock and Vibration Studies," University of Florida Engineering and Industrial Experiment Station, Proj. 8-91-06-002, Engineer Research and Development Laboratories, Fort Belvoir, Virginia, February, 1952.

2. The Applicability of Existing Truck and Rail Shock and Vibration Data to Freight Shipment Criteria, Vitro Corporation of America, Silver Springs Laboratory, *Tech. Rept.* 58, March, 1954.

3. "Climatic Extremes for Military Equipment," Military Standard Specification 210, 1953.

4. Environmental Criteria for Guided Missile Systems, *USAF Spec. Bull.* 106, February, 1954.

5. "Missiles, Guided; Design and Construction, General Specification for," MIL-M-8555.

6. "Strength of Metal Aircraft Elements," ANC-5, Government Printing Office, Washington, D.C., March, 1955.

7. Peery, D. J.: "Aircraft Structures," McGraw-Hill Book Company, Inc., New York, 1950.

8. Timoshenko, S. P., and D. H. Young: "Theory of Structures," McGraw-Hill Book Company, Inc., New York, 1945.

9. Wang, C. T.: "Applied Elasticity," McGraw-Hill Book Company, Inc., New York, 1953.

10. Bonney, E. A., M. J. Zucrow, and C. W. Besserer: "Aerodynamics, Propulsion, Structures, and Design Practice," D. Van Nostrand Company, Inc., Princeton, N.J., 1956.

11. Niles, A. S., and J. S. Newell: "Airplane Structures," vols. I and II, John Wiley & Sons, Inc., New York, 1943.

12. *Aircraft and Missiles*, vol. 2, no. 11, November, 1959.

13. Bruhn, E. F.: "Analysis and Design of Aircraft Structures," Tri-State Offset Co., Cincinnati, Ohio, 1950.

APPENDIX A

DETERMINATION OF RADIUS AND VOLUME OF TANGENT OGIVES

A-1. RADIUS

From Fig. A-1, the radius of the ogive is derived as follows:

$$R = \frac{d}{2} + R\cos\theta \tag{A-1}$$

Since $l = R\sin\theta$ and $\sin\theta = \sqrt{1 - \cos^2\theta}$ we get

$$\frac{l}{R} = \sqrt{1 - \cos^2\theta} \tag{A-2}$$

or

$$\cos\theta = \sqrt{1 - \frac{l^2}{R^2}} \tag{A-3}$$

Substituting Eq. (A-3) into (A-1), we get

$$R = \frac{d}{2} + R\sqrt{1 - \frac{l^2}{R^2}} \tag{A-4}$$

Rearranging Eq. (A-4), we get

$$1 - \frac{d}{2R} = \sqrt{1 - \frac{l^2}{R^2}} \tag{A-5}$$

Squaring both sides of Eq. (A-5) and rearranging terms, we get

$$R = \frac{d}{4} + \frac{l^2}{d} \tag{A-6}$$

The length-to-diameter ratio of the tangent ogive l/d may be

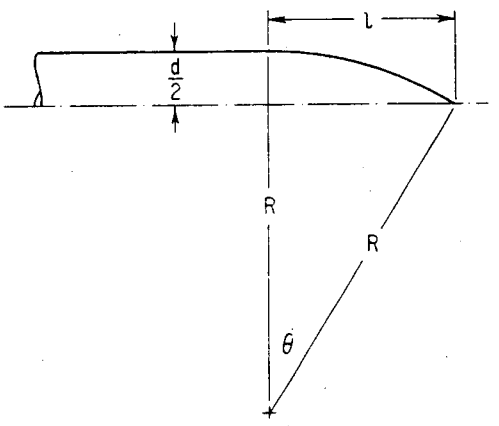

FIG. A-1. Radius of tangent ogive.

expressed in terms of the ogive caliber R/d as follows: Dividing Eq. (A-6) by d and rearranging, we get

$$\frac{l^2}{d^2} = \frac{R}{d} - \frac{1}{4} \tag{A-7}$$

or

$$\frac{l}{d} = \sqrt{\frac{R}{d} - 0.25} = \sqrt{C - 0.25} \tag{A-8}$$

where C is the caliber of the ogive.

A-2. VOLUME

From Fig. A-2*A*, the following relationship is obtained:

$$x = x_1 \tag{A-9}$$

and

$$y_1 = \left(R - \frac{d}{2}\right) + y = a + y \tag{A-9a}$$

where $a = R - \frac{d}{2}$

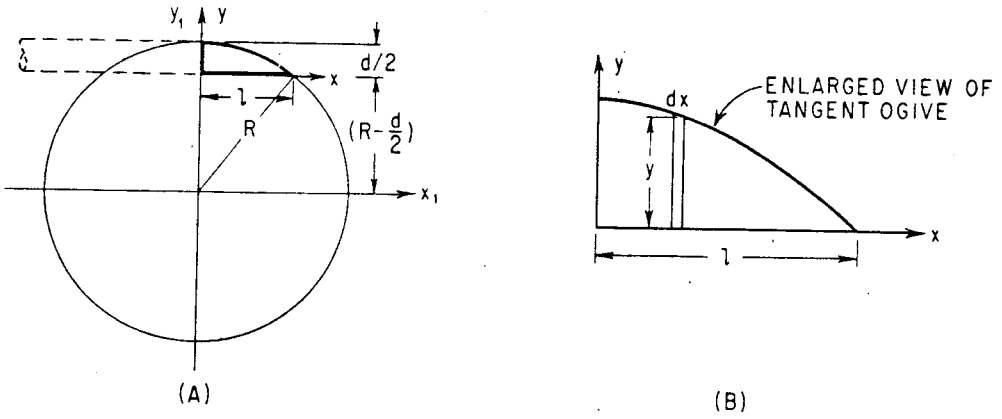

FIG. A-2. Volume of tangent ogive.

From the equation of a circle, we can write

$$x_1^2 + y_1^2 = R^2 \tag{A-10}$$

or

$$x^2 + (a + y)^2 = R^2 \tag{A-10a}$$

Hence

$$y = \sqrt{R^2 - x^2} - a \tag{A-11}$$

or

$$y^2 = R^2 - x^2 - 2a\sqrt{R^2 - x^2} + a^2 \tag{A-12}$$

From Fig. A-2B, the volume of the tangent ogive V may be expressed as

$$V = \pi \int_0^l y^2 \, dx \tag{A-13}$$

Substituting Eq. (A-12) in Eq. (A-13), we get

$$V = \pi \int_0^l [R^2 + a^2 - x^2 - 2a\sqrt{R^2 - x^2}] \, dx \tag{A-14}$$

or $$V = \pi \left[\int_0^l (R^2 + a^2) \, dx - \int_0^l x^2 \, dx - \int_0^l (2a\sqrt{R^2 - x^2}) \, dx \right] \tag{A-15}$$

Integrating Eq. (A-15), we get

$$V = \pi \left\{ (R^2 + a^2) \left[x \right]_{x=0}^{x=l} - \left[\frac{x^3}{3} \right]_{x=0}^{x=l} - 2a \left[\frac{x}{2}\sqrt{R^2 - x^2} + \frac{R^2}{2} \sin x \sqrt{\frac{1}{R^2}} \right]_{x=0}^{x=l} \right\} \tag{A-16}$$

Hence

$$V = \pi \left[(R^2 + a^2)l - \frac{l^3}{3} - al\sqrt{R^2 - l^2} - aR^2 \sin^{-1} \frac{l}{R} \right] \tag{A-17}$$

Substituting $a = R - (d/2)$ in Eq. (A-17), we get

$$V = \pi \left[l\left(R^2 + R^2 - Rd - \frac{d^2}{4} \right) - \frac{l^3}{3} - \left(R - \frac{d}{2} \right) l\sqrt{R^2 - l^2} - \left(R - \frac{d}{2} \right) R^2 \sin^{-1} \frac{l}{d} \right] \tag{A-18}$$

or $$V = \pi \left[l\left(2R^2 - Rd + \frac{d^2}{4} \right) - \frac{l^3}{3} - \left(R - \frac{d}{2} \right) l\sqrt{R^2 - l^2} - \left(R - \frac{d}{2} \right) R^2 \sin^{-1} \frac{l}{R} \right] \tag{A-18a}$$

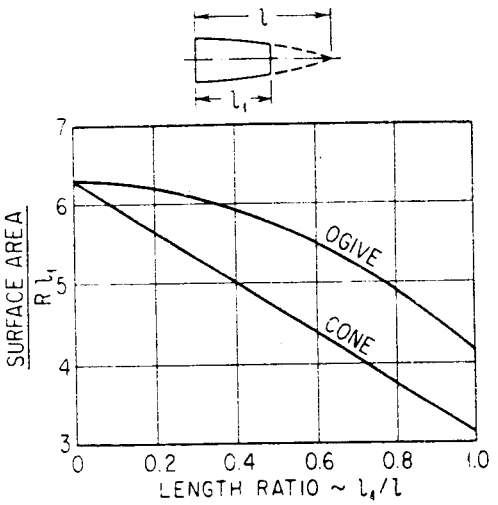

FIG. A-3. Surface area of tangent ogive and truncated conical bodies of revolution.

A-3. SURFACE AREA

In the determination of skin-friction drag coefficient, the surface (wetted) area of the aerodynamic component must be known [see Sec. 4-2, Eq. (4-7)]. Figure A-3 is a plot of the surface area of tangent ogive and truncated conical bodies of revolution.

APPENDIX B

EXPRESSIONS AND COORDINATES OF DIFFERENT NOSE SHAPES*

B-1. POWER SERIES

$$r = x^n \qquad \text{for } (0 \leqq x \leqq 1) \tag{B-1}$$

where $n = 1$ for a cone
$n = \frac{1}{2}$ for a parabola with vertex at $x = 0$

B-2. PARABOLIC SERIES

$$r = \frac{2x - Kx^2}{2 - K} \tag{B-2}$$

where $K = 0$ for a cone
$K = 1$ for a parabolic nose
$K = 0.75$ for a "¾ power" parabolic series
$K = 0.50$ for a "½ power" parabolic series

B-3. HAACK SERIES

$$r = \frac{1}{\sqrt{\pi}} \sqrt{\varphi - \tfrac{1}{2} \sin 2\varphi + C \sin 3\varphi} \tag{B-3}$$

where $\varphi = \cos^{-1}(1 - 2x)$
$C = 0$ for the Von Kármán nose shape (also known as the L-D Haack nose)
$C = \frac{1}{3}$ for the L-V Haack nose.

The letters L-D and L-V refer to the boundary conditions for which the drag was minimized. The L-D signifies given length and diameter and L-V length and volume. Profiles of these nose shapes are shown

* *NACA Research Mem.* L53K17.

in Fig. 3-11 with coordinates presented in Table B-1. The terms x and r used in Table B-1 are defined as

$$x = \frac{\text{distance from nose station}}{\text{total nose length}}$$

$$r = \frac{\text{radius at any nose station}}{\text{maximum radius (i.e., at the base of the nose)}}$$

TABLE B-1. COORDINATES OF DIFFERENT NOSE SHAPES

Nose station	Power series		Parabolic series			Haack series	
	$x^{1/2}$	$x^{3/4}$	Parabola ($K = 1$)	¾ Power ($K = 0.75$)	½ Power ($K = 0.50$)	Von Kármán, L-D Haack ($C = 0$)	L-V Haack ($C = 1/3$)
x	r	r	r	r	r	r	r
0	0	0	0	0	0	0	0
0.05	0.2236	0.1057	0.0975	0.0785	0.0658	0.1368	0.1658
0.10	0.3170	0.1779	0.1900	0.1540	0.1300	0.2281	0.2738
0.15	0.3873	0.2410	0.2750	0.2250	0.1917	0.3066	0.3642
0.20	0.4472	0.2991	0.3600	0.2960	0.2533	0.3774	0.4435
0.25	0.5000	0.3536	0.4375	0.3625	0.3125	0.4422	0.5142
0.30	0.5477	0.4054	0.5100	0.4260	0.3700	0.5022	0.5779
0.35	0.5916	0.4550	0.5775	0.4865	0.4258	0.5585	0.6357
0.40	0.6325	0.5030	0.6400	0.5440	0.4800	0.6112	0.6880
0.45	0.6708	0.5494	0.6975	0.5985	0.5325	0.6607	0.7355
0.50	0.7071	0.5946	0.7500	0.6500	0.5850	0.7071	0.7785
0.55	0.7416	0.6387	0.7975	0.6985	0.6325	0.7506	0.8173
0.60	0.7746	0.6817	0.8400	0.7440	0.6800	0.7914	0.8522
0.65	0.8062	0.7239	0.8775	0.7865	0.7258	0.8295	0.8833
0.70	0.8367	0.7653	0.9100	0.8260	0.7700	0.8647	0.9107
0.75	0.8660	0.8059	0.9375	0.8625	0.8125	0.8969	0.9346
0.80	0.8944	0.8459	0.9600	0.8960	0.8533	0.9261	0.9549
0.85	0.9220	0.8853	0.9775	0.9265	0.8925	0.9518	0.9719
0.90	0.9487	0.9240	0.9900	0.9540	0.9300	0.9736	0.9853
0.95	0.9747	0.9622	0.9975	0.9785	0.9658	0.9905	0.9950
1.00	1.0000	1.0000	1.0000	1.0000	1.0000	1.0000	1.0000

APPENDIX C

OPTIMUM WING STUDY

As stated in Sec. 3-15, maximum L/D is obtained when the induced drag is equal to the drag at zero lift, i.e., $C_{D_i} = C_{D_0}$ or $C_D = 2C_{D_0}$. The proof of this statement is given below. In addition, the expressions for the value of C_L at $(L/D)_{max}$ and $(L/D)_{max}$ are derived as a function of C_{D_0} and the induced drag factor $dC_{D_i}/dC_L{}^2$.

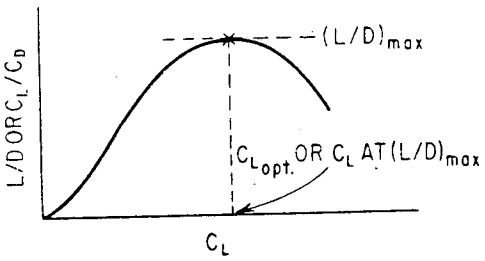

FIG. C-1. Optimum wing study.

C-1. C_D at $(L/D)_{max}$

From the basic definition of lift and drag, we get

$$\frac{L}{D} = \frac{C_L qS}{C_D qS} = \frac{C_L}{C_D} \tag{C-1}$$

Since $C_D = C_{D_0} + C_{D_i} = C_{D_0} + (dC_{D_i}/dC_L{}^2)\, C_L{}^2$, Eq. (C-1) becomes

$$\frac{C_L}{C_D} = \frac{C_L}{C_{D_0} + KC_L{}^2} \tag{C-2}$$

where $K = dC_{D_i}/dC_L{}^2$

From Fig. C-1, it is apparent that $(L/D)_{max}$ is obtained when

$$\frac{d(C_L/C_D)}{dC_L} = 0 \tag{C-3}$$

Hence
$$\frac{d(C_L/C_D)}{dC_L} = \frac{d[C_L/(C_{D_0} + KC_L{}^2)]}{dC_L}$$

$$= \frac{(C_{D_0} + KC_L{}^2)(1) - C_L(0 + 2KC_L)}{(C_{D_0} + KC_L{}^2)^2} = 0 \tag{C-4}$$

or
$$C_{D_0} - KC_L{}^2 = 0 \tag{C-5}$$

From Eq. (C-5), it is seen that

$$C_{D_0} = KC_L^2 = C_{D_i} \tag{C-6}$$

or
$$C_D = C_{D_0} + C_{D_i} = 2C_{D_0} \tag{C-7}$$

Hence
$$C_D \text{ at } (L/D)_{\max} = 2C_{D_0} \tag{C-8}$$

C-2. C_L at $(L/D)_{\max}$ or $C_{L_{\text{opt}}}$

From Eq. (C-6), we get

$$C_L = \sqrt{\frac{C_{D_0}}{K}} = \sqrt{\frac{C_{D_0}}{dC_{D_i}/dC_L^2}} \tag{C-9}$$

Hence
$$C_L \text{ at } (L/D)_{\max} = \sqrt{\frac{C_{D_0}}{dC_{D_i}/dC_L^2}} \tag{C-10}$$

C-3. $(L/D)_{\max}$

The value of $(L/D)_{\max}$ is determined by taking the ratio of C_L and C_D at $(L/D)_{\max}$ as shown in Fig. C-1. Hence, from Eqs. (C-10) and (C-8), we get

$$\left(\frac{L}{D}\right)_{\max} = \frac{C_L \text{ at } (L/D)_{\max}}{C_D \text{ at } (L/D)_{\max}} = \sqrt{\frac{C_{D_0}/K}{2C_{D_0}}} \tag{C-11}$$

or
$$\left(\frac{L}{D}\right)_{\max} = \tfrac{1}{2}\sqrt{\frac{1}{(dC_{D_i}/dC_L^2)C_{D_0}}} \tag{C-12}$$

APPENDIX D

DERIVATION OF INCREMENTAL VELOCITY DUE TO BOOST

D-1. VACUUM (DRAG-FREE CONDITION)

The incremental velocity the missile attained during its accelerating phase of flight can be expressed mathematically as follows:

$$\Delta V_b = \int_0^{t_b} a\, dt \tag{D-1}$$

where ΔV_b = incremental velocity
a = axial acceleration of missile
t_b = burning time of rocket motor

From Fig. D-1, the axial acceleration may be expressed in terms of rocket-motor thrust T and weight W as follows:

$$a = \frac{Tg}{W} + g \sin \gamma_L \tag{D-2}$$

Hence

$$\Delta V_b = g\int_0^{t_b} \frac{T}{W}\, dt + g\int_0^{t_b} \sin \gamma_L\, dt \tag{D-3}$$

Since $W = W_L - W_P\,(t/t_b)$, we get (D-4)

$$\Delta V_b = g\int_0^{t_b} \frac{T}{W_L - W_P(t/t_b)}\, dt + g\int_0^{t_b} \sin \gamma_L\, dt \tag{D-5}$$

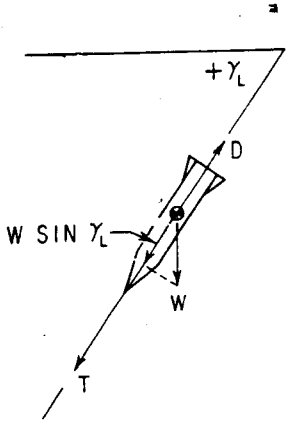

FIG. D-1. Force diagram.

where W_L = missile weight at launch
W_P = propellant weight

Assuming T, γ_L, and t_b are constants, Eq. (D-5) becomes

$$\Delta V_b = Tg\int_0^{t_b} \frac{t_b}{W_L t_b - W_P t}\, dt + g \sin \gamma_L \int_0^{t_b} dt \tag{D-6}$$

Integrating Eq. (D-6), we get

$$\Delta V_b = Tg\left(-\frac{t_b}{W_P}\right)\left[\ln\left(W_L t_b - W_P t\right)\right]_{t=0}^{t=t_b} + g\sin\gamma_L\left[t\right]_{t=0}^{t=t_b} \tag{D-7}$$

or $$\Delta V_b = -\frac{Tt_b}{W_P}g[\ln\left(W_L t_b - W_P t_b\right) - \ln\left(W_L t_b\right)] + gt_b\sin\gamma_L \tag{D-8}$$

Since $Tt_b/W_P = I/W_P = I_{sp}$ [see Eq. (13-13)], Eq. (D-8) becomes

$$\Delta V_b = I_{sp}g\ln\left(\frac{W_L}{W_E}\right) + gt_b\sin\gamma_L \tag{D-9}$$

where $W_E = W_L - W_P$

D-2. GENERAL SOLUTION

For the general solution, the drag term must be included in Eq. (D-2). Hence

$$a = \frac{Tg}{W} - \frac{Dg}{W} + g\sin\gamma_L \tag{D-10}$$

or $$a = \frac{Tg}{W} - \frac{C_D\,\frac{1}{2}\rho V^2 Sg}{W} + g\sin\gamma_L \tag{D-10a}$$

Because of the nature of the drag term, a closed analytical solution cannot be obtained. Hence, for most analysis, Eq. (*D*-10*a*) must be solved by a method of iteration such as that described in Sec. 4-6 or on the automatic computing machines. However, for certain applications whereby the thrust-to-weight ratio is relatively high (i.e., high axial acceleration), it is permissible to use an approximation for the drag effect in calculating a value of ΔV_b. For these cases, an estimated average drag $\bar{D}$ is used in Eq. (*D*-10). Hence Eq. (D-6) may be modified as follows:

$$\Delta V_b = (T - \bar{D})g\int_0^{t_b}\frac{t_b}{W_L t_b - W_P t)}\,dt + g\sin\gamma_L\int_0^{t_b}dt \tag{D-11}$$

Hence Eq. (D-11) becomes

$$\Delta V_b = -\left[(T - \bar{D})\frac{t_b g}{W_P}\right][\ln\left(W_L t_b - W_P t_b\right) - \ln\left(W_L t_b\right)] + gt_b\sin\gamma_L \tag{D-12}$$

Multiplying Eq. (D-12) by T/T and rearranging, we get

$$\Delta V_b = \frac{T - \bar{D}}{T} I_{sp} g \ln \frac{W_L}{W_E} + g t_b \sin \gamma_L \tag{D-13}$$

or

$$\Delta V_b = K' I_{sp} g \ln \frac{W_L}{W_E} + g t_b \sin \gamma_L \tag{D-13a}$$

where $K' = (T - \bar{D}/T)$ as used in Eq. (4-12)

APPENDIX E

DERIVATION OF EXPRESSION FOR ΔV FOR ITERATION METHOD

In the derivation of ΔV [see Eq. (4-21)] for the iteration method used to calculate missile performance, two basic assumptions are made: (1) the acceleration vs. time curve (see Fig. E-1) is linear over the time interval Δt used, and (2) the time interval used throughout the procedure is a constant value. From Fig. E-1, the value of velocity V at any time t may be expressed as

$$V = V_{n-1} + a_{av}\,\Delta t \qquad \text{(E-1)}$$

where the subscript $n - 1$ denotes the first interval previous to t (and $n - 2$ is the second interval previous to t, etc.). Hence Eq. (E-1) becomes

$$V = V_{n-1} + (a + a_{n-1})\frac{\Delta t}{2} \qquad \text{(E-2)}$$

But for a constant Δt, we get

$$a - a_{n-1} = a_{n-1} - a_{n-2} \qquad \text{(E-3)}$$

or

$$a = 2a_{n-1} - a_{n-2} \qquad \text{(E-4)}$$

Substituting Eq. (E-4) into Eq. (E-2), we get

$$V = V_{n-1} + (3a_{n-1} - a_{n-2})\frac{\Delta t}{2} \qquad \text{(E-5)}$$

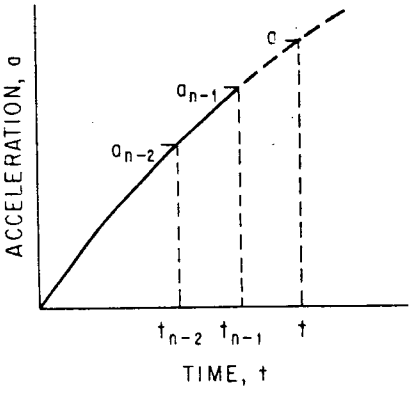

FIG. E-1. Acceleration vs. time.

APPENDIX F

DETERMINATION OF DOWNWASH FROM WIND-TUNNEL-TEST RESULTS

F-1. ANALYTICAL SOLUTION

For the purpose of illustration, a canard configuration has been arbitrarily selected. Hence, from Fig. (F-1), the complete model pitching moment M_{CM} may be expressed as

$$M_{CM} = N_B x_B + N_C x_C + N_T x_T \tag{F-1}$$

where N_B, N_C, and N_T = normal force on body, canard, and tail surfaces

x_B, x_C, and x_T = center-of-pressure location of N_B, N_C, and N_T

Expressed in coefficient form, Eq. (F-1) becomes

$$M_{CM} = (M_\alpha \alpha)_{CM} = [(C_{N_\alpha})_B \alpha x_B + (C_{N_\alpha})_C \alpha x_C + (C_{N_\alpha})_T (\alpha - \epsilon) x_T] q S_\pi \tag{F-2}$$

Dividing by $qS_\pi d$, Eq. (F-2) becomes

$$(C_m)_{CM} = \frac{M_{CM}}{qS_\pi d} = (C_{N_\alpha})_B \alpha \left(\frac{x}{d}\right)_B + (C_{N_\alpha})_C \alpha \left(\frac{x}{d}\right)_C + (C_{N_\alpha})_T (\alpha - \epsilon) \left(\frac{x}{d}\right)_T \tag{F-3}$$

Hence

$$(C_m)_{CM} = (C_m)_{BC} + (C_m)_T (\alpha - \epsilon) \tag{F-4}$$

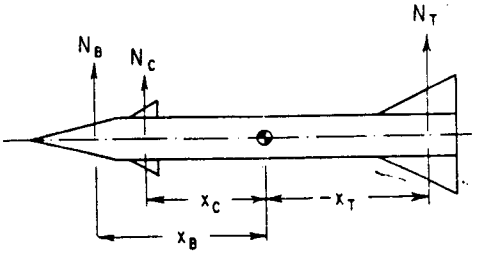

FIG. F-1. Analytical solution of downwash.

where the subscript BC denotes body-plus-tail configuration, etc. Therefore, at a given α, we get

$$\frac{-\alpha - \epsilon}{\alpha} = \frac{(C_m)_{CM} - (C_m)_{BC}}{(C_m)_T} = \frac{(C_m)_{CM} - (C_m)_{BC}}{(C_m)_{BT} - (C_m)_B} \tag{F-5}$$

Equation (F-5) may be described as

$$\frac{\alpha - \epsilon}{\alpha} = \frac{\text{tail contribution in the presence of downwash}}{\text{tail contribution in the absence of downwash}} \qquad \text{(F-5}a\text{)}$$

If the moment curves are linear, then the slopes of C_m vs. α may be used as follows:

$$1 - \epsilon_\alpha = \frac{(C_{m_\alpha})_{CM} - (C_{m_\alpha})_{BC}}{(C_{m_\alpha})_{BT} - (C_{m_\alpha})_B} = \frac{(\Delta C_{m_\alpha})'_T}{(\Delta C_{m_\alpha})_T} \qquad \text{(F-6)}$$

where $(\Delta C_{m_\alpha})'_T$ = tail contribution in presence of downwash
$(\Delta C_{m_\alpha})_T$ = tail contribution in absence of downwash

Similarly, it can be shown that the downwash due to control (canard) surface deflection ϵ_δ, may be expressed as

$$(1 - \epsilon_\delta) = \frac{(\Delta C_{m_\delta})_T}{(\Delta C_{m_\alpha})_T} \qquad \text{(F-7)}$$

F-2. GRAPHICAL SOLUTION

The downwash angle ϵ may also be determined graphically from wind-tunnel-test results. This is done by plotting the pitching-moment contributions of the tail in the presence of and absence of downwash vs. angle of attack as shown in Fig. F-2. It is apparent that, at a given α (i.e., α_1), the value of ΔC_{m_T} in the absence of downwash (i.e., BT-B) is point B in Fig. F-2. The value of ΔC_{m_T} in the presence of downwash is A (BCT-BC) at α_1. This represents a loss of ΔC_m of B-A, which is equivalent to a downwash angle ϵ as shown in Fig. F-2. Hence the value of ϵ can be readily determined at any or all values of α desired. Hence nonlinearity imposes no limitation on this graphical solution.

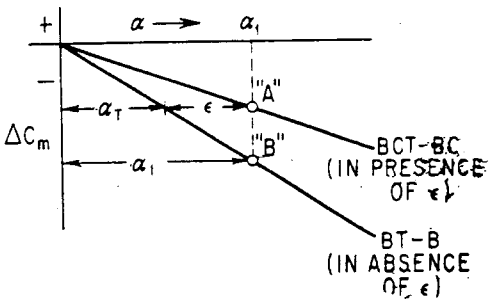

FIG. F-2. Graphical solution of downwash.

The normal-force coefficients may also be used in lieu of the pitching-moment coefficients. However, since the moment coefficients are generally somewhat more accurate than the normal-force coefficients, the former are preferred.

APPENDIX G

DETERMINATION OF DAMPING DERIVATIVES FROM WIND-TUNNEL-TEST RESULTS

G-1. DAMPING IN PITCH

The value of the pitch damping or rotary derivatives $C_{m_{\dot{\theta}}}$, $C_{m_{\dot{\alpha}}}$, and $C_{m_{\dot{\delta}}}$, as discussed in Sec. 9-3, may be determined from the static derivatives (i.e., C_{N_α} and C_{m_α}) which are obtained from wind-tunnel tests. In Sec. 9-3 it was shown that the value of $C_{m_{\dot{\theta}}}$ for the complete model configuration consists of contributions from the forebody, canard (or any other control surfaces ahead of the tail), and tail surfaces as expressed below:

$$(C_{m_{\dot{\theta}}})_{CM} = -2\left\{(C_{N_\alpha})_B\left(\frac{x}{d}\right)_B^2 + (C_{N_\alpha})_C[K_{C(B)} + K_{B(C)}]\frac{S_c}{S_\pi}\left(\frac{x}{d}\right)_C^2 + (C_{N_\alpha})_T \times [K_{T(B)} + K_{B(T)}]\frac{S_T}{S_\pi}\left(\frac{x}{d}\right)_T^2\right\} \quad \text{(G-1)}$$

From Eq. (G-1) [which is identical to Eq. (9-39)], it is apparent that the first two terms represent the contributions from the combined effects of the body and canards. The third or last term represents the tail contribution which includes the mutual interference between the body and tail. These contributions may also be expressed in terms of the moment derivative C_{m_α}, in the following general form:

$$(C_{N_\alpha})_B\left(\frac{x}{d}\right)_B^2 \rightarrow (C_{N_\alpha})_B\frac{(C_{m_\alpha})_B^2}{(C_{N_\alpha})_B} \rightarrow \frac{(C_{m_\alpha})_B^2}{(C_{N_\alpha})_B}$$

Hence Eq. (G-1) becomes

$$(C_{m_{\dot{\theta}}})_{CM} = -2\left\{\frac{(C_{m_\alpha})_{BC}^2}{(C_{N_\alpha})_{BC}} + \frac{[(C_{m_\alpha})_{BT} - (C_{m_\alpha})_B]^2}{(C_{N_\alpha})_{BT} - (C_{N_\alpha})_B}\right\} \quad \text{(G-2)}$$

where the subscripts denote the components of the configuration (i.e., B body, T tail, etc.).

Similarly, the expressions for $C_{m_{\dot{\alpha}}}$ and $C_{m_{\dot{\delta}}}$ [see Eqs. (9-44) and (9-46)] become

$$(C_{m_{\dot{\alpha}}})_{CM} = -2[(C_{m_\alpha})_{BT} - (C_{m_\alpha})_B]\frac{x_{C\text{-}T}}{d}\epsilon_\alpha \tag{G-3}$$

and

$$(C_{m_{\dot{\delta}}})_{CM} = -2[(C_{m_\alpha})_{BT} - (C_{m_\alpha})_B]\frac{x_{C\text{-}T}}{d}\epsilon_\delta \tag{G-4}$$

where $x_{C\text{-}T}$ is the distance between the canard and the tail surfaces as shown in Fig. 9-4, and ϵ_α and ϵ_δ are determined in Appendix F.

G-2. DAMPING IN ROLL

In order to determine the damping-in-roll derivative C_{l_p} [see Sec. 8-5 or Eq. (8-4)] in the wind tunnel, several techniques may be employed. Perhaps the simplest method is to roll the model on the mounting

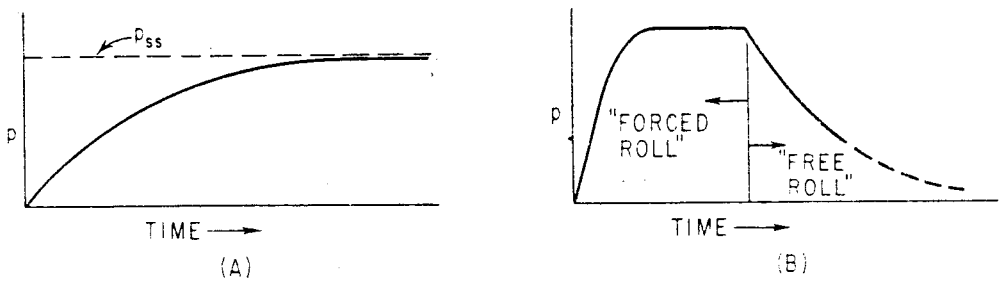

FIG. G-1. Damping-in-roll tests.

sting by means of fixed aerodynamic lateral-control surfaces. In this technique, the model is initially restrained from rolling while the tunnel builds up to speed, whereupon the model is released and commences to spin up to its steady-state rolling velocity, as indicated in Fig. G-1*a*.

The transient response of the missile in roll is expressed as

$$I_x\dot{p} = C_{l_\delta}\delta qSd + C_{l_p}p\frac{qSd^2}{2V} + L_0 \tag{G-5}$$

where I_x = moment of inertia of model in roll
C_{l_δ} = lateral-control effectiveness which is determined from conventional wind-tunnel test
L_0 = term to account for friction in the system and may be accounted for or, if it is small, neglected

From the time history of the measured rolling velocity as shown in Fig. G-1*a*, the roll acceleration $\dot{p}$ and hence C_{l_p} may be calculated. However, the value of C_{l_p} is more accurately calculated for the steady-state rolling condition, i.e., $\dot{p} = 0$. For this condition, C_{l_p} is

determined by setting Eq. (G-5) equal to zero. Hence, if friction is neglected, we get

$$C_{l_p} = \frac{C_{l_\delta}\delta}{p_{ss}d/2V} \tag{G-6}$$

where p_{ss} = steady-state rolling velocity

Another method of determining C_{l_p} is to spin the model mechanically. In this technique, a driving device is employed to spin the model with the aerodynamic lateral-control surfaces in their neutral position. By measuring the rolling moment required to spin the model at various constant rolling velocities, the value of C_{l_p} is calculated as follows (again, assuming $L_0 = 0$):

$$C_{l_p} = \frac{\mathscr{L}_p}{qSd^2/2V} \tag{G-7}$$

where $\mathscr{L}_p$ = measured variation of required rolling moment with rolling velocity, ft-lb/radian/sec

A third method of determining C_{l_p} is simply to spin the model to an arbitrary rolling velocity and then allow the spin rate of the model to decrease toward zero velocity as shown in Fig. G-1*B*. In this technique, the aerodynamic lateral-control surfaces are set in their neutral positions. The value of C_{l_p} may be calculated by Eq. (G-5), which may be simplified to the following expression:

$$C_{l_p} = \frac{I_x\dot{p}}{pqSd^2/2V} \tag{G-8}$$

APPENDIX H

DETERMINATION OF AERODYNAMIC DERIVATIVES FROM FLIGHT-TEST DATA

H-1. "PULSED MODEL"

One technique most commonly used in scaled-model flight testing is the "pulsed-model" method. In this method, the model is usually ground-launched and accelerated to the desired speed by means of a booster rocket which drops off at the end of its burning. The model then commences its free flight wherein small rocket charges are set off at fixed time intervals which provide the desired impulse to "disturb" the model in pitch and/or in yaw during its zero-lift flight trajectory. The model used in this technique is generally completely uncontrolled and must be statically stable. By carefully controlling the manufacturing and installation fin misalignments, the rolling velocity of the model is kept low in order to reduce the cross-coupling effects during the "disturbed" conditions. A typical plot of the model transient response in the "disturbed" condition is shown in Fig. 9-3. Telemetered data for this technique generally consist of time history of axial acceleration, normal acceleration about the model center of gravity, and angle of attack. A history of the model speed, Mach number, and dynamic pressure is also required and may be obtained from external coverage such as radar, theodolite, and radiosonde data.

The aerodynamic derivatives obtained from this method are C_{D_0}, C_{N_α}, C_{m_α}, and $(C_{m_{\dot\theta}} + C_{m_{\dot\alpha}})$. The value of C_{D_0} may be determined when the model is flying in the undisturbed conditions.

$$C_{D_0} = \frac{n_x W}{qS} \tag{H-1}$$

where n_x = axial acceleration
W = weight of model

The value of C_{N_α} may be determined from the telemetered data of

normal acceleration and angle of attack during the "disturbed" condition of the model. The value of C_N is evaluated as follows:

$$C_N = \frac{nW}{qS} \tag{H-2}$$

where n is the normal acceleration at the model center of gravity. By plotting the value of C_N vs. α, the value of C_{N_α} may be determined throughout the speed or Mach-number range of the model. Since the angle of attack is generally measured by an α indicator located at or ahead of the nose of the model (see Fig. H-1), the telemetered data of α must be corrected for the incremental angle of attack $\Delta\alpha$ induced by the angular motion of the model. The induced angle of attack may be expressed as [see Eq. (9-34)]

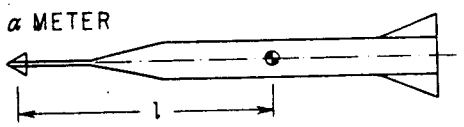

FIG. H-1. Angle-of-attack correction.

$$\Delta\alpha = \tan^{-1}\frac{\dot{\theta}l}{V} \tag{H-3}$$

For small angles, Eq. (H-3) becomes

$$\Delta\alpha \cong \frac{\dot{\theta}l}{V} \tag{H-3a}$$

Since $\dot{\theta} = \dot{\alpha} + \dot{\gamma}$ [see Eq. (5-3)] and

$$\dot{\gamma} = \frac{g}{WV}(nW - W\cos\theta)$$

we get

$$\Delta\alpha = \frac{l}{V}\left(\dot{\alpha} + g\frac{n - \cos\theta}{V}\right) \tag{H-4}$$

Hence

$$\alpha_{cg} = \alpha_{\text{measured}} - \Delta\alpha \tag{H-5}$$

The value of C_{m_α} and $(C_{m_{\dot{\theta}}} + C_{m_{\dot{\alpha}}})$ may be determined by solving the equation of motion assuming a single degree of freedom. Hence

$$I\ddot{\theta} = M_\alpha\alpha + M_{\dot{\theta}}\dot{\theta} + M_{\dot{\alpha}}\dot{\alpha} \tag{H-6}$$

Since $\dot{\theta} \cong \dot{\alpha}$ (assumption of single degree of freedom), we may rewrite Eq. (H-6) as follows:

$$I\ddot{\theta} - (M_{\dot{\theta}} + M_{\dot{\alpha}})\dot{\theta} - M_\theta\dot{\theta} = 0 \tag{H-7}$$

or

$$\ddot{\theta} - (m_{\dot{\theta}} + m_{\dot{\alpha}})\dot{\theta} - m_\theta\theta = 0 \tag{H-7a}$$

Solving for the roots of Eq. (H-7a), we get

$$\lambda_{1,2} = \tfrac{1}{2}(m_{\dot\theta} + m_{\dot\alpha}) \pm \tfrac{1}{2}\sqrt{(m_{\dot\theta} + m_{\dot\alpha})^2 + 4m_\theta} \tag{H-8}$$

From Sec. 9-3, it is apparent that

$$T_{1/2} = -\frac{2 \ln 2}{m_{\dot\theta} + m_{\dot\alpha}} \tag{H-9}$$

and

$$P = \frac{4\pi}{\sqrt{(m_{\dot\theta} + m_{\dot\alpha})^2 + 4m_\theta}} \tag{H-10}$$

From Eq. (H-9), the values of $(M_{\dot\theta} + M_{\dot\alpha})$ become

$$M_{\dot\theta} + M_{\dot\alpha} = \frac{-2I \ln 2}{T_{1/2}} = (C_{m_{\dot\theta}} + C_{m_{\dot\alpha}})\frac{qSd^2}{2V} \tag{H-9a}$$

Hence

$$C_{m_{\dot\theta}} + C_{m_{\dot\alpha}} = \frac{-4IV \ln 2}{qSd^2 T_{1/2}} \tag{H-9b}$$

The value of C_{m_α} may be determined by first squaring both sides of Eq. (H-10) and rearranging terms as shown below:

$$\left(\frac{4\pi}{P}\right)^2 = (m_{\dot\theta} + m_{\dot\alpha})^2 + 4m_\theta \tag{H-10a}$$

or

$$m_\theta = \left(\frac{2\pi}{P}\right)^2 - \frac{(m_{\dot\theta} + m_{\dot\alpha})^2}{4} \tag{H-10b}$$

Substituting Eq. (H-9) into Eq. (H-10b), we get

$$m_\theta = \frac{M_\theta}{I} = \left(\frac{2\pi}{P}\right)^2 - \left(\frac{\ln 2}{T_{1/2}}\right)^2 \tag{H-11}$$

Since M_θ is equal to M_α for this single-degree-of-freedom analysis and is negative we get

$$C_{m_\alpha} = \frac{M_\alpha}{qSd} = \frac{-I}{qSd}\left[\left(\frac{2\pi}{P}\right)^2 - \left(\frac{\ln 2}{T_{1/2}}\right)^2\right] \tag{H-11a}$$

Hence the value of C_{m_α} and $(C_{m_{\dot\theta}} + C_{m_{\dot\alpha}})$ may be readily calculated by Eqs. (H-11a) and (H-9b) by measuring the period of oscillation P and time to damp to half amplitude $T_{1/2}$ from the telemetered record of the model transient response as shown in Fig. 9-3. The change in Mach number, dynamic pressure, etc., during this transient is assumed to be negligible.

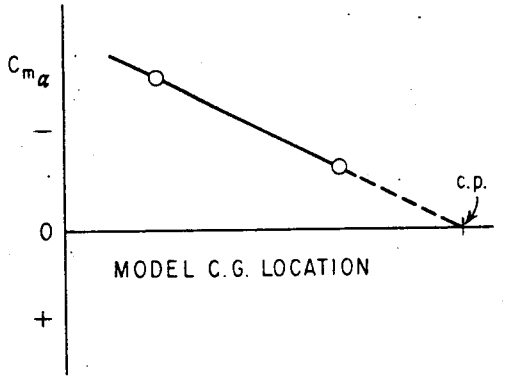

FIG. H-2. Determination of C_{N_α}.

By flight testing the model with two different center-of-gravity locations, the values of C_{m_α} thus obtained may be used to check the value of C_{N_α} previously determined with telemetered α data. This may be accomplished by plotting the values of C_{m_α} vs. center of gravity as shown in Fig. H-2. The center-of-pressure (or neutral-point) location is determined by extrapolating the curve of C_{m_α} vs. center of gravity to C_{m_α} equal to zero. Hence, from Eq. (5-19) and Fig. H-2, we get

$$\text{cp} = \text{cg} - \frac{\bar{X}}{d} = \text{cg} - \frac{C_{m_\alpha}}{C_{N_\alpha}} \tag{H-12}$$

or

$$C_{N_\alpha} = \frac{C_{m_\alpha}}{\text{cg} - \text{cp}} \tag{H-12a}$$

It is therefore apparent that C_{N_α} is simply the slope of the C_{m_α} vs. center-of-gravity curve shown in Fig. H-2.

H-2. STEP-COMMAND INPUT

Another method commonly used consists of programming step-control surface deflections of sufficient duration to assure that the model or missile approaches its steady-state trimmed condition. In conditions wherein the missile is continually decelerating, the duration of command may be reduced somewhat in order that the change in Mach number, q, etc., be small. In these cases, the missile may not reach its steady-state trimmed condition but will have experienced a sufficient number of oscillations about its nominal trimmed condition to permit an accurate determination of the period of oscillation and time to damp to half amplitude. For this type of command a two-degree-of-freedom analysis is generally acceptable.

From the analysis presented in Sec. 9-5, it was shown that the period of oscillation P and the time to damp to half amplitude $T_{\frac{1}{2}}$ may be related to the aerodynamic coefficient as follows [see Eqs. (9-91) and (9-92)]:

$$P = \frac{2\pi}{\sqrt{-\omega^2(1 - \zeta^2)}} \tag{H-13}$$

and $$T_{1/2} = \frac{\ln 2}{\zeta\omega} \tag{H-13a}$$

Equation (H-13) may be rewritten as

$$-\omega^2(1-\zeta^2) = \left(\frac{2\pi}{P}\right)^2 \tag{H-13b}$$

From Eq. (9-77) and the definition of ω and ζ (see Sec. 9-5), we may rewrite Eq. (H-13a) as

$$\omega^2(1-\zeta^2) = -\left(\frac{2\pi}{P}\right)^2 = (m_\alpha + m_{\dot\theta} f_\alpha)\left[1 - \frac{(-f_\alpha + m_{\dot\theta} + m_{\dot\alpha})^2}{4(m_\alpha + m_{\dot\theta} f_\alpha)}\right] \tag{H-14}$$

Defining $\sqrt{-\omega^2(1-\zeta^2)}$ as the damped natural frequency of the missile ω_d, we may write Eq. (H-14) as follows:

$$\omega_d{}^2 = (m_\alpha + m_{\dot\theta} f_\alpha)\left[1 - \frac{(-f_\alpha + m_{\dot\theta} + m_{\dot\alpha})^2}{4(m_\alpha + m_{\dot\theta} f_\alpha)}\right] \tag{H-15}$$

or $$\omega_d{}^2 = m_\alpha + m_{\dot\theta} f_\alpha - \tfrac{1}{4}(-f_\alpha + m_{\dot\theta} + m_{\dot\alpha})^2 \tag{H-15a}$$

Hence $$m_\alpha = \omega_d{}^2 + \left(\frac{-f_\alpha + m_{\dot\theta} + m_{\dot\alpha}}{2}\right)^2 - m_{\dot\theta} f_\alpha \tag{H-16}$$

or $$m_\alpha = \left(\frac{2\pi}{P}\right)^2 + \left(\frac{-f_\alpha + m_{\dot\theta} + m_{\dot\alpha}}{2}\right)^2 - m_{\dot\theta} f_\alpha \tag{H-16a}$$

From Sec. 9-5 and Eq. (9-77), we get

$$\zeta\omega = \frac{-e}{2} = -\frac{m_{\dot\theta} + m_\alpha - f_\alpha}{2} = \frac{\ln 2}{T_{1/2}} \tag{H-17}$$

Rearranging, we get

$$m_{\dot\theta} + m_{\dot\alpha} = -2\zeta\omega + f_\alpha \tag{H-18}$$

Substituting Eq. (H-17) into Eq. (H-18), we get

$$m_{\dot\theta} + m_{\dot\alpha} = \frac{-2\ln 2}{T_{1/2}} + f_\alpha \tag{H-19}$$

Hence $$C_{m_{\dot\theta}} + C_{m_{\dot\alpha}} = \frac{-2VI}{qSd^2}\left(\frac{2\ln 2}{T_{1/2}} - \frac{C_{N_\alpha} qS}{mV}\right) \tag{H-20}$$

Substituting Eq. (H-17) into Eq. (H-16a), we get

$$C_{m_\alpha} = \frac{-I}{qSd}\left[\left(\frac{2\pi}{P}\right)^2 - \left(\frac{\ln 2}{T_{1/2}}\right)^2 + C_{m_{\dot\theta}} \frac{qSd^2}{2VI} \frac{C_{N_\alpha} qSd}{mV}\right] \tag{H-21}$$

In most practical cases, the last term in Eq. (H-21) may be neglected. Hence

$$C_{m_\alpha} = \frac{-I}{qSd}\left[\left(\frac{2\pi}{P}\right)^2 - \left(\frac{\ln 2}{T_{1/2}}\right)^2\right] \tag{H-21a}$$

Other aerodynamic coefficients obtainable from this method include C_{D_0}, C_{N_α}, C_{N_δ}, and C_{m_δ}. The values of C_{D_0} and C_{N_α} may be determined by the methods previously described. The value of C_{N_δ} may be calculated from Eq. (5-23) as follows:

$$C_{N_\delta} = \frac{C_{N_{TR}} - C_{N_\alpha}\alpha_{TR}}{\delta} \tag{H-22}$$

where α_{TR}, δ, C_{N_α} are known and

$$C_{N_{TR}} = \frac{n_{ss}W}{qS} \tag{H-23}$$

The value of C_{m_δ} may be determined from Eq. (5-21) as follows:

$$C_{m_\delta} = -\frac{C_{m_\alpha}\alpha_{TR}}{\delta} \tag{H-24}$$

Aerodynamic hinge-moment characteristics of the control surfaces may also be determined from flight by telemetered strain-gauge data.

H-3. FORCED OSCILLATION

The forced-oscillation technique is commonly used to determine the combined lateral-control effectiveness and damping-in-roll characteristic of the missile. In this method the model or missile is forced to roll by deflecting the lateral-control surfaces throughout the missile flight trajectory. The combined effect of the lateral-control effectiveness and damping in roll may be determined from Eq. (9-93) as follows:

$$I_x\dot{p} = C_{l_p}p\frac{qSd^2}{2V} + C_{l_\delta}\delta qSd \tag{H-25}$$

From the telemetered trace of rolling velocity (measured by a roll-rate gyro) vs. time, the value of $pd/2V$ per degree of lateral control deflection δ may be determined by assuming $\dot{p} = 0$. Hence Eq. (H-25) becomes

$$\frac{pd/2V}{\delta} = \frac{-C_{l_\delta}}{C_{l_p}} \tag{H-26}$$

The assumption that $\dot{p} = 0$ at any instant of flight is generally valid, particularly for cases where the moment of inertia I_x is low or the

damping-in-roll derivative is large. This is readily apparent if the dynamic response of the missile in roll is treated essentially as a first-order system as indicated below [see Eq. (9-96)],

$$\frac{p}{\delta} = \frac{l_\delta}{-l_p + s} = -\frac{l_\delta/l_p}{1 + (1/l_p)s} \rightarrow \frac{K}{1 + Ts} \tag{H-27}$$

where

$$T = \frac{I_x}{C_{l_p} q S d^2/2V} \tag{H-28}$$

Hence, for low values of I_x or large values of C_{l_p}, the value of T is also small. Hence, for most designs, the value of T is sufficiently low that it is generally valid to assume $\dot{p} = 0$ or that steady-state rolling velocity is realized throughout the flight of the missile.

H-4. MACH-NUMBER DETERMINATION

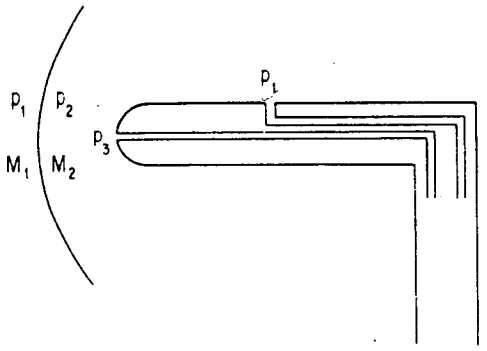

FIG. H-3. Pitot-static tube.

In order to reduce the flight-test data to aerodynamic coefficients, it is necessary that the Mach number, velocity, and dynamic-pressure history be known. The Mach number may be determined either from telemetered stagnation and static-pressure data from a pitot-static tube as shown in Fig. H-3, or from external data such as radar, theodolite coverage, and radiosonde information. From telemetered pressure data, the Mach number may be determined as follows:

1. For $M < 1$,

$$\frac{p_{\text{stagnation}}}{p_{\text{static}}} = \left(1 + \frac{\gamma - 1}{2} M^2\right)^{\gamma/\gamma-1} \tag{H-29}$$

Substituting $\gamma = 1.4$ for air, Eq. (H-29) becomes

$$\frac{p_{\text{stagnation}}}{p_{\text{static}}} = (1 + 0.2M^2)^{3.5} \tag{H-29a}$$

2. For $M > 1$ (see Fig. H-3),

$$\frac{p_{\text{stagnation}}}{p_{\text{static}}} = \frac{p_3}{p_2}\frac{p_2}{p_1} = \frac{p_3}{p_1} \tag{H-30}$$

where p_3 = stagnation pressure.
p_1 = free-stream static pressure
p_2 = pressure behind a normal shock

From the normal shock equations, we get

$$\frac{p_2}{p_1} = \frac{7M_1^2 - 1}{6} \tag{H-31}$$

From isentropic compression [see Eq. (H-29a) we get

$$\frac{p_3}{p_2} = (1 + 0.2M_2^2)^{3.5} \tag{H-32}$$

Since $$M_2 = \frac{M_1^2 + 5}{7M_1^2 - 1} \tag{H-33}$$

Eq. (H-32) becomes

$$\frac{p_3}{p_2} = \left[1 + 0.2\left(\frac{M_1^2 + 5}{7M_1^2 - 1}\right)^2\right]^{3.5} \tag{H-34}$$

Substituting Eqs. (H-31) and (H-34) into Eq. (H-30), we get

$$\frac{p_{\text{stagnation}}}{p_{\text{static}}} = \frac{p_3}{p_1} = \frac{7M_1^2 - 1}{6} \times \left[1 + 0.2\left(\frac{M_1^2 + 5}{7M_1^2 - 1}\right)^2\right]^{3.5} \tag{H-35}$$

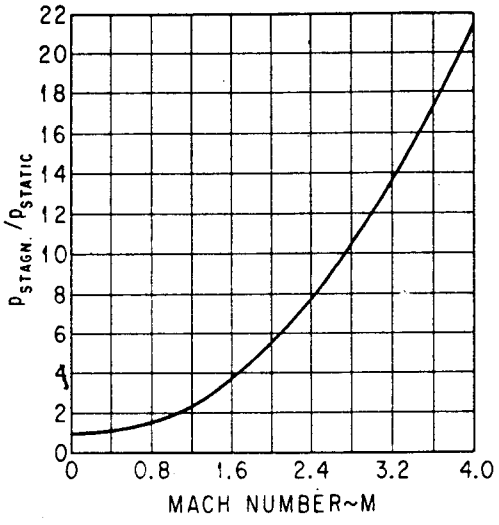

FIG. H-4. Variation of ratio of stagnation pressure to static pressure with Mach number.

Equation (H-35) is commonly known as the Rayleigh pitot-tube formula. A plot of Eqs. (H-29a) and (H-35) is presented in Fig. H-4. It is noted that Eq. (H-29a) may be used for Mach number up to 1.3 without appreciable error.

The velocity of the missile may be calculated from the Mach number as

$$V = Ma \tag{H-36}$$

where a is the speed of sound and is related to the outside air temperature as follows:

$$a = 49.02\sqrt{T_{(°F)} + 459.7} \tag{H-37}$$

The velocity of the missile may also be determined from radar or theodolite data.

The dynamic pressure q, may be calculated as follows:

$$q = \tfrac{1}{2}\gamma p_1 M_1^2 \tag{H-38}$$

or

$$q = \tfrac{1}{2}\rho V^2 \tag{H-38a}$$

where ρ is the density of the air and may be determined from radiosonde data.

INDEX